







Electronically Steerable Antennas for Future Heterogeneous Communication Networks: Review and Perspectives

TOBIAS CHALOUN ¹ (Member, IEEE), **LUIGI BOCCIA** ² (Senior Member, IEEE),
EMILIO ARNIERI ² (Member, IEEE), **MICHAEL FISCHER** ¹ (Student Member, IEEE),
VACLAV VALENTA³ (Member, IEEE), **NELSON J. G. FONSECA** ³ (Senior Member, IEEE),
AND CHRISTIAN WALDSCHMIDT ¹ (Fellow, IEEE)

(Invited Paper)

¹Institute Of Microwave Engineering, University of Ulm, 89081 Ulm, Germany

²Department of Computer Science, Modeling, Electronics and Systems Engineering (DIMES), University of Calabria, 87036 Rende, Italy

³Antenna and Sub-Millimetre Waves Section, European Space Agency, 2200 Noordwijk, The Netherlands

CORRESPONDING AUTHOR: Tobias Chaloun (e-mail: tobias.chaloun@uni-ulm.de).

This work was supported in part by the European Union's Horizon 2020 Research and Innovation Programme under Grant 101004233 and in part by the German Research Foundation under Grant CH 2226/2-1.

ABSTRACT Satellite, fifth generation (5G), and sixth generation (6G) mobile communication systems operating at micro- and millimeter wave frequencies are an essential pillar in advanced network architectures for high-throughput low latency services. The decisive factors for this current development were the significant technological advances accomplished over the last two decades, which meanwhile enable highly integrated, feature-rich, and cost-effective realizations of complete phased array transceiver topologies. Motivated through the today's trend for heterogeneous constellation types to provide truly global coverage, this contribution reviews the current state-of-the-art of electronically steerable antennas for terrestrial and non-terrestrial communication systems up to 100 GHz. First, the potential benefits and limitations of the most relevant technologies are contrasted and put into context with recent system architectures for adaptive beamforming. Their operating principles along with various experimental implementation and achievements providing advanced capabilities such as multi-band/multi-beam operation, polarization agility, and wide-angle scanning are thoroughly presented. Particular emphasis is laid on the review of direct radiating arrays, quasi-optical antenna configurations, and metasurface-based antennas.

INDEX TERMS Satellite communications on the move (SOTM), fifth generation (5G), sixth generation (6G), hybrid satellite constellations, aerial networks, electronic steering, phased array, antennas.

I. INTRODUCTION

Modern telecommunication systems have become an integral part of our daily lives, having a lasting impact on both our private and professional activities. Their role is under constant affirmation and is receiving continuous impulses from the increasing number of applications being developed.

The “anyone to anything, anytime and anywhere” paradigm, originally conceived for the 5G New Radio (NR), is progressively becoming a reality. The key drivers of this change are related to three needs: i) enhanced mobile

broadband; ii) ultra-reliable and low latency communications; iii) massive machine type communications [1]. In the eyes of an engineer, this trend is driving technological advancements across all segments of the network service ecosystem, from its infrastructure hierarchy to its spectrum layer [2]. Accordingly, the use of millimeter and sub-millimeter waves is crucial to implement networks with low latency and high capacity. However, because of the low output power [3] and inherently high link loss, implementing a wireless network becomes increasingly difficult as the frequency increases. Millimeter

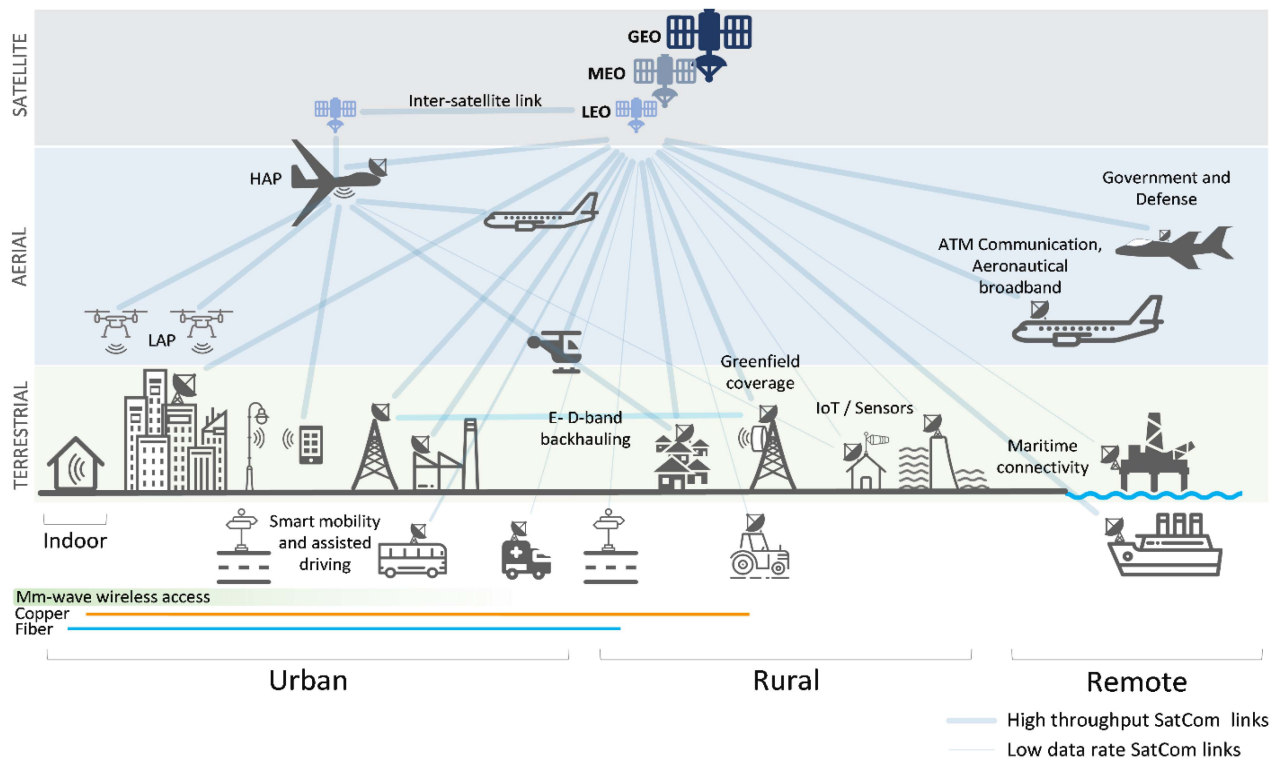


FIGURE 1. Integration between terrestrial, aerial, and satellite networks.

wave (mm-wave) electronically reconfigurable antennas are therefore an essential technological pillar of future telecommunication systems as they allow more efficient radio links.

The use of mm-wave systems (see Fig. 1) is becoming prevalent in all segments of the network infrastructure and even a valid alternative to copper and fiber connections in urban areas. Their role, already crucial in the 5G infrastructure, will become even more important in the future. The architecture of the 6G network currently under development is strongly oriented to a hierarchical infrastructure referred to as Vertical Heterogeneous Network (VHetNet) [4]. According to this vision, future networks can rely on three layers: terrestrial network, space network and aerial network.

A. TERRESTRIAL NETWORKS

The market for high-capacity mm-wave wireless indoor communications is expected to rapidly expand over the next few years in licensed 26/28/40 GHz or unlicensed 60/100/300 GHz spectrum. Thanks to the availability of wide bandwidths, enhanced local area access networks can be deployed reaching 10 Gbps of data rates and latencies smaller than 1 ms [5]. Main application drivers include private homes (e.g., entertainment, sensing), public transportation (e.g., railway or metro stations), commercial spaces, public buildings (e.g., museums, theaters), manufacturing areas (Industry 4.0) or hospitals [4]. Similarly, 5G is expected to benefit from broadband millimeter wave links with reconfigurable directional properties. Consequently, millions of nodes will be

deployed, posing technological and production challenges that cannot be addressed through evolutionary solutions. A multidisciplinary revolutionary approach is instead required involving heterogeneous integration into 3D high density packages [6], as well as multichannel transceivers utilizing silicon technologies (SiGe or CMOS) [7]. With the proliferation of cells and the huge fronthaul data rate, wireless backhauling will be required in large scales. Such links are typically operated in the E-band [8] with D-band as the next frequency target [9], [10]. Although these systems do not require phased arrays, it is necessary to use electronic beam steering to compensate for environmental constraints such as mast sways caused by thermal deformation [11].

The use of electronically steerable antennas in mm-wave frequency ranges is also prevalent in smart mobility and as-sistive driving. In addition to the well-established automotive radar market [12], a new range of applications for info-tainment as well as road safety can be hence enabled by mm-wave vehicle-to-vehicle communications and vehicle-to-infrastructure communications in urban environments. With the extremely low latency supported by the 5G technology, namely less than 10 ms regardless of the frequency range [13], road information can be shared in real-time and traffic controllers can implement real-time congestion-free regulations [14], [15]. These developments are inevitably accompanied by the transformation of the infrastructure to a sensing network comprising of joint radar-communication nodes. Unlike most commercial automotive radar sensors,

these future automotive-related RF platforms are supposed to deploy digital modulation schemes and more radiating elements in order to meet both higher data rates and better sensing qualities [16].

B. SATELLITE NETWORKS

Satellite Communication (SatCom) were initially introduced mainly to serve media broadcasting, defense applications and, more recently, for backhauling applications. Since their inception, these services were operated through geostationary (GEO) satellites which allow a wide coverage using a single satellite, typically serving a regional or continental area suitable for point-to-multipoint communications. In the last few years, a wide range of new applicative scenarios emerged, primarily due to the increased demand of SatCom internet connections and media streaming enabled with multi-spot high throughput satellite (HTS) technology suitable for point-to-point communications. As a result, a rapid adoption of SatCom links developed for a broad spectrum of mobile platforms, resulting in an explosion of SatCom-on-the-move (SOTM) terminal demand. First civil applications of this type, typically based on reflector antennas with electromechanical pointing, were limited to long-range airplanes, cruise ships and emergency scenarios. However, the constantly growing demand for these types of services, on the one hand, and the availability of new reconfigurable phased array technologies, on the other hand, are boosting the diffusion of SatCom systems. In perfect accordance with the cost-size reduction paradigm, the proven maturity of new user terminal technologies is creating new SatCom market areas and new applications which are in turn attracting new public and private investments.

Another significant milestone in this context is the convergence of different wireless technologies enabled by the 5G network that greatly benefits the development of new ambitious SatCom constellations based on Low Earth Orbit (LEO) [17] or Medium Earth Orbit (MEO) satellites. With an altitude of the most recent constellations as low as 320 km, broadband services with interface latency of 3 ms can be provided [18]. Due to the high diffusion potential of such LEO-based SatCom services, many private companies have announced the creation of their own constellations [19], [20]. With thousands of satellites to be launched in the next few years, these constellations will by far be the largest satellite fleet ever deployed and it is expected to provide a very relevant market opportunity for the satellite sector. Besides, this shift does also represent an exceptional stimulus for the development of new K-Ka band electronically reconfigurable antennas. Interestingly, LEO SatCom terminals can generally have less stringent requirements in terms in terms of EIRP, G/T and scanning range than their GEO counterparts, thus resulting in a significantly reduced cost and size of the user terminal as well as in less stringent modem requirements. This is mainly because present and future LEO satellite communication systems operate in mega-constellations at much lower altitudes.

As a result, more competitive phased array solutions [21] and a completely new range of applications [22] can be developed in the near future. For example, industries, energy generation activities or agriculture practice, typically operated in scarcely populated areas, can benefit for SatCom LEO links. Another sector where LEO SatCom services will produce a strong impact is the one related to the internet of things (IoT). An increasing number of industrial sectors, including not only telecommunications but also transportation and logistics, energy, agriculture, healthcare, natural resources extractions and maritime will adopt IoT technologies. In this sector, which is foreseen to grow by more than 180% over the next few years [23], LEO-based connectivity will bring coverage of remote or isolated geographical areas where terrestrial infrastructures are not present or unreliable [24]. These services typically require lower data rates associated with relaxed signal to noise ratio (SNR) requirements and hence smaller and cheaper antennas can be employed to have wider beams and, consequently, slower tracking requirements. One of the main drawbacks of LEO constellations is the inherently high deployment cost associated to the high number of satellites to be launched. In this context MEO SatCom satellites play a key role as their orbit is a good compromise between latency and complexity as they allow a coverage of virtually the entire Globe with less satellites. LEO, MEO, and GEO SatCom ecosystems give rise to a stratified infrastructure targeting different types of applications and market segments.

C. AERIAL NETWORKS

Aerial networks are a newly conceived network node [25] of the telecommunication infrastructure that can be implemented using airships, unmanned aerial vehicles (UAV) or balloons located at different altitudes. This new layer combines some of the benefits of both satellite and terrestrial communication systems and it can deliver broadband wireless connections at a low cost.

High Altitude Platforms (HAP) are an integral node of the aerial networks [26]. They are network nodes located in the stratosphere at an altitude of 20 km. With the advances of solar panel, composite material and antenna technologies, their deployment and maintenance in future networks will become not only economically feasible but more convenient than terrestrial networks [27]. HAP should provide a footprint of about 500 km in radius, and they can operate as an intelligent network layer capable to bridge satellite and terrestrial communications. For instance, HAP can provide fast internet access by operating as a macro base station linked to the satellite network. Furthermore, HAP can operate also as a hub for a fleet of unmanned aerial vehicles (UAV) flying at lower altitudes and referred to as Low Altitude Platforms (LAP). Hence, LAPs are another VHetNet layer flying at lower altitudes over densely populated urban areas. They have a narrower coverage and a shorter communication persistence. Within the VHetNet framework, LAP and HAP along with LEO, MEO and GEO satellites constitutes an integrated non

terrestrial communication network which can provide an opportunity for the development of a variety of new services [28]. Nevertheless, aerial networks do also pose new technological challenges [25]. With the exclusion of GEO nodes, all the other nodes of the aerial network are mobile platforms thus demanding user terminals with reconfigurable antenna patterns. Besides, the proliferation of aerial networks will augment the trend toward employing higher link frequencies. HAPs, for instance, are going to be linked to satellites through dedicated frequency bands at Q-, V-, or even E-band [21], [29] which were preferably allocated as far as possible from the broad O^2 resonance at 60 GHz [30], [31]. By comparison, LAP could operate through Ka-band spot coverages. In this perspective, a technology convergence should be expected to achieve the required equivalent isotropic radiated power (EIRP) either using high power solid-state power amplifiers or high-gain antennas with electronic beam steering.

D. MOTIVATION, CONTRIBUTION, AND OUTLINE

Motivated by the current architectural transformation towards seamlessly integrated heterogeneous wireless networks, a large variety of overview and surveys papers have been published on the vision, use cases, and requirements of this multi-layer communications infrastructure [21], [27], [32], [33], [34], [35]. In the envisioned scenario, microwave and mm-wave phased array technologies play a central role in enabling communication links between the mobile platforms with enhanced data throughput and reliability. The evolution of phased array technologies is generally discussed in [36], while [37] and [38] specifically reviews digital and wideband antenna array architecture, respectively. A broad picture on reconfigurable reflect- and transmitarray topologies are provided in [39], [40], [41], [42]. A summary of current and potential antenna packaging technologies for terrestrial 5G and beyond applications were given in [43], [44], [45], [46], whereas the authors of [47], [48] provided a review of recent mn-wave integrated circuits.

By contrast, the aim of this article is to present a broader view on phased array related developments for high throughput communication links in future heterogeneous networks which are envisioned to operate from K- to E-band. Since these communication systems are characterized by a plurality of operation purposes with diverse requirements, an application-centric review of state-of-the-art system architectures, components, integration techniques across various technologies are given. For the first time, this also includes a comprehensive and comparative study of numerous antenna elements and phased arrays for satellite, aerial, as well as terrestrial communication systems. Special emphasis is drawn to the many interrelated implementation aspects in electronically steerable antenna systems.

The rest of this article is organized as follows. Section II first provides a general view on system architectures for electronic steerable antennas emphasizing on different beamforming techniques, array configurations, and functional partitioning. Subsequently, the paper reviews the underlying

technologies and components of these wireless communication systems in Section III. This includes integration opportunities for RF modules and packages as well as RF interconnects between these technologies. Then, passive beamforming technologies are highlighted, followed by a brief overview on electronic components. The section concludes with a comprehensive review on planar radiating elements suitable for antenna-in-module and antenna-in-package integration, respectively. These discussions progress to electronically steerable antenna systems in Section IV, which deals with recent developments in direct radiating arrays, quasi-optical antenna arrays, and holographic antennas for terrestrial and satellite communications up to 100 GHz. Finally, Section V concludes this article.

II. SYSTEM ARCHITECTURES

In light of the envisioned multi-layer communications architecture including terrestrial, aerial, and satellite networks (see Fig. 1), a plurality of wireless communications systems with diverse requirements and specifications across the microwave and mm-wave regime are going to be deployed. Consequently, different solutions for electronically steerable antennas have evolved depending on their specific application. Emphasizing on high-level design aspects, the following paragraphs contrasts contemporary system architectures in terms of beamforming technique, array configuration, and functional partitioning.

A. BEAMFORMING TECHNIQUES

The choice of the beamforming technique has a pervasive influence on the system architecture. In addition to fully analog [49], [50], [51], [52] or digital [53], [54], [55], [56], [57] beamforming solutions, various hybrid beamforming topologies with different emphasis to the analog/digital partitioning have been proposed [58], [59], [60], [61]. Analog beamformers are still widely employed in active phased array systems in which the signals at the radiating elements are manipulated in amplitude and phase through analog circuits (see Fig. 2). Depending on where the analog beamformer (ABF) is implemented in the system, a distinction is generally made between radio frequency (RF) [62], [63], [64], [65], [66], local oscillator (LO) [49], [67], [68], intermediate frequency (IF)/baseband (BB) [69], [70], [71], [72], [73], [74] beamforming. Towards increasingly larger phased array systems, the complexity and scalability of the integrated circuits is becoming a major design aspect [44]. As a results of this, RF beamforming architectures have emerged as a common solution because their component count is the lowest [44], [75]. However, while the true virtue of analog beamformers lies in the unmatched ability to realize affordable antenna systems for point-to-point communications with a relatively low hardware complexity and power consumption, beam steering solely in the RF domain reveals to be a major burden when designing multi-beam antenna systems.

The ease of the analog beamforming network, which basically combines/splits the individual signals coherently,

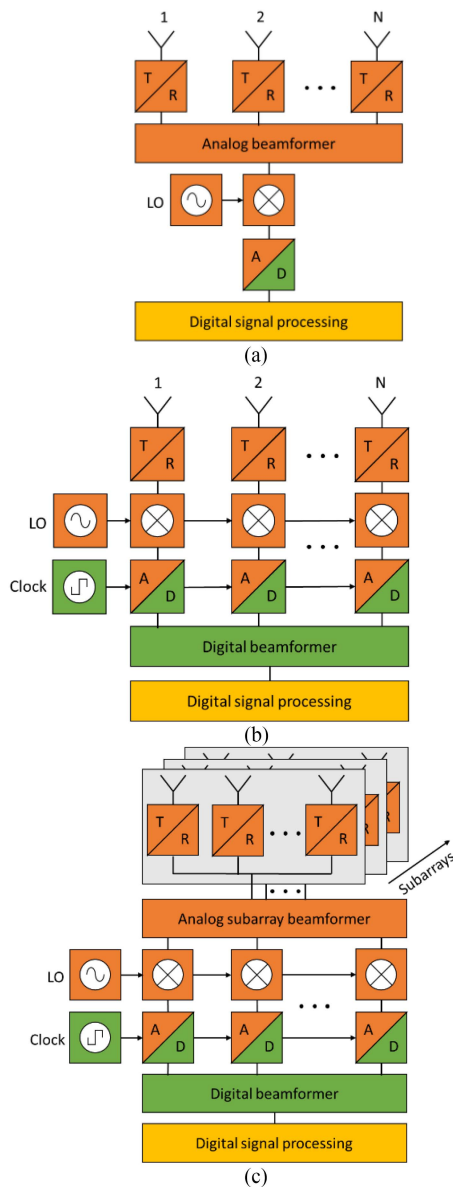


FIGURE 2. Overview schematic beamforming architecture (a) analog beamforming (b) digital beamforming (c) hybrid beamforming.

prevents the reuse of its building blocks across independent channels separated in space. It is thus evident that these spatial multiplexing systems typically suffer from inherently space constraints as the amount of required circuitry for the analog beamforming network directly scales with the number of beams to be supported. In comparison, analog IF/BB beamformers can potentially handle higher numbers of concurrent independent beams as they feature of a smaller circuit area and relaxed routing complexity [73], [74], [76]. On the other hand, multi-beam communication systems using IF/BB domain beamformers pose narrower instantaneous bandwidths and comes with the design challenge in providing coherent LO distribution across subarray beamformer ICs [44], [75].

In comparison, fully digital beamforming techniques, as the name suggests, have shifted the beam steering functionalities entirely into the digital back-end. This results in the necessity of only a simplified RF front-end containing an amplifier and frequency conversion stage for transmit and receive, respectively. As depicted in Fig. 2(b), each antenna element is therefore connected to a dedicated RF chain followed by analog-digital-converters. The element-level digital beamformer (DBF) processing offers the highest degree of flexibility in synthesizing simultaneous beams because those digital signals can be modified, duplicated, and combined in any arbitrary manner without a detrimental effect on the signal quality. In addition, DBF facilitate the use of frequency-dependent amplitude tapering and phase shifting including the corrections of hardware impairments through channel-level equalization, I/Q correction, static LO phase offsets [37]. This approach becomes increasingly attractive for wideband multi-beam systems to avoid analog true time delay beamformers [38]. Regardless of the digital architecture, however, the implementation effort of the signal processing back-end strongly scales up as the number of antenna elements and the instantaneous channel bandwidth of the system increases, respectively [77]. On these grounds, analog beamformers are still seen as a more viable solution for large-scale phased array systems across many applications from a performance/economical point of view.

Compared to analog and digital beamformers, hybrid beam steering techniques may provide a trade-off between the system complexity and performance. Hybrid beamformers are based on a joint analog and digital processing whose architecture depends on the properties of the propagation channel. Subarray HBF architecture as depicted in Fig. 2(c), are widely used due to its simplicity. In this topology, the antenna array is subdivided into subarrays whose input and output signals are processed digitally, whereas the signals on element level are manipulated in the analog domain. As a result, the number of antenna elements greatly exceeds the number of RF chains which likewise represents the maximum number of independent beams supported by the hybrid beamformer. Spatial multiplexing can be achieved using the analog subarrays to synthesize overlapping sector patterns, through which a set of pencil beams is produced in the digital signal processor [36], [78].

However, hybrid analog/digital beamforming architectures are currently not widely deployed in multi-beam antenna systems for mobile SatCom terminals requiring both tracking and satellite-to-satellite handovers to maintain connectivity [56]. On the one hand, the reason can be found in sectorization problem of subarray HBF limiting the angular range in which a set of simultaneous beams can be generated due to the focusing effect of the sector patterns [36]. The angular spread of these spatial multiplexing systems can be enhanced by wider sector patterns, but at the expense of a lower antenna gain and a reduced suppression of grating lobes. On the other hand, fully connected HBF configurations can overcome these limitations as each RF chain is fully connected to all

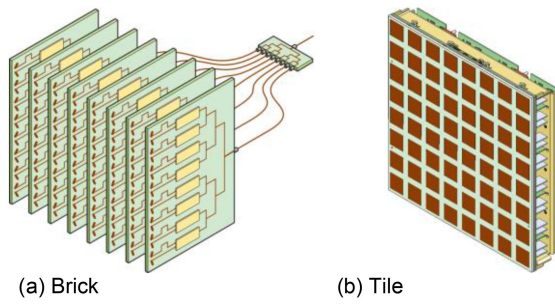


FIGURE 3. Basic array implementations (a) brick (b) tile [36].

available antenna elements. This comes along with substantially higher hardware and computational complexity in return. In addition, the fully connected HBF type achieves higher array gain, narrow beamwidth, and a better spectral efficiency than the subarray HBF topology because the architecture supports MIMO beamforming. But these advantages cannot not be exploited in SatCom scenarios having highly decorrelated channels. The true virtue of fully-connected HBFs become apparent in terrestrial MU-MIMO applications, where the channel capacity for the spatially non-located users is mainly limited by signal to interference noise ratio (SINR). Unlike the SatCom sector, hybrid beamformers have thus been identified as promising solution for 5G and 6G communication systems [73], [79], [80], [81], [82] as the data processing and hardware efforts and hence the overall power consumption is significantly lower compared to their fully digital counterparts.

B. ARRAY CONFIGURATIONS

The conceptual design of the beamformer as a part of the system architecture already allows to draw some conclusions how the antenna array should in principle be organized. At this level of abstraction, constraints with respect to the antenna aperture such as the array size and lattice can be specified. However, the concrete arrangement of the components below the aperture plane cannot be derived from this angle. Since the lateral dimensions of planar antenna arrays are dictated by the operating frequency, its depth must be taken into account for integration. In order to meet requirements on the integration density, different strategies for constructing large array architecture have become well established.

1) BASIC ARRAY IMPLEMENTATIONS

In general, planar antenna arrays can be categorized into two basic implementation approaches: a brick and a tile configuration [83], [84], [85]. Fig. 3(a) shows an exemplary array of printed end-fire antenna elements in a brick configuration. In this array architecture, the electronic components are typically integrated together with the radiating elements on a series of printed circuit boards (PCB) that are oriented perpendicular to the array's aperture [86]. In doing so, the integration density is hardly dependent on the operating frequency as

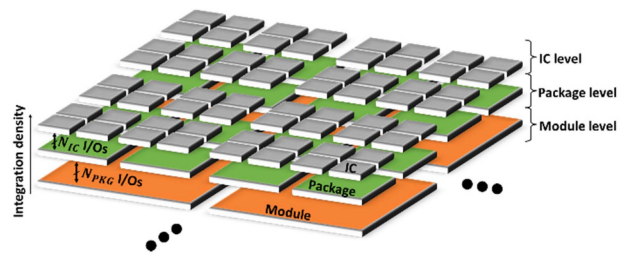


FIGURE 4. Abstract representation of the functional partitioning in large electronically steerable antenna systems.

the depth profile of the individual PCBs does not reach their technological limits in practical applications. This allows the integration of multiple ICs whose dedicated functions can be realized in the most appropriate semiconductor technology. The heat dissipation of the active components can thus be spread over a large surface area. A major disadvantage of this approach is that it requires a considerable amount of RF boards, adapters, and cables to route the RF, bias, and control signals. This aspect is one of the main cost drivers and prevents a mostly automated fabrication and assembly process to address high-volume market segments [36]. The alternative array configuration, commonly referred to as a tile architecture, is illustrated in Fig. 3(b). In this implementation approach, the required components are integrated in multiple layers oriented parallel to aperture plane.

A key challenge is to incorporate all required electronic components into the area occupied by the corresponding antenna elements. Since the integration density of a tile increases quadratically with the frequency, the functional partitioning of the necessary building blocks across different technologies becomes increasingly important in designing electronically steerable antenna systems at higher operating frequencies (see Section II-B-2). Compared to brick configurations, tile architectures have the impact of substantially lowering the construction depth and dramatically reducing the number of required connectors.

2) FUNCTIONAL PARTITIONING

Electronically steerable antennas can functionally be subdivided into several parts, regardless of the specific array implementation or beamforming topology. Although there are manifold options for the arrangement of the building blocks in the system, some basic design considerations are universally applicable. In order to create large phased array antennas, it has proven useful to combine repeatable assembly units since these unique systems consist of large numbers of identical circuits. Scaling is typically done across technologies, for instance on module, package, and IC level as abstractly depicted in Fig. 4.

The overarching task when developing such systems is to optimally leverage high-volume commercial manufacturing and packaging techniques [87]. Generally speaking, the more mature the underlying technology, the larger the repeatable

units might be realized. The highest integration density can be achieved by monolithic technologies, whereas the packaging primarily acts as interposer to the module level in order to make the integrated circuits technically usable in a system. Hence moving to higher operating frequency inevitably leads to a monolithic-centric system partitioning.

Driven by the inherent space constraints of phased array antennas, which scales with wavelength, the latest developments show that multi-channel IC solutions may absorb a large portion of the system complexity. The decisive factor for this development was primarily the enormous advances in silicon-germanium (SiGe) and CMOS semiconductor technology, which meanwhile enables highly miniaturized and cost-effective realizations of complete transceiver topologies. However, a sweet spot in terms of the system's integration density can only be achieved, if the number of I/Os among the different ICs, packages, and modules is likewise minimized by proper functional partitioning of the electronic components. In particular, millimeter-wave interconnects occupy relatively large surface areas as their minimum feature size is typically limited by technological and mechanical constraints. In case the components and the external I/Os do not fit into the superior package and module units, respectively, they must be enlarged accordingly. As result of this and as a result of the minimum practicable distance between the assembly units, gaps in the discrete aperture configuration must be accepted which degrade the radiating performance of electronically steerable antennas through the onset of subarray grating lobes.

Fig. 5 shows an exemplary solution of a phased array antenna with 16×16 elements to address this scaling problem. Compared to the ideal case of an equidistant array lattice, the irregular sampling of the aperture, either due to a finite inter-package or inter-module spacing, manifests in a distorted radiation pattern. Since the defects on the aperture induced by the package spacing appear more frequently, the resultant spectral ambiguities in the radiating diagram are more severe. On the other hand, the grating lobes which are associated with the module spacing are more critical in terms of EIRP off-axis requirements [88] as they emerge closer to boresight.

Apart from the challenge to realize highly directive and wide-angle scanning radiation characteristics, oversized module and package dimensions are also prone to thermo-mechanical issues [89]. Likewise, smaller module and package dimensions may enhance the flexibility and scalability to create different aperture sizes or make them conformal to curved surfaces like the fuselage of an aircraft. These system design aspects are closely associated with the available technologies and components, which are discussed in the following section.

III. KEY TECHNOLOGIES AND COMPONENTS

There are various enabling technologies for electronically steerable antennas which show great differences in terms of integration, performance, maturity, and availability. Therefore, it is crucial to select the most suitable technologies for the underlying building blocks based on a given set of

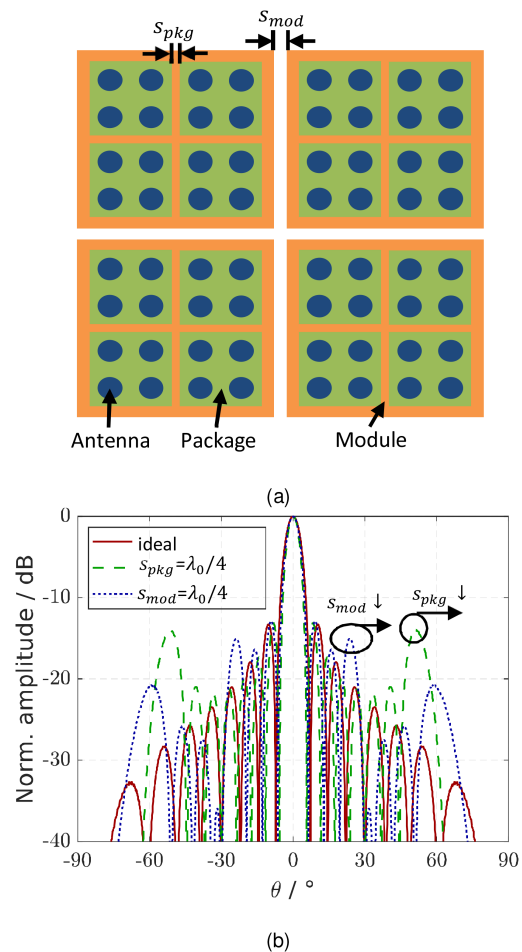


FIGURE 5. Exemplary phased array antenna with 16×16 elements (a) array configuration (b) radiation diagram (s_{pkg} and s_{mod} is the package and module spacing, respectively).

requirements. Since an in-depth and equal review on all components is beyond the scope of this paper, the focus is placed on integration and passive beamformer technologies as well as on planar radiating elements, while the paragraphs on RF interconnects and electronic components overview the main solutions available.

A. INTEGRATION OPTIONS

For the implementation of modules and packages, representing the first and second level system building blocks of large phased array antennas, various technologies have been established. Since these micro- and millimeter-wave systems require solutions for dense integration, the module and/or package design must be organized with a three-dimensional approach. For this reason, planar multilayer configurations are predominately used in industry and academia to realize high performance modules and packages at relatively low costs. The various multilayer technologies of major relevance can be categorized into organic- and ceramic-based material systems, respectively [45], [90].

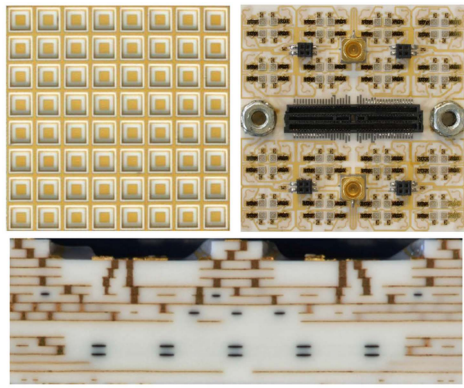


FIGURE 6. Highly-integrated 8×8 TX antenna array module comprising of 17 LTCC and 18 metallization layers [91].

Apart from the chosen system architecture (see Section II), the module and package complexity, respectively, is mainly determined by which of these two system building blocks the antennas are accommodated in. With the antenna-in-module (AiM) approach, the radiating elements are directly implemented on the module, whereas in the antenna-in-package (AiP) approach the antenna elements are integrated at package level.

Manufacturing techniques for ceramic multilayer modules such as low-temperature cofired ceramics (LTCC) have long been preferred as they may provide both a small feature size and a high layer count. Furthermore, the glass-ceramic materials used have a higher thermal conductivity compared to organic laminates, and their thermal expansion coefficients closely match those of SiGe or GaAs semiconductors [95], [96]. An AiM implementation on LTCC with 64 radiating elements for mobile SatCom terminals at 30 GHz is shown in Fig. 6 [91]. The multilayer module, which supports fully digital beamforming, incorporates all RF frontend functionalities such as the antenna elements, active RF circuitries, LO distribution and calibration networks, and the liquid cooling system on 17 LTCC and 18 metallization layers. While ceramic-based multilayer technologies still play a vital role in application scenarios with harsh environmental conditions, for instance in the military or space segment [97], the vast majority of commercially-driven module implementations rely nowadays on low-cost organic materials. In retrospect these developments have been spurred by significant advances of PCB technology in the last two decades driven by the automotive industry. The core material for low-frequency planar circuits usually consists of a glass fiber reinforced epoxy resin e.g., FR4. Since the dielectric losses of epoxy-based materials increase rapidly with frequency, polymer dielectrics such as PTFE (polytetrafluoroethylene) and PPE (polyphenylene ether) are mainly used for microwave and millimeter-wave multilayer modules [45]. By adding fine ceramic particles and glass particles/fibers, the relatively low dielectric constant can be increased in small increments and likewise the thermal expansion coefficient along the vertical direction is reduced [90].

Due to the simple manufacturing process, a large number of laminates have become commercially available providing the highest flexibility in terms of material choice for multilayer module designs. Furthermore, the superior properties of the LTCC technology, such as the potentially high degree of integration, are increasingly losing relevance in modern mm-wave phased array modules not least because of the pervasive use of multi-channel SiGe (Bi)CMOS transceiver chipsets [87], [98]. As a result, the latest module trends for electronically steerable antennas up to the Ka-band are almost exclusively realized with PPE- or PTFE-based dielectric materials albeit the use of low-loss insulator materials such as bis-maleimide & Triazine resins [99] are increasingly gaining momentum in advanced packaging for 5G applications [100]. Fig. 7 depicts several representative cross sections of PCB-based AiM developments for mobile SatCom and 5G radio access applications up to the Ka-band [51], [52], [63], [64], [67], [92], [93], [94].

Technology-wise, this integration method has proven itself as the most appropriate to realize planar antennas with highly efficient radiation characteristics in the lower mm-wave regime. The mainstream solution here is to place the RFICs on the opposite side of the tile-based multilayer module. These integrated circuits come either in bare die form or encapsulated using a quad flat no-leads (QFN) or wafer level chip scale (WLCS) package. As a consequence of this arrangement, the antenna feeding lines, passive components (e.g., filters, duplexers), RF/LO/IF distribution networks, and power supply and control lines must be considered in the multilayer PCB design. Moving to higher operating frequencies exacerbates the module's integration density pushing the PCB technology to its limits. In particular, miniaturized low-loss transitions between module and package (chip) are becoming increasingly difficult to realize. Therefore, AiP solutions rapidly turn out to be most viable and economical option for large phased array antennas above the Ka-band [43], [101], [102].

Through implementing the antennas on the package, their feeding lines to the RFIC can be realized in the same technology. In this way, low-loss transitions beyond 150 GHz have recently been demonstrated which effectively helps to improve the RF system performance in terms of EIRP and noise figure (NF), respectively [108], [109]. In conjunction with a popular functional partitioning, which foresees dedicated frequency conversion stages on each RFIC, the routing of mm-wave signals from/to the module can be avoided [44], [110]. This approach enables the use low-cost laminates as well as standard PCB and assembly processes, since only low-frequency IF signals must be routed on the module. At present, this extremely cost-effective AiP approach – albeit with lower radiation performance than module-integrated antennas at Ka-band – has emerged as a serious option to capture high-volume markets such as 5G radio access applications below 30 GHz [110], [111], [112], [113]. There is a wide range of different substrate technologies that are considered favorable to integrate both the antennas and the RFICs into

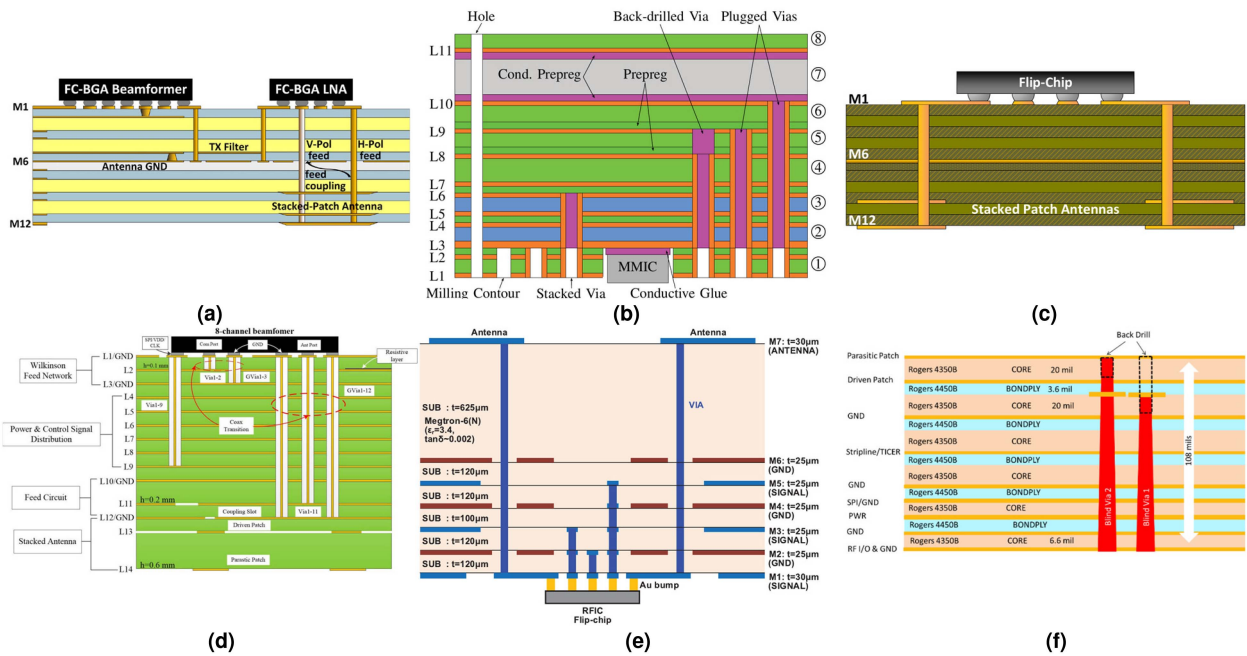


FIGURE 7. PCB-based phased array multilayer modules (a) Ku-band SatCom [52], [64], (b) Ka-band SatCom [51], [92] (c) Ka-band SatCom [93] (d) Ka-Band SatCom [63] (e) mm-wave 5G (n260) [67] (f) mm-wave 5G [94].

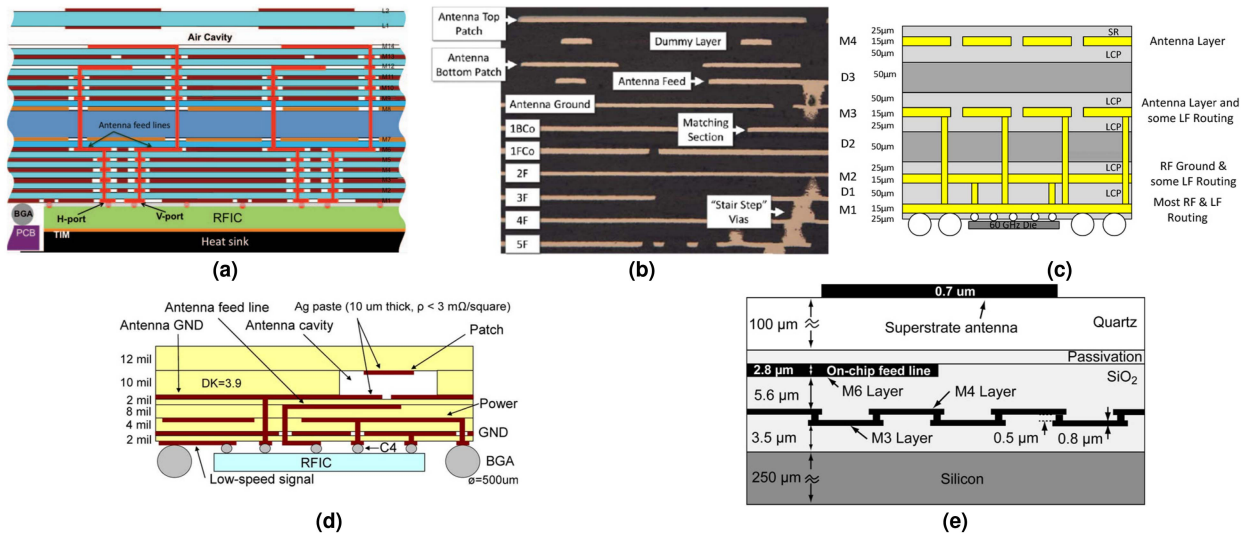


FIGURE 8. AiP implementations for mm-wave communications (a) Build-up package for 5G at 28 GHz [103] (b) PCB package for 5G (73 GHz) [104] (c) LCP package for WiGig (60GHz), (d) LTCC package for WiGig (60GHz) [105], (e) Glass-on-silicon package for 5G (60 GHz) [106], [107].

a mm-wave package. Regarding terrestrial and non-terrestrial communication applications up to 100 GHz, numerous AiP implementations have been demonstrated using multilayer organic laminates for conventional PCB [104], [114], [115], [116], (mixed-) liquid crystal polymer (LCP) [117], [118], and build-up packages [110], [113], [119].

As an example, Fig. 8(a) illustrates a multilayer package from IBM for 5G communication at 28 GHz using an organic build-up substrate technology [113]. More specifically, the layer stack up of the entire package consists of a 2-layer lid

substrate, a 2-layer frame, and a 14-layer base substrate. In addition, a uniform air cavity is implemented between the lid and base substrate to enhance the bandwidth and efficiency of the 64 dual-polarized antenna elements which are individually driven by four SiGe BiCMOS RFICs. Intel has recently described a multichip PCB package of an E-band phased array transceiver [104]. Besides the 4×4 radiating elements, the package (see Fig. 8(b)) hosts analog baseband splitters and four transceiver IC, whose thermal dissipation is conducted via a high-performance through-PCB cooling structure to the

TABLE 1. Comparison of Planar Integration Options for Microwave and mm-Wave Communication Systems Up to 100 GHz

Integration Technique	Material	Main Application	Scalability	Fractional BW	Integration density		Radiation Efficiency	Thermal Management	Ref.
					Lateral	Vertical			
AiM	LTCC	SatCom	●●●●●	●●●	●●●●●	●●●●●	●●●	●●●	[91]
	PCB	SatCom	●●●●●	●●●●●	●●●	●●●●	●●●●	●●●	[52, 64, 92, 93]
AiP	LTCC	mm-wave 5G	●●●	●●●	●●●●●	●●●●●	●●●	●●	[105, 121, 122]
	LCP	Wireless networks	●●●	●●	●●●	●●	●●●●	●●	[117, 118]
	Glass	mm-wave Sat-Com/5G	●●●	●●●	●●●●●	●●	●●●●●	●●	[107, 125]
	Organic build up	mm-wave 5G	●●●	●●●	●●●●	●●●●●	●●●	●●	[115, 104, 124]

Legend: ●●●●● = excellent, ●●●● = very good, ●●● = good, ●● = fair, ● = poor

heat sink. In addition, a uniform air cavity is implemented between the lid and base substrate to enhance the bandwidth and efficiency of the 64 dual-polarized antenna elements which are individually driven by four SiGe BiCMOS RFICs. Intel has recently described a multichip PCB package of an E-band phased array transceiver [104]. Since this proposed system architecture follows a scalable approach, it can be adopted to 5G user equipment or base-station applications through package tiling. Another demonstration of a multilayer organic package from Intel using LCP has been reported in [117]. As depicted in Fig. 8(c), the layer stack up of the AiP for wireless communications at 60 GHz is designed to have four metal layers with the die flip-chip RFIC assembled on the backside. LCP has emerged as a promising alternative for low-cost mm-wave AiP realization as the dielectric constants range from 2.8 to 4, and the loss tangents are typically lower than 0.005 up to 110 GHz [120]. Furthermore, LCP packages are particularly suitable for (nearly) hermetic encapsulation of integrated circuits due to their low moisture absorption and low-temperature bonding process required. On the downside, the thermal expansion coefficient of LCP laminates is up to ten times greater in the vertical direction than for commercial PTFE-based materials. This can be problematic for thicker multilayer packages, which are exposed to high temperature loading, as cracks may damage the planar circuits. In the context of inorganic material systems, the LTCC technology has been widely used to fabricate AiPs for the unlicensed band around 60 GHz [105], [121], [122], [123]. IBM achieved some of the earliest AiP implementations based on a multilayered LTCC technology [105] (see Fig. 8(d)). The fully-integrated AiP solution for electronically steerable antenna systems at 60 GHz consists of 16 patch antennas with either a flip-chip attached transmitter or receiver RFIC. Although excellent RF performance can be achieved in LTCC, only a few AiP designs for 5G mm-wave communications have recently been published, for instance [124]. Again, the reason can be found in the prohibitive fabrication costs of LTCC based AiPs for consumer electronics markets targeting especially low-cost mass production. In recent years, glass-based AiPs have increasingly gained attention for mm-wave applications [6], [106], [107], [109], [125],

[126], [127]. The advantage of the glass substrates are their low-loss electrical properties beyond 150 GHz, dimensional stability, ability to form fine-pitch lines, spaces, and vias, and potential availability in large-scale low-cost panels [45]. The works in [106], [107] have proposed a wafer-scale phased array at 60 GHz with 64 and 256 antenna elements realized on a quartz substrate (see Fig. 8(e)). It's worth noting that both designs deploy the same building blocks, but the 256-element antenna array make use of a subreticle stitching technique to increase the reticle sizes. A similar wafer-scale package approach that integrates a 16-element transceiver architecture for SatCom at 44 GHz has been reported in [125]. A detailed comparison of planar integration options for microwave and mm-wave communication systems up to 100 GHz is given in Table 1.

B. MICRO- AND MM-WAVE INTERCONNECTS

The properties of the interconnects have an essential impact on the performance, reliability, and costs of phased array systems [36]. In particular for mm-wave systems, it becomes a major and ubiquitous design challenge to realize both high-performance and miniaturized guided-wave structures. While coaxial transmission lines and metallic waveguides exhibit unparalleled shielding and power handling properties, these low-loss non-planar transmission lines are bulky, heavy, and unfavorable for integration [102], [128]. As the latter properties are in contradiction to meet the system integration requirements at higher operating frequencies, planar transmission line techniques such as microstrip lines and coplanar waveguides are preferred. Unlike their non-planar counterparts, they allow a dense three-dimensional circuit integration on multiple layers. Without reference to any specific planar integration technology, vertical transitions between circuit parts on different layers are often realized as quasi-coaxial lines and three-wire lines, respectively [129], [130], [131]. For a single-ended configuration, these galvanically coupled transitions consist of a signal via and a number of surrounding ground vias through the layered medium. Another possible approach is the use of vertical transitions based on electromagnetic field coupling [132], [133]. These structures are generally easier to

manufacture because the use of a via process can be avoided. However, the lateral dimensions are relatively large – typically in the order of a quarter wavelength – making broadband and vialess vertical transitions less suitable for highly integrated phased array systems.

Cross-technology interconnects between the RFICs and the package (module) are implemented either with wire-bonding or flip-chip techniques. Bond wire transitions, which were among the first interconnects used at microwave frequencies, are still omnipresent in mm-wave systems [43], [134]. They owe their popularity to their robust and inexpensive fabrication process being seamlessly compatible with overmolded QFN packages. Another striking advantage of wire-bonding interconnects is their insensitivity to thermal expansion being a crucial requirement for conservative phased array systems in the aerospace and defense electronics sector. In fact, bond wire interconnects can be applied for operating frequencies beyond 100 GHz [135], [136] using symmetrical or asymmetrical matching networks to compensate the wire inductance, albeit at the expense of a poor yield and a limited down-scaling of dimensions. By comparison, flip-chip interconnects have better electrical performance, in particular at mm-wave frequencies, as the possible height and diameter of the solder bumps are smaller and larger, respectively, than that of bond wires. This facilitates the further miniaturization of the interconnect dimensions down to a fraction of the wavelength and thus makes complex matching circuits redundant to provide superior bandwidth capabilities [134]. Moving to higher frequencies, ball grid array-based (BGA) packages are consequently more popular than QFN-based packages due to lower packaging efforts and the higher I/O density. In spite of all the advantages, flip-chip interconnects are vulnerable to thermo-mechanical stress due to the mismatch of the thermal expansion coefficients. The reliability of BGAs under thermal cycling can be improved, for instance by using thermal bumps and epoxy-based underfiller to distribute the force and stabilize the interface structure, needless to mention their deteriorating effects on the interconnects' RF performance.

C. PASSIVE BEAMFORMING TECHNOLOGIES

Beamforming techniques and technologies have a long history very much linked to the developments of electromagnetics and more specifically radar surveillance and wireless communications, where narrow focused beams are desired. Some of the earlier solutions were inspired from optical principles and form a family of concepts generally referred to as quasi-optical beamformers, which includes reflector solutions and lenses. For example, focusing devices based on graded refractive index lenses originated from the early works of Maxwell himself on the so-called Maxwell fisheye lens [137], which eventually inspired the ground breaking work of Luneburg [138] in the 1940's and still inspires theoretical developments to these days [139]–[140]. Various concepts of parallel plate waveguide beamformers were also proposed, including the pillbox antenna [141] and the geodesic lens [142].

Quasi-optical beamformers are particular well suited to illuminate continuous apertures, such as line sources, and were mostly developed at first for directive mechanically scanned radar systems, although they tend to be bulky at lower frequencies. These drawbacks are mitigated at mm-wave frequencies and a number of quasi-optical antenna systems supporting electronic beam steering have been reported over recent years. State-of-the-art reconfigurable quasi-optical solutions are reviewed in Section IV-B-2).

At about the same time, another family of beamforming solutions developed in parallel of the theoretical work on ar-ray antennas in the 1940's and 1950's. These are generally referred to as beamforming networks as they are formed of a network of interconnected elementary microwave components, such as power dividers, couplers, and phase shifters, through adequate transmission lines, and are well adapted to feed discrete apertures. The simplest forms of beamforming networks are the parallel, also called corporate, and serial feeding techniques. Fig. 2(a) provides an illustration of a corporate beamforming network, where successive layers of reactive power dividers are used to split the signal. This topology of beamforming network has the advantage of producing a wide band response as all electrical paths are equalized. On the contrary, a series-fed topology, which feeds all elements in a serial way as indicated by its name, produces a frequency dependent response [147]. Such networks are much more compact than corporate networks and of interest for applications with a narrow operating bandwidth or using frequency scanning. Multiple beams may be produced combining several corporate or serial beamforming networks, one per beam, through another layer of beamforming, which may comprise corporate or serial beamforming networks, one per radiating element. Due to their ease of integration into planar technologies, they are widely used, for instance in direct radiation arrays on module and circuit level (cf. Section IV-A). While simple and effective to produce fully independent beams, this technique introduces losses in the combination network equal to $10 \log N$, where N is the number of beams.

Alternative beamforming techniques have been developed to produce multiple beams, while reducing intrinsic losses. The first multiple beamforming matrix discussed in the literature is the Blass matrix [148] based on serial feeding techniques. This solution uses loaded transmission lines to produce a travelling wave operation, like in some leaky-wave antennas. Shortly after, the Butler matrix was proposed [149] which provides a theoretically lossless design [150]. This solution shows the tight link between beamforming theory and signal processing theory, as the concept behind the Butler matrix is equivalent to the Fast Fourier Transform [151]. The Nolen matrix was later proposed as a solution combining advantages of Blass and Butler matrices and is a general form of Discrete Fourier transform [152]. Recently, a generalized parallel beamforming network has been proposed with reduced dimensions when compared to the equivalent Nolen matrix [153]. Some beamforming solutions may be seen as hybrid solutions. This is the case of the constrained lenses,

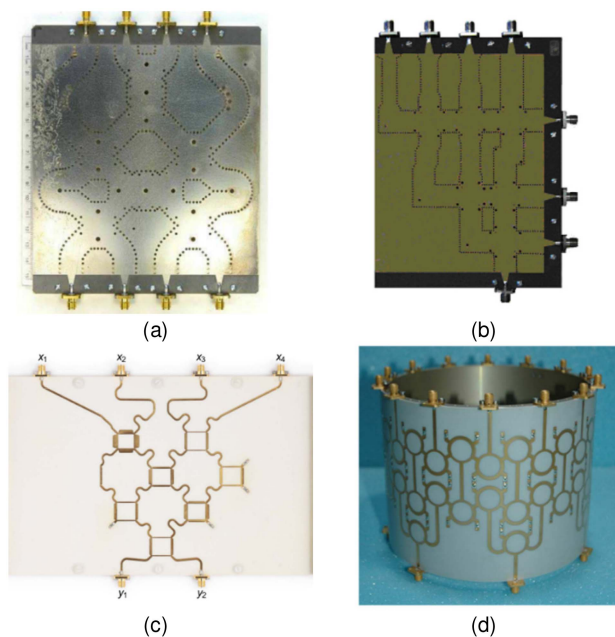


FIGURE 9. Practical implementation of analogue beamforming networks: (a) Butler matrix [143], (b) Nolen matrix [144], (c) checkered network for overlapped sub-arrays [145] and (d) coherently fed circular array [146].

or bootlace lenses [154] which are lenses with a discretized aperture using transmission lines of adjusted lengths to produce focusing properties beyond optical principles.

Early solutions included the Ruze lens [155], and the well-known Rotman lens [156]. The latter is particularly attractive to feed linear arrays producing a wide scanning range with a true time delay response, thus producing no beam squint over a wide fractional bandwidth. These solutions eventually led to the development of reflectarrays [157] and transmitarrays [158], which can be seamlessly enhanced by electronic components to perform electronic beam steering as discussed in Section IV-B-2).

While beamforming theory is still an active field of research, most of the works report on practical implementations as there is a significant regain of interest on multiple beam antennas for mm-wave applications, including applications in automotive radars, wireless communication systems and imaging systems. Beamforming networks are particularly attractive for applications requiring high integration and may be implemented in hybrid beamforming devices [159]. Fig. 9 provides some examples of beamforming networks, including a Butler matrix [143] and a Nolen matrix [144], highlighting the differences between parallel and serial topologies, both implemented in substrate integrated waveguide technology [128]. It also provides examples of beamforming networks producing overlapped sub-arrays, in which each feeding port excites a sub-set of the array ports, including a linear checkered network design [145] and a coherently fed circular array design [146].

Quasi-optical solutions also find applications in the mm-wave and sub-terahertz range as physical dimensions are not

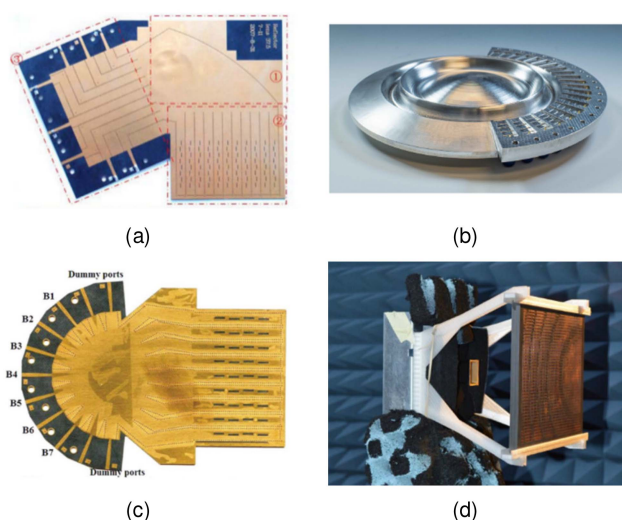


FIGURE 10. Practical implementation of quasi-optical beam-formers: (a) pillbox antenna [160], (b) modulated geodesic lens [161], (c) checkered network for overlapped sub-arrays [162] and (d) coherently fed circular array [163].

as problematic due to much smaller wavelengths and higher gain values are required to compensate for higher propagation losses [42]. Fig. 10 provides examples of quasi-optical beamformers, including a single-layer pillbox antenna [160] and a geodesic lens [161], both for mm-wave applications. Fig. 10 also illustrates an example of a Rotman lens in SIW technology [162] and a dual-band transmitarray using PCB multilayer technology [163]. The reader may refer to [42], [159] for more exhaustive listing of technological implementations. These passive beamforming techniques provided the foundation for the emergence of reconfigurable beamforming techniques, and in particular the highly integrated solutions developed over recent years.

D. ELECTRONIC COMPONENTS

Although we have gained vast, over-a-century long experience in developments of phased-arrays, large-volume and economically viable commercial solutions started to emerge only during the last decade. The latter has been enabled through maturing and affordability of SiGe and RF-CMOS technologies and advances in packaging (QFN, BGA, WL-CSP, etc.) as discussed in Section III-A. Over more than a decade, various R&D centers have been showing capabilities of multi-channel phased array transceiver RFICs, suitable for Ku and Ka-band SatCom terminals or more recently for 5G at 28 GHz, all implemented in SiGe or advanced RF CMOS technologies [164], [165], [166], [167]. From that point on-wards, several industrial players such as Analog Devices, Anokiwave, IDT/Renesas, Satixfy, Movandi, Qualcomm, MixComm, Ensilica, Sivers Semiconductors, NXP, DigiMimic and others have been introducing advanced RFIC solutions for 5G and SatCom active antennas covering both analog and digital beamforming solutions and striving for the best performance under the lowest costs.

Developments of SatCom beamformer ICs benefit from the momentum gained in terrestrial 5G however there are several key differentiators between 5G and SatCom that make the IC solutions incompatible. While SatCom terminal antennas rely on frequency division multiplexing, mm-wave 5G radios make use of time division multiplexing. It is primarily due to this fact that SatCom links are operating in full duplex mode (although not always used in existing SatCom terminals) with a wider TX/RX band separation and wider channel bandwidths compared to their mm-wave 5G counterparts, but at the expense of a higher sensitivity to beam-squint. Furthermore, beamformer ICs for SatCom typically provide higher output power and polarization agility, whereas circuit implementations for 5G radios typically come with higher beam counts or even support (massive) multi-user MIMO communication [168].

SatCom terminals and 5G mm-wave radios based on electronically steerable antennas rely on multiple electrical components such as transmit and receive RF frontends, beamforming ICs, RF splitters and combiners, frequency synthesizers and converters, amplifiers, attenuators and switches, data converters, digital signal processors and power management systems. Depending on the beamforming architecture (cf. Section II-A), the level of complexity and degree of monolithic integration of these elements vary as well as the semiconductor technology used for their implementation. Given the large market volume, predominantly bulk CMOS, RF-SOI and SiGe BiCMOS technologies are chosen to answer the needs for performance and low cost. High non-recurring costs (NRE) of the most advanced RF-SOI technology nodes, mainly related to the mask set, are absorbed only under large production volume. On the other hand, SiGe with inherently lower initial NRE costs that could be several times lower than those for advanced SOI nodes (e.g., 130-nm SiGe vs. advanced RF-SOI nodes), will make sense in applications where lower volume and high-end RF performance (e.g., higher linearity, higher 1-dB compression point) are required.

The trade-off between the RF hardware complexity of analog beamforming solutions versus the complexity of the digital subsystem requires careful assessment as the advantage of the low hardware complexity of digital solutions may transfer into excessive power consumption in the digital subsystem, especially in arrays with large number of radiating elements, simultaneous beams, and large processing bandwidths [169]. This is the case for example in large active antenna satellite payloads that need to serve multiple users and where hybrid beamforming appears more suitable. Hybrid beamforming is also of interest in larger arrays where beam-squint becomes an issue and time delay range of beamforming ICs cannot cover the whole aperture. In such cases, a hybrid solution allows compensating the delay at sub-array level in the digital domain. For smaller SatCom terminal where lower beam counts are required, fully digital beamforming architectures have recently become a technologically and commercially viable solution, not least because their substantial advantages (e.g., flexibility of beam shape, multiple beams, or beams

with steered nulls, etc.) in future LEO or MEO constellations. The latter has been demonstrated by Satixfy, who brings to market the first electronically steered multi-beam antenna based on digital beamforming [170]. In the following, some exemplary implementation of analog and digital beamformer as well as amplification stages are shown without claiming to be exhaustive. For the sake of conciseness, the interested reader is referred to [47], [48] for a comprehensive overview on mm-wave RF ICs.

1) ANALOG BEAMFORMER ICs

Analog beamformer ICs interface the antenna elements and beam-splitting/combining networks. In TX, their role is to map input signals to multiple outputs with specific gain and phase coefficients that correspond to the specific position of the antenna element, whereas in the RX direction the functional role is reversed. The number of splitting/combining stages is an important system design consideration as the intrinsic beamforming losses, as discussed in Section III-C, must be compensated (i.e., mandatory RF gain stages within beamforming IC, hence impact on overall power efficiency). Moreover, the signal-to-noise ratio is decreased with every splitting, which may become the key limiting factor in large multibeam active antennas. Implementation of the phase and time delay control can be done in multiple ways, using vector or polar modulators, switchable delay lines or fully passive elements. The choice of the time delay and phase shifting element is crucial as it eventually determines the overall power consumption of the terminal. For the sake of conciseness, the reader is referred to [38] for an extended discussion on the use of true time and phase delays in wideband phased arrays. As demonstrated by Analog Devices recently, the power consumption per beam-steering node within a four-beam and 16-channel time delay beamformer IC can be as low as 12 mW [172].

Analog beamforming ICs are now available as (components of the shelf) COTS in many different flavors, mainly for 5G market, including 5G spectra in Ka-, V- and E-bands [47]. The SatCom market is still significantly smaller, which is reflected in the choice of beamforming ICs, however, even here several products exist which are suitable for X, Ku and Ka bands. From the implementation perspective, both beamforming solutions on phase shifters, true time delay, and combination of both are commercially available today [47].

One of the limitations of the latest commercial true time delay beamformer ICs for SatCom is the limited time delay range, which is typically <60 ps (covering less than a single wavelength at Ka-band downlink frequencies), which is insufficient to compensate for the delay across larger antenna array over the full communication bandwidth and hence the beamforming becomes dispersive. However, this is an issue especially in satellite payload where the antenna apertures are significantly larger in terms of wavelengths compared to those of SatCom terminals and where hybrid beamforming becomes de-facto a must [173], [174], [175].

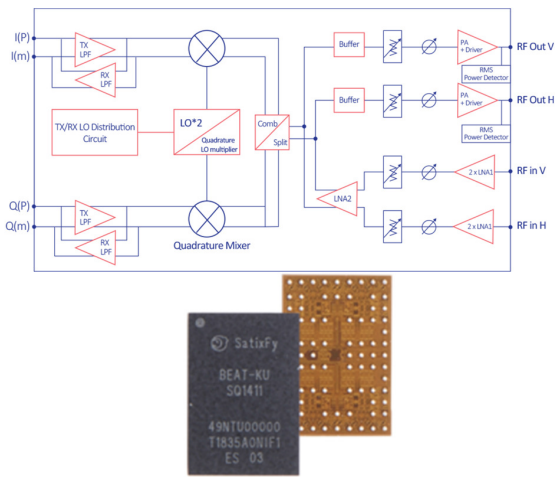


FIGURE 11. High level block diagram of one of the four transceiver branches implemented in Ku-band SatCom transceiver IC “Beat” (Courtesy of SatixFy U.K. Ltd.) [171].

Complete transceiver ICs incorporate in addition to analog beamforming functionality also other functions such as frequency conversion, IF amplification and filtering, frequency generation and distribution or polarization switching functionalities.

An example of a complete four-channel Ku-band SatCom transceiver for digital beamforming antennas developed by Satixfy in the frame of an ESA contract is shown in Fig. 11. For simplicity, only one of four on-chip channels is shown. Each of the four channels features I/Q up and down-conversion, polarization control with a 1-dB compression point (P1dB) of +10 dBm for transmit and a NF of 2 dB for receive, respectively.

Ensilica is another company that introduced a versatile multi-channel beamforming transceiver at Ka-band implemented in 40-nm bulk CMOS and suitable for both analog and digital beamforming applications. The transceiver integrates four receive and four transmit paths operating at 17.7–21.2 GHz and 27.5–30.5 GHz, respectively, with each path containing independent 5-bit phase control and fine gain control to achieve accurate beam steering and gain compensation or tapering across the antenna elements. The transceiver achieves 3.3 dB average NF across frequency per RX path and +10 dBm output power per TX path across frequency [166]. The corresponding block diagram, a die photograph, and a test board are shown in Fig. 12.

A complete end-to-end beamforming solution has been presented by Siverson Semiconductors, targeting the 24.0–29.5 GHz band [177] as well as the full 57 to 71 GHz unlicensed band [176] (shown in Fig. 13) and demonstrating feasibility of wafer level packaging concepts for commercial applications at mm-waves. Both transceivers incorporate complete 16-channel transmit/receive beamforming functionality, including on-chip frequency synthesis, TX/RX baseband and digital control blocks, validating the capabilities of SiGe BiCMOS at mm-waves.

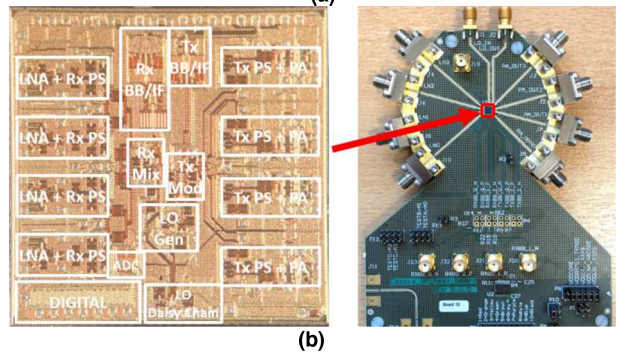
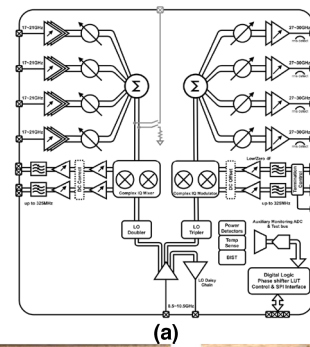


FIGURE 12. 8-channel Ka-band beamforming transceiver IC ENS92030 (a) Block diagram (b) die photograph and evaluation PCB (Courtesy of Ensilica) [166].

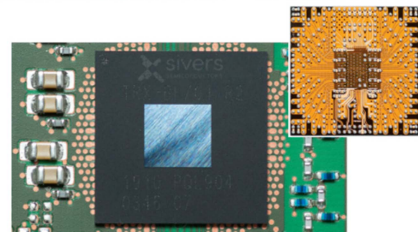
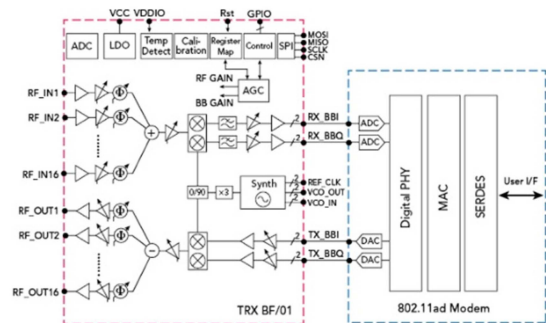


FIGURE 13. 57 to 71 GHz transceiver combining the TRXBF01 RFIC with a separate modem. SiGe BiCMOS transceiver MMIC is packaged using Embedded Wafer Level Ball Grid Array (eWLB) technology (Courtesy of Siverson Semiconductors) [176].

While many beamformer ICs are still predominantly developed for single and multi-beam communication links, there have been significant efforts over the last years to implement full transceiver RF ICs supporting MIMO beamforming. Aiming to provide higher data rates by pushing spectral efficiency has led to the development of numerous MIMO transceiver chipsets for mm-wave 5G applications up to the E-Band. This

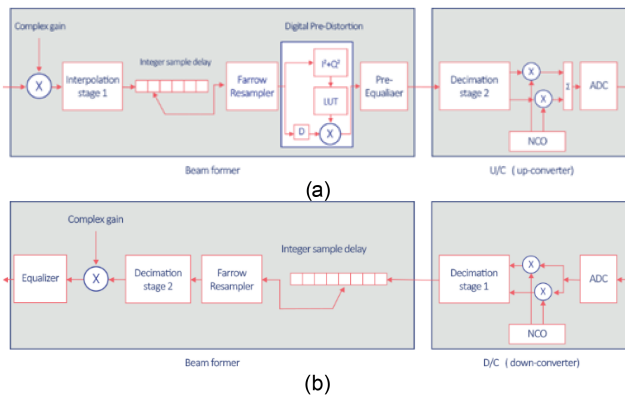


FIGURE 14. Block diagrams of digital implementation of a single channel (a) TX and (b) RX digital beamformer (Courtesy of Satixfy) [179].

includes analog beamformer ICs based on fully connected structures [61], [73], [168], frequency-domain multiplexing [74], and polarization multiplexing [178], to name a few.

2) DIGITAL BEAMFORMER ASICS

In most of the commercial cases, digital beamforming requires custom made ASICs and AD/DA converters, designed for specific active antenna configurations. An example of a DBF ASIC for SatCom terminals from SatixFy is shown in Fig. 14 [179]. True time delay in both TX and RX is implemented via sample buffering where shift registers delay samples of the baseband signal at resolution related to the sampling time, possibly after interpolation to improve delay resolution. High-frequency AD/DA converters are likewise part of the beamforming ASIC to answer the needs for specific sampling rates, signal purity and required bandwidth to be processed. Moreover, the beamformer ASIC incorporates other additional digital functions such as signal equalization, pre-distortion, or calibration or dedicated functions to support simultaneous operation in two polarization schemes.

Owing to the enormous advances in CMOS semiconductor technologies, meanwhile also enables the commercial realization of data converters for direct RF sampling up to the Ka-band [180]. Although, power consumption is still the most significant technical hurdle for this technology to be used on element level in mobile DBF antenna terminals, the availability of high-performance data converters has paved the path for new code-based DBF architectures [76], [181]. In these contributions, more specifically, a code division multiplexing technique is used to aggregate the IF signals from multiple antenna elements into a single ADC. Power consumption is also major concern in the design of mm-wave 5G/6G massive MIMO communication systems.

3) AMPLIFICATION: INTEGRATED PAS AND LNAS

Today, bulk CMOS and RF-SOI can provide at Ku and Ka bands output power levels in the range of 10–15 dBm using classical PA architectures. The output power limit is determined by the device breakdown voltage. Device stacking

is used to overcome the breakdown limits however at the cost of higher complexity and potential stability and reliability issues [182].

In array configurations where higher P1dB is required, SiGe BiCMOS with higher voltage breakdown levels will out-perform bulk CMOS and RF-SOI amplifiers by several dBs even without applying transistor stacking techniques and risks associated with the time-dependent dielectric breakdown which is known to be one of the most important degradation mechanisms affecting the reliability of CMOS devices [183]. In terms of NF performance, 22-nm and 45-nm SOI nodes have recently demonstrated at Ka-band NF below 1.5 dB, approaching to state-of-the-art levels obtained in GaAs [184]. NF of SiGe BiCMOS counterparts is at least 0.5 dB higher. Excellent NF performance of RF-SOI LNAs is achieved mainly thanks to the low substrate losses the technology offers, which allows implementation of very low-loss passive components (e.g., input matching and source degeneration inductors). In specific SatCom applications where the RF power of 10–15 dBm available from today’s beamformers is no longer sufficient, Gallium Nitride (GaN) output amplification can very efficiently boost the RF power, however at the expense of increased complexity and end-product costs. The latter is the usual baseline in satellite payloads, however, the same approach will likely appear also in high-performance antenna arrays for SatCom and aerial communications (cf. Section I-C) that will offer higher EIRP or will rely on lower number of radiating elements hence providing the same service in more compact hardware implementation.

E. RADIATING ELEMENTS

The choice of the antenna element also plays a key role in successfully designing direct radiating arrays. Their properties must satisfy the systems requirements in terms of bandwidth, polarization, gain, and integrability. While electronically steerable antenna arrays have become very much mainstream at microwave and mm-wave frequencies, they are still confronted with technological constraints, if large scan volumes should be covered across a wide relative bandwidth. It is well-known that the onset of surface wave, leaky wave, or parallel plate resonances may manifest in scan blindness at certain scanning angles due to the periodic nature of phased array antennas [185], [186].

As a consequence, the achievable scan volume is always limited by these scan blindness effects as they appear closer to boresight than those associated to the onset of grating lobes. Independently of the specific antenna design, these scan anomalies can be alleviated through oversampling of the antenna aperture using array lattices smaller than $\lambda_0/2$. This general design approach is very often in contradiction to the achievable integration level at high operational frequencies as it leads to a denser implementation of the phased array systems in which more active antenna elements must be populated to produce the same aperture size.

In view of these aspects, many planar radiating elements for terrestrial and non-terrestrial communications systems have

TABLE 2. Overview of Antenna Designs for Planar Direct Radiating Arrays (S: Simulation Results)

Ref.	Antenna Type	Technology	Element size (# of elements)	Min. Gain (boresight)	BW (GHz)	Pol.	Inter-port decoupling	Scan range (E-/H-plane)	Max. scan loss	Cross-pol. rejection
[187]	Tapered slot	Hybrid	3.8×3.8mm ² (8×8)	19 dBi	26.0-40.0	Dual-linear	30 dB ^S	60°/60°	≈ 3 dB	20 dB
[188]	Coupled Dipoles	AiM	11.5×11.5mm ² (8×8)	11 dBi	8.0-12.5	Linear	-	70°/60°	≈ 4 dB	20 dB
[189]	Coupled Dipoles	AiM	2.06×2.06mm ² (3×3)	5 dBi	24.0-72.0	Linear	-	45°/45°	-	8 dB
[190]	Coupled Dipoles	AiM	7×7 mm ² (16×16)	-6 dBi	7.0-21.0	Dual-linear	20 dB ^S	45°/45°	≈ 5 dB	15 dB
[191]	Coupled Dipoles	AiM	4×4mm ² (16x16)	-5dBi	12.0-32.0	Dual-linear	-	60°/60°	≈ 5 dB	10 dB
[192]	Coupled Dipoles	AiM	7×7mm ² (16×16)	-10dBi	3.53-21.2	Dual-linear	9.5 dB ^S	60°/60°	≈ 2.5 dB	10 dB ^S
[193]	Coupled Dipoles	AiM	5.4×5.4mm ² (12×12)	15dBi	23.5-29.5	Dual-linear	10 dB ^S	60°/60°	≈ 3 dB	25 dB
[194]	Connected Slot	AiM	9×9mm ² (16×16)	12 dBi	6.0-15.0	Dual-linear	-	80°/60°	≈ 6 dB	12 dB ^S
[46]	ME Dipole	AiP	5.1×5.1 mm ² (8×8)	0 dBi	24.3-29.5	Dual-linear	-	60°/60°	≈ 8 dB	10 dB
[195]	ME Dipole	AiP	3.0×3.4 mm ² (2×2)	9 dBi	25.0-43.0	Dual-linear	20 dB	40°/40°	≈ 3 dB	20 dB
[196]	ME Dipole	AiP	4.6×4.6 mm ² (4×4)	14 dBi	26.5-40.8	Dual-linear	24 dB ^S	60°/60°	≈ 4 dB	15 dB
[197]	ME Dipole	AiM	3×3mm ² (2×2)	10.5 dBi ^S	53.4-66.0	Dual-linear	15 dB ^S	45°/45°	≈ 5 dB	23 dB
[198]	ME Dipole	AiM	2.83×2.83 mm ² (8×8)	9 dBi	56.0-66.0	Dual-linear	15 dB ^S	55°/55°	≈ 3 dB	28 dB
[52]	Stacked Patch	AiM	12.3×10.65 mm ² (32×32)	30 dBi ^S	10.7-12.7	Dual-linear	15 dB ^S	70°/70°	≈ 5 dB	20 dB ^S
[66]	Stacked Patch	AiM	5.3×5.74 mm ² (8×8)	21.7dBi	23.5-29.5	Linear	-	60°/40°	≈ 4 dB	28 dB
[199]	Stacked patch	PCB	5×5 mm ² -	3.9 dBi	26.5-32.7	Dual-linear	24.5 dB	60°/60°	≈ 5 dB	15 dB
[200]	Probe-fed patch	AiP	5×5 mm ² (16×16)	21.2 dBi	29.1-30.9	Dual-circular	-	60°/60°	≈ 6 dB	-

been proposed. An overview of antenna element designs published in scientific literature is given in Table 2, which are specifically discussed in the following paragraphs.

1) WAVEGUIDE-BASED AND TAPERED SLOT ANTENNAS

Open-ended metallic waveguide antennas and their derivatives are still widely used in electronically scanned arrays whose intended field of operation requires for highly stable, efficient, and broadband radiation performance, e.g., for the space segment. Although, additive fabrication technologies have recently spurred the development of waveguide-based antenna arrays [201], they are not very attractive for terrestrial applications, expect for mechanical tracking systems [202], [203], [204], due to their large dimensions, high fabrication costs, and complex electronic integration compared to planar antenna technologies. Nowadays, some of these limitations have been overcome by the substrate-integrated waveguide (SIW) technology bridging the performance gap between planar and waveguide technologies [128]. An open SIW antenna element for mobile user terminal SatCom applications at Ka band,

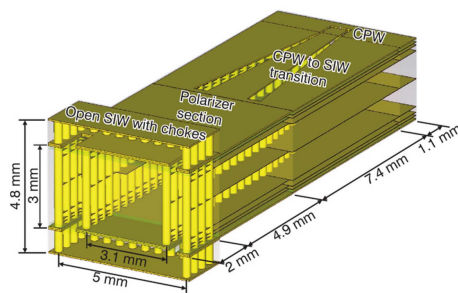


FIGURE 15. Dual-polarized open SIW antenna element with chokes for SatCom at Ka band [206].

which is capable of polarization multiplexing, is described in [205], [206]. Fig. 15 shows the choked radiating element including the septum polarizer and the feeding structures realized as grounded coplanar waveguides in the top and bottom metal layers of the SIW.

Such edge radiating elements in PCB technology including tapered slot antennas (TSA) are particularly suitable to

construct brick array architectures (cf. Section II-B). Owing to their traveling-wave principle, they can provide a wide-band impedance response as a trade-off for a low-profile array configuration. While waveguide-based antenna arrays can cover scanning angles beyond 60° in elevation in all azimuth planes, TSA arrays, by comparison, show typically a lower scanning capability and radiation efficiency, especially in the non-principal planes. The reason for this limitation is that the operating bandwidth of TSAs can be increased primarily by longer flare elements exacerbating the imbalance between vertical and horizontal current potentials [207]. Notably in [187], a surface-mounted Vivaldi antenna array for the entire Ka-band has been presented with a scanning range of $\pm 60^\circ$ in the principal and $\pm 50^\circ$ in the diagonal planes, respectively.

2) CONNECTED DIPOLE AND SLOT ANTENNAS

Conversely, connected antenna arrays can guarantee comparable broad matching bandwidths, but at the same time lower cross-polarization levels are attained as the vertical radiating currents are negligibly small. Connected antenna arrays are either composed of slot or dipole elements which are galvanically or strongly capacitively coupled with each other. In this way, the currents are weakly frequency-dependent since this design technique mimics a single radiating element of the size of the antenna array that is periodically fed [208]. From a practical point of view, however, connected antenna arrays typically show a bandpass response, albeit with a low-Q factor, due to the presence of a back reflector ensuring unidirectional radiation characteristics [209], [210]. Most of the designs of connected dipole arrays at lower frequencies, for instance covering the Ku SatCom bands, are realized on vertically arranged PCBs [86], [188], [211]. This is because the vertical feeding lines through the back reflector are often too long to be reliably implemented in that case by standard through-hole vias within the realm of the multilayer PCB technology. Particularly in [86], a connected dipole array in an egg-crate configuration has been presented whose wide-band unit cell elements accommodate both the dedicated Ku transmit and receive SatCom bands. Since the two orthogonal dipoles and their corresponding feeding structures have been realized primarily by printed transmissions lines, only short vias were necessary for the balun de-sign (see Fig. 16).

Across the whole operating frequency range, the connected dipole array loaded with a wide-angle impedance matching (WAIM) layer maintains a good radiation performance with a polarization purity larger than 10 dB while scanning down to 60° in all azimuth planes. On the contrary, fully planar dipole antenna arrays have become a prevalent solution when scaling down the array lattice to operate at higher frequencies [212]. This class of tightly coupled dipole antennas are referred as planar ultra-wideband modular arrays (PUMA). It has been found practicable to implement the differentially fed dipole elements and the balun transformers on the same multilayer PCB to avoid a bulky external matching network and to retain a convenient single-ended interface to the RFICs [189].

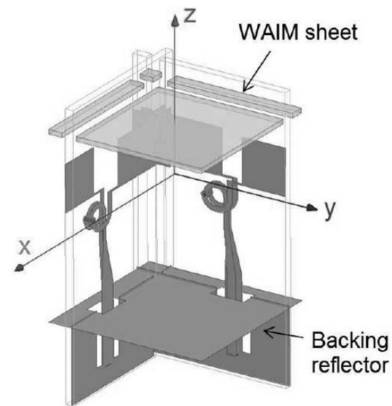


FIGURE 16. Dual-polarized connected dipole element on vertically nested printed circuit boards [211].

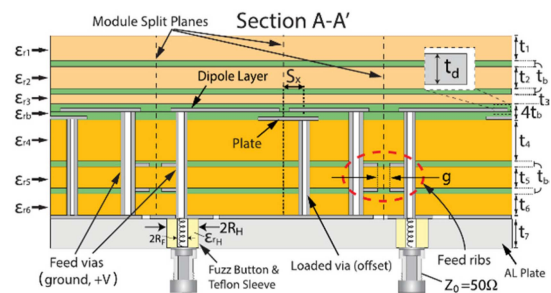


FIGURE 17. Wideband connected dipole array using capacitively-loaded vias for in-band common-mode rejection [103].

The first planar designs of a wideband connected dipole array are excited by an unbalanced feeding topology using additional shorting vias between to dipole arms and the ground plane to shift the parasitic common-mode resonance above the operating band [190], [213]. The reported low-cost dual-polarized array prototype operates in a 3:1 bandwidth up to 21 GHz for scans out to 45° in elevation. In another contribution, this rather simple antenna array design has also proven suitable up to mm-wave frequencies with 60° scanning in all azimuth planes [191]. More recently, an improved arrangement of a connected dipole array with a bandwidth of 6:1 for scanning up to 60° was presented in [192]. As illustrated in Fig. 17, the improved array arrangement uses a capacitively-loaded via below the dipole arms instead of a shorting via. By means of this enhanced suppression technique, the in-band common-mode resonance is pushed beneath rather than above the operating frequency band without sacrificing the low-frequency performance of the unbalanced-fed dipole array. Following a similar design technique, a coupled dipole antenna for mm-wave 5G base station applications has been proposed in [193]. Despite the fact that connected slot antennas can be conveniently fed by unbalanced transmission lines (e.g., microstrip or strip lines), they are barely deployed in phased array systems compared to their complementary counterparts. The reason can be found in the limited impedance bandwidth of about 2:1, because connected slot antenna arrays

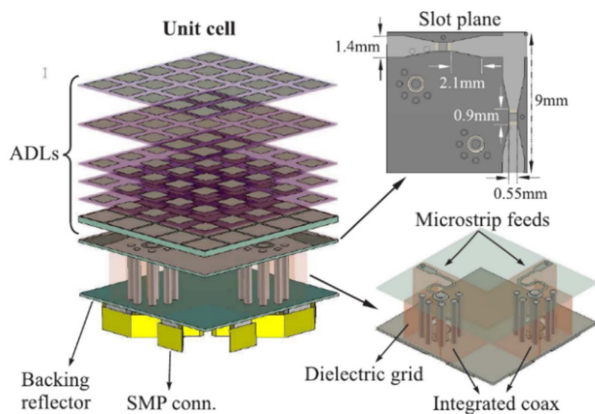


FIGURE 18. Connected slot antenna array with an artificial superstrate [194].

are preferably excited asymmetrically and not symmetrically to avoid a complex and lossy planar feeding network at higher operating frequencies. In addition, connected slot antenna arrays are prone to support leaky-wave resonances which further limits the scanning range [209]. More recently however, connected slot antenna arrays have regained noticeable interest thanks to the use of artificial superstrates to enhance their scanning capabilities [194]. Through careful manipulation of the dispersion properties of the anisotropic WAIM layer, the onset of transverse resonances, where the phase synchronism with the Floquet modes is met, can effectively be suppressed. As a result of these efforts, superstrate-loaded connected slot antenna arrays (see Fig. 18), have demonstrated comparable properties in terms of impedance bandwidth and scanning range as dipole arrays. These developments have just provided the breeding ground for new phased array architectures that may simultaneously cover the Ku- and Ka-transmit bands for satellite communication [214].

3) MAGNETO-ELECTRIC DIPOLE ANTENNAS

Regarding terrestrial mobile networks, similar trends aim at the development of wideband radio front-ends to operate across multiple mm-wave bands in the 5G Frequency Range 2 (FR2). In comparison to antenna terminals for SOTM connectivity at Ku-/Ka-band, their link budget requirements are typically less stringent and consequently leads to lower element count for these electronically steerable antenna systems. Since connected antenna arrays inherently unfold their full performance capabilities only for larger aperture sizes, magneto-electric (ME) dipoles have recently emerged as a viable alternative for small- and medium-sized planar antenna arrays whose operating fractional bandwidth spans up to 50%. ME dipoles can achieve a large impedance bandwidth and wide-angle scanning by nesting complementary electric and magnetic dipoles without demanding for strong coupling between radiating elements. Furthermore, this class of wideband antenna element owes its popularity to its great compatibility with a large range of planar integration technologies.

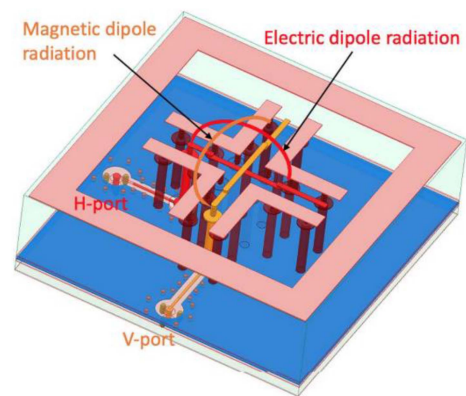


FIGURE 19. Dual-polarized magneto-electric dipole antenna for 5G applications using an organic build-up substrate technology [46].

Regardless of whether the ME dipole is implemented by an antenna-on-board (AoB) or antenna-in-package (AiP) approach, the electric dipole is commonly constructed by a pair of metal plates, whereas the magnetic dipole is formed by shorting vias. Fig. 19 illustrates a dual-polarized ME dipole array element in a 14-layer organic build-up package for mm-wave communication [46]. The vertical and horizontal polarizations are both fed by L-probes through the ground plane to ensure very similar behavior for both ports, as well as to maintain a scalable and low complex package solution. The wideband variant of the array element supports the n257, n258, and n261 5G frequency bands ranging from 24.25 to 29.5 GHz. Based on a state-of-the-art fan-out wafer level packaging (FOWLP) technology, another dual-polarized ME dipole antenna has been described in [195]. The experimental verification of the complementary AiP design shows a wideband impedance response across 25 GHz to 43 GHz coinciding with most of the allocated and planned frequency bands for 5G mm-wave communications. For larger phased array systems as they are going to be deployed in 5G micro base stations, the proposed ME dipole element may operate within a 50° scan cone exhibiting a gain degradation of less than 4 dB.

An LTCC-based dual-polarized ME dipole antenna covering an overlapping fractional bandwidth of 45% across the entire Ka-band has been reported [196]. Moreover, this wideband antenna type has been implemented in various different ways on multilayer PCBs at Ka-band [215], [216] and at Q-band [197], [198], respectively. Following a similar design concept as proposed in [198], a wideband ME monopole antenna fed by a SIW port has recently been presented in [217]. The linearly polarized endfire antenna element complementary combines an opened-ended SIW with two top-loaded electric monopoles. Despite the fact that the linear ME monopole array has demonstrated a very wide operating fractional bandwidth of more than 60% and a large scanning range of $\pm 52^\circ$ at Ka-band, this end-fire element design is not immediately applicable to create planar array configurations as the extended lower broadwall of the SIW

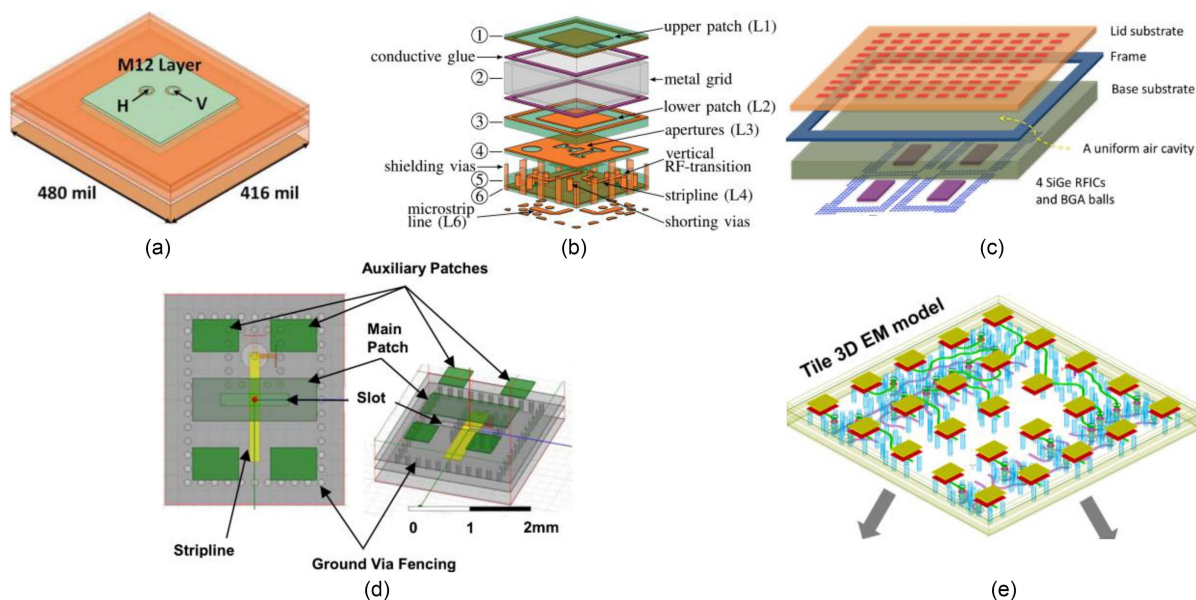


FIGURE 20. Millimeter-wave patch antenna array elements for (a) Ku-band SatCom [52] (b) Ka-band SatCom [199] (c) mm-wave 5G at 28 GHz [113] (d) for WiGig at V-band [118] (e) mm-wave 5G at E-band [115].

would create a parallel plate waveguide which in turn would change the loading of the electric monopoles.

4) MICROSTRIP PATCH ANTENNAS

Despite all existing planar antenna types, microstrip patch antennas remain the unchallenged candidates for modern phased array systems. In comparison with the previously discussed antenna elements, they combine ease of integration, versatile usability, and low-cost realization in various technologies. Like ME dipole antenna arrays, arrays of microstrip patch elements show a sinusoidal and strongly frequency-dependent current distribution due to their resonant nature. Hence, they do not intrinsically provide broadband properties, but in many practical implementations it has become a viable approach to improve the antenna's operating bandwidth and scanning range by increasing the isolation between neighboring elements. This can be sufficiently achieved for most communication applications by reducing the mode interactions between the free-space Floquet modes and the guided modes which are supported by periodic antenna array [186]. In this respect, a large variety of techniques has been proposed aiming specifically at the manipulation of the dispersion characteristic of the latter ones in the three-dimensional antenna structure. Unless specific measures are taken in the design process, patch antenna arrays can typically operate within a 45° scan cone until their efficiency drops noticeably due to scan anomalies in the E-plane. For example, in [52] the authors developed a dual-polarized stacked-patch antenna array for Ku-band SatCom whose active reflection coefficients increase to about -9 dB in the band from 10.7 to 12.7 GHz for E- and H-plane scanning down to 60° . A more broadband and single linearly polarized patch antenna design (see

Fig. 20a)) for terrestrial communication applications from 23.5–29.5 GHz has been presented in [66] by lowering the radiator's Q-factor through expansion of the unit cell dimensions but in return of a smaller scanning range of 30° and 45° in the E- and H-plane, respectively. Considerable efforts have also been devoted over almost three decades to cavity-backed patch antennas to alleviate scan blindness effects by means of galvanic isolation [91], [199], [200], [218]. Fig. 20(b) depicts a stacked patch antenna for wide-angle scanning SatCom terminals at Ka-band [199]. The metal-plated FR4 grid structure between the lower and the upper patch adjusts their coupling ratio but also improves mutual coupling by moving the onset of possible leaky and surface wave resonances to larger elevation angles. In addition, the large air volume below the upper patch leads to highly efficient scan performance up to $\pm 60^\circ$ in both E- and H-planes across an operational bandwidth from 27.8 to 30.8 GHz. In a similar way, a stacked patch antenna array has been implemented at 28 GHz on an organic package in which a uniform air cavity is formed between the lid and base substrates (see Fig. 20(c)) [113]. In another contribution from IBM, a patch antenna loaded by a non-shielded air cavity has been realized within a multilayer LTCC package in order to provide a 15% fractional bandwidth at 60 GHz. More recently, a patch antenna array using parasitic loading (see Fig. 20(d)) has been proposed by Broadcom for wideband backhaul communications at V-band [118]. Since the radiating structures are implemented on the same metal layer, the wafer-level chip-scale package (WLCSPP) is greatly simplified. However, in line with the intended application scenario, the patch antenna array has a very unbalanced scanning range of $\pm 10^\circ$ and $\pm 60^\circ$ in the E- and H-plane, respectively, across the band 57–66 GHz. Finally, the integration of stacked patch antennas

(see Fig. 20(e)) into a fully integrated phased array system for wireless 5G backhaul links at W-band are presented in [115].

IV. ELECTRONICALLY STEERABLE ANTENNAS

In this section a comprehensive overview on recent implementations of electronically steerable antennas for terrestrial and non-terrestrial networks up to 100 GHz is given. Reflected by the fact that these wireless communications systems have very diverse performance requirements and economical constraints, the three most commonly used antenna array topologies are highlighted here with their distinctive features. Apart from direct radiating arrays, which can be seen as the today’s mainstream solution, also quasi-optical and holographic antenna systems are thoroughly discussed.

A. DIRECT RADIATING ARRAYS

In a direct radiating array, all individual antenna elements contribute to the radiation characteristics simultaneously, regardless of whether the wireless communication system is operating in point-to-point or point-to-multipoint mode. It is particularly an interesting solution for large phased array systems as the RF power is inherently distributed across the whole aperture. In line with the recent developments, a large number of low-cost, low-power SiGe (BiCMOS) transceiver are deployed, whose contributions are spatially combined by the antenna arrays, in order to achieve the desired link margin. This circumvents the need for a single centralized high-performance transceiver chain e.g., using GaN technology. Hence, a moderate number of element failures in phased arrays with distributed amplification leads to a graceful degradation of the system performance and by implication no individual redundancy is required. At the turn of the last century, the satellite communication segment has increasingly gained interest to exploit higher operational frequencies at Ka-band in order to provide high data throughput for a large variety of end users.

The idea at the time of continuously replacing Ku-band transponders onboard GEO satellites was recently superseded by a more radical paradigm shift towards hybrid mega constellations. In this envisioned scenario, which may provide a truly global coverage by integrating terrestrial networks, phased array technologies at Ku-, Ka-, V- and E-band play nowadays an equally important role in this bigger orchestra (see Section I). Hence, this section provides a review of the significant developments in electronically steerable antenna systems for communication applications across these frequency bands of interest.

1) SATELLITE COMMUNICATION AT KU-/KA-BAND

In [94] the design and development of a phased array transceiver module at Ku-band has been presented. The active phased array demonstrator with 4×4 radiating elements was implemented on a multilayer PCB. In order to support dual-circular polarization, a probe-fed stacked patch antenna design with truncated corners was chosen. Since the proposed

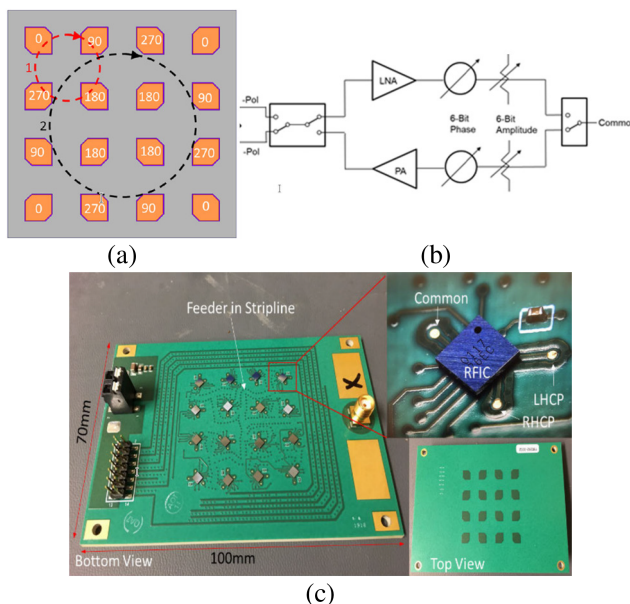


FIGURE 21. Dual circularly polarized phased array transceiver module at Ku-band (a) Antenna array configuration showing the applied nested sequential rotation (b) Schematic silicon beamformer IC Anokiwave AWMF-0117 (c) Photographs of the realized prototype [94].

antenna element typically covers only a relatively narrow bandwidth in terms of axial ratio (AR), a nested sequential rotation approach at both element and sub-array level was applied as depicted in Fig. 21(a). Moreover, the remaining hardware impairments including but not limited to antenna properties can be corrected to some extent by the beamformer ICs. In this work, each antenna element is individually driven by the commercial beamformer chipset Anokiwave AWMF-0117 [219] which is based on a common-leg architecture and thus supports half-duplex operation (see Fig. 21(b)). The single channel silicon beamforming RFIC comes in a WLCS flip-chip package attached to the bottom side of the phase array module as shown in Fig. 21(c). For both left-handed circular polarization (LHCP) and right-handed circular polarization (RHCP), the phased array module at Ku-band demonstrates a scanning capability of $\pm 45^\circ$. Fig. 22 shows the block diagram and realization of a 256-element phased array receiver using dual-polarized quad receive beamformer ICs for Ku-band SatCom [64]. The 12-layer PCB module as shown in Fig. 22(b) is composed of Panasonic Megtron-6 laminates in which 16×16 dual linearly polarized antenna elements and a 64:1 Wilkinson RF power combiner network are implemented, while the 64 dual-polarized beamformer chips are assembled on the bottom side. Since the analog beamformer IC has four receive channels assigned for vertical and horizontal polarization, respectively, the phased array module can operate at any polarization from 10.7–12.5 GHz within 70° scan cone. Due to the RF connector on the bottom edge, the tile is scalable along the remaining three directions allowing the realization of large-scale phased array systems using $2 \times N$ tiles.

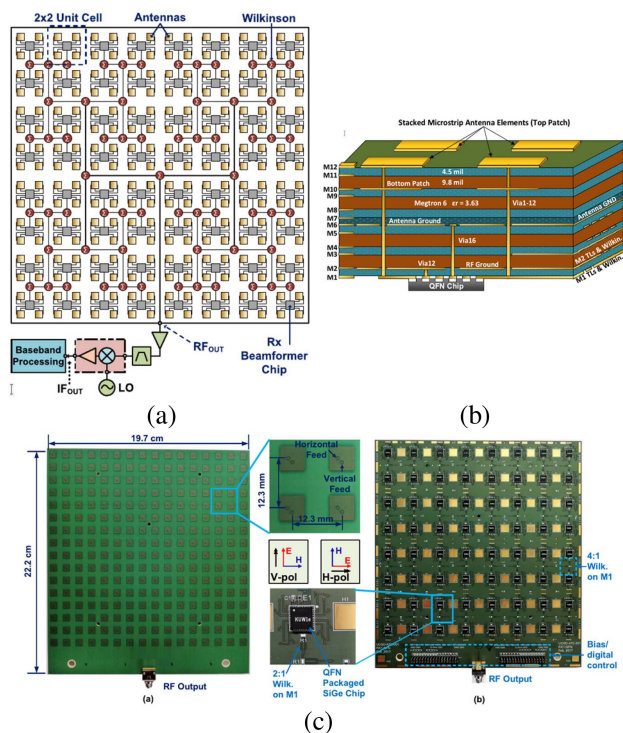


FIGURE 22. 256-element phased array receiver module at Ku-band (a) block diagram (b) PCB layer stack up (c) Top and bottom view of the realized demonstrator [64].

It is worth noting that such a phased array system can either support analog RF, analog RF/IF, or hybrid beamforming (cf. Section II-A).

Specifically, the work in [52] expands this design approach presenting a low-cost phased array system with 1024 dual-polarized patch antennas for use in Ku-band downlink terminals. The active antenna array illustrated in Fig. 23 provides single-beam operation and consists of four 16×16 subarray tiles, whose RF signals are coherently superimposed using a 4:1 Wilkinson power combiner followed by a down-conversion stage and a baseband processor. In contrast to the module design in [64], the dual-polarized antennas are arranged in an equilateral triangular grid to improve the scan performance within the very same scan volume. In addition, each dual-polarized antenna element is connected to a dual-channel LNA for an increased G/T of the overall receive system to 10.5 dB/K. However, this approach makes it more likely that the silicon beamformer RFICs are driven into saturation, if the transmit and receive units operate under a shared radome. Consequently, a two-pole notch filter is placed between each external LNA and beamformer channel to sufficiently attenuate any transmit leakage by means of reflections from the radome at the Ku-band uplink frequencies. To enable ground terminals to track multiple satellites simultaneously, a similar phased array receiver topology for dual-beam operation at Ku-band has been proposed in [220]. Since the electronically steerable antenna is based on an analog beamformer topology, the employed beamformer IC must generate

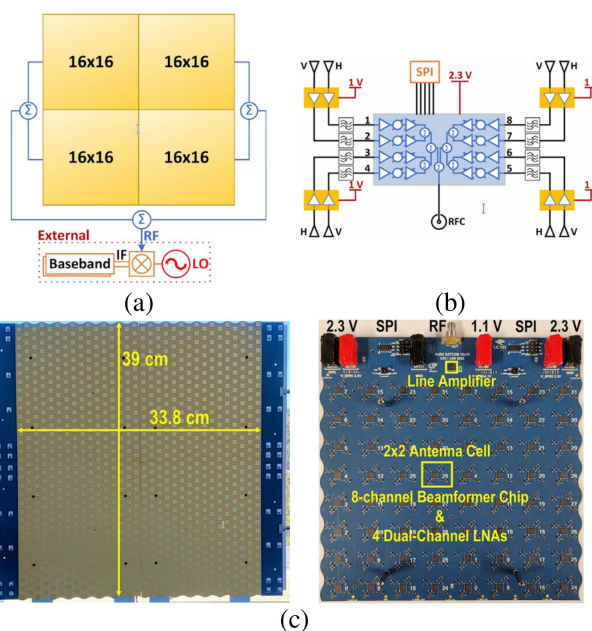


FIGURE 23. 1024-element Ku-Band SatCom dual-polarized receiver array (a) system configuration based on four 16×16 array tiles (b) eight-channel beamformer RFIC connected to dual-channel LNAs and embedded transmit filters (c) photographs of the realized receiver front-end [52].

two independent beams in the RF domain, with each beam having any polarization and steering angles. For this purpose, the receive signals are split within the beamformer RFIC after the embedded LNA to avoid doubling of some analog components, such as the external LNAs and transmit rejection filters. Both required 64:1 distribution networks, which are based on Wilkinson power combiners, are implemented on the multilayer PCB. Beyond that, also a widespread use of analog beamformers in commercial Ku-band SatCom terminals (e.g., Qest, OneWeb, SpaceX, Rockwell Collins, Boeing, Coxsat) can be observed thanks to the mature PCB and SiGe technologies.

Driven by the ambitious high throughput goals of near-future LEO and MEO SatCom constellations [221], [222], it becomes increasingly difficult to build satellite ground terminals for more than two beams in a pure analog fashion (see Section II-A). Mobile SatCom antennas are now being specified to meet large instantaneous bandwidths of 300–500 MHz, while flexibly connect to multiple satellites concurrently on geostationary and non-geostationary orbit constellations. Although previously seen as theoretical solution, DBF-based antenna arrays have recently emerged as a viable design approach to tackle these challenges [170].

Fig. 24 shows a DBF half-duplex antenna prototype from SatixFy comprising 256 patch antennas for transmit and receive across the dedicated frequency bands for Ku-band SatCom [223]. Apart from the analog circular polarization control within the 4-channel up-/down-converting transceiver RFIC [171], up to 32 beams with independent phase, gain and delay control for each beam are supported by the digital

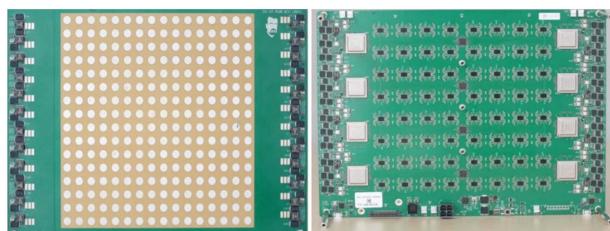


FIGURE 24. Top and bottom view of 16×16 DBF transceiver array for Ku-band SatCom terminals (Courtesy of SatixFy U.K. Ltd.) [223].

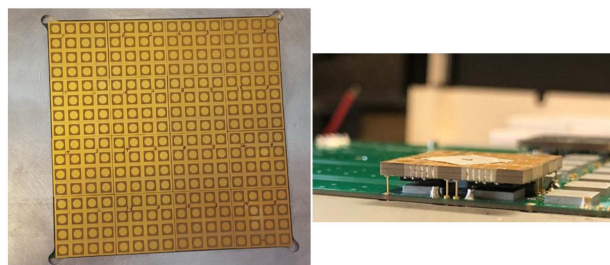


FIGURE 25. 256-element phased array demonstrator at Ka-band composed of 16 modules (a) top view (b) module integration [224].

true time delay beamformer IC [179] (see Section III-D). In this way, the electronically steerable prototype system has demonstrated an unparalleled wideband signal transmission and reception across 1 GHz, 888 MHz, 444 MHz of bandwidth in single, double, quad beam mode, respectively. Ahead of current developments, the first DBF antenna modules for mobile SatCom terminals at Ka-band have been presented in [56], [206]. In these pioneering achievements, the digital baseband processing unit could handle the individual signals of up to 64 radiating elements, but within a limited bandwidth of a few tens of MHz. A completely different situation from 10 years ago, when the use of COTS was prevalent in the antenna array design process, nowadays the custom design of affordable application-specific integrated circuits (ASIC) paved the way for Ka-band DBF antenna terminals with superior performance, even though they are currently in the development phase [223].

Thus, phased array systems based on analog beamforming are still the preferred choice for antenna terminals at Ka band as reflected by the following discussion on state-of-the-art direct radiating arrays. A modular phased array architecture for Ka-band SatCom has been proposed in [224] following the same design approach for the transmit as well as the receive array antennas. In this work, a patch antenna design compatible with half-wavelength separation between the elements at 30/20 GHz has been implemented in the first top five layer of the multilayer PCB as shown in Fig. 25, whereas the 8-channel commercial beamformer RFICs for the up- and downlink bands, respectively, are soldered on the opposite side. The low-profile 16:1 RF feeding network was realized as a SIW to minimize the signal attenuation from/to each 16-element multilayer module. The experimental verification

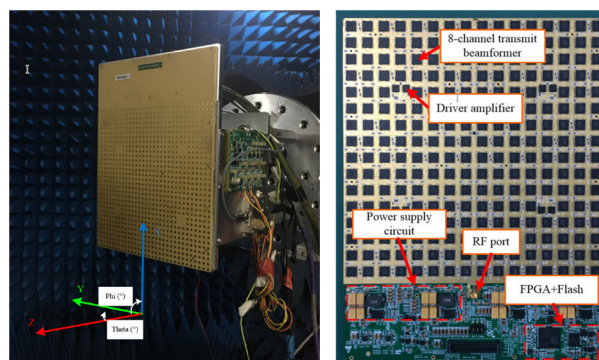


FIGURE 26. 1024-element dual circularly polarized phased array transmit antenna at 30 GHz (a) perspective view (b) bottom view [63].

of both phased array module has successfully demonstrated beam steering capabilities up to $\pm 70^\circ$ off-boresight at 20 GHz and 30 GHz, respectively.

A radically different approach has been pursued by the authors of [63] presenting a large monolithic PCB-based phased array antenna at 30 GHz with 1024 radiating elements (see Fig. 26). Another distinguishing feature is the use 8-channel beamformer RFICs realized in a 65-nm CMOS technology. Both rather uncommon implementation approaches are aiming to tremendously reduce the cost of future active phased arrays at mm wave frequencies. As a result of the fact that all dual circularly polarized patch antennas are realized on a common multilayer PCB, the 1:256 Wilkinson power divider to the dedicated CMOS beamformer chipsets was seamlessly integrated into the same board as well. Due to the large insertion loss of the planar feeding network, eight driver amplifiers are considered between the third and four hierarchy level to compensate some of the induced losses. Under the overarching goal of providing an all-in-one solution, the system board also contains the power supply circuit as well as the FPGA, and the flash memory acting as the antenna control unit. The proposed single-beam system achieves an EIRP of 74 dBm at boresight and can steer the beam up to $\pm 60^\circ$ with a gain degradation of 4.5 dB from 29.5 GHz to 30 GHz. In both LHCP and RHCP mode, the reported axial ratio is below 3 dB for 30° elevation scans.

Very recently, a similar phased array transmitter architecture for Ka-band SatCom application has been presented by Low et al. [225]. In direct comparison to [63], a total of 1024 dual linearly polarized patch antenna elements, which are fed by 256 SiGe beamformer RFICs [226], are deployed (see Fig. 27). The antenna elements were placed in a square grid with a lattice constant of $0.48\lambda_0$ at the highest operating frequency of 31 GHz. By means of slight oversampling of the antenna's aperture, the electronically steerable antenna system demonstrates the ability to efficiency scan to $\pm 70^\circ$ in all azimuth planes from 27–31 GHz, while maintaining an axial ratio of 1.8 dB and a cross polarization discrimination of -35 dB, respectively. Since all the radiating elements, and beamformer RFIC are implemented on a single multilayer

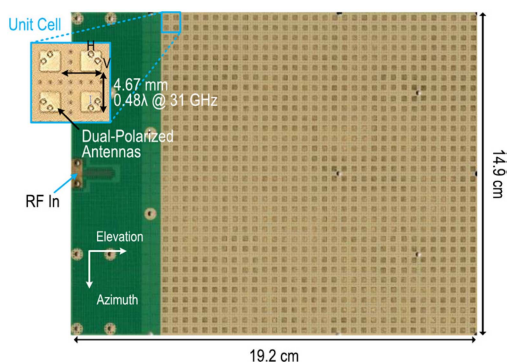


FIGURE 27. 1024-Element K a-Band SatCom phased-array transmitter with 49.5-dBW Peak EIRP [225].

PCB, the most obvious solution was also to incorporate the 1:256 Wilkinson power divider network distributing the RF input signals to the individual beamformer chips. In contrast to the work in [63], however, only four instead of eight RF driver amplifiers are used between the second and third stage of the cooperate feeding networks to overcome ohmic and splitting losses.

For the 1024-element phased array, an EIRP of 48 dBW was achieved at boresight and thus a transmitter system composed of four of these subarrays is suitable for GEO satellite communication. The technical counterpart of the phased array transmitter for the dedicated downlink band at K-band has been presented by the same authors in [227]. The 1024-element phased-array receiver closely follows the same design concepts as shown in [225] for the opposite communication direction. It demonstrates a measured G/T at least of 3.4 dB/K per polarization, a cross-polarization purity of more than 25 dB for scanning up 70° . Furthermore, the TX band filters in the RF receiver chains provide more than 80 dB isolation. It is evident in the large variety of current phased array developments that the massive advances of the PCB, IC, and packaging technologies have enabled an affordable realization of SatCom terminals at Ka-band. In particular, the widespread availability of commercial beamformer RFICs serves as a catalyzer for multifaceted product innovations in the aerospace industry. Besides electronically steerable antenna terminals at Ku-band, various companies (e.g., ViaSat, Rockwell Collins, OneWeb, Phasor) have extended their product portfolio in the meantime with equivalent Ka-band solutions, not at least because of the prospective high-volume market in the new space era, in which uninterrupted communications links to GEO and moving satellites in LEO/MEO are vitally important.

As an example, Fig. 28 shows different terminal solutions from Viasat for airborne as well as fixed backhaul applications being able to connect to different constellations (GEO, MEO, LEO). The chosen technology platform for the 2D electronically scanned arrays is based on analog beamforming and allows the terminals to cover the complete allocated up- and downlink spectra at K-/Ka-band with a large instantaneous bandwidth. A modular approach in the form of rhomboidal

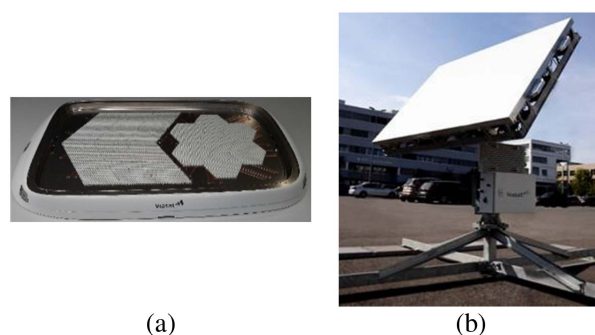


FIGURE 28. SatCom terminals at Ka-band from Viasat for (a) airborne (b) fixed backhaul MEO applications (Courtesy of ViaSat Antenna Systems SA).

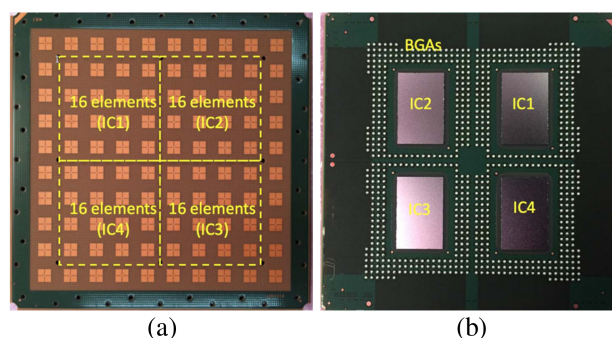


FIGURE 29. 64-element dual-polarized phased array transceiver module at 28 GHz (a) top view (b) bottom view [113].

and hexagonal tiles has proved to be a key point for a scalable design that facilitates addressing various markets with different performance requirements. Compared with these, current developments of direct radiating arrays for terrestrial communications follow a more pluralistic design approach. From the technological perspective the reason can be found in less stringent system requirements of terrestrial phased-array radios due to much lower path losses as for SatCom applications.

As a consequence, recent phased array developments for HAPS [228], [229] closely resemble their terrestrial counterparts, although such 5G radios are coined as non-terrestrial infrastructure under the 5G standardization [33] (cf. Section I-C).

2) TERRESTRIAL/ARIAL COMMUNICATION FROM K- TO Q-BAND

Depending on the specific application, terrestrial 5G base stations and user terminals typically have different requirements (see Section I). While electronically steerable antennas for 5G single- /dual-beam user terminals often rely on analog beamforming [7], [66], [68], [113], [228], [229], [230], [231], base station antennas are making use of massive MIMO through hybrid [58], [232] or digital beamforming schemes [54], [233], [234]. Fig. 29 illustrates a 28-GHz phased array

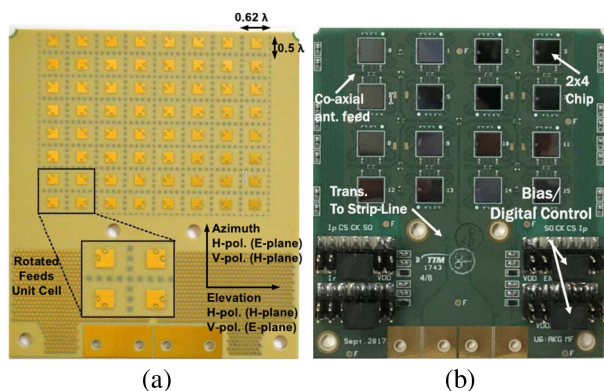


FIGURE 30. A dual-beam phased array transceiver module at 28 GHz with 64 dual-polarized antennas (a) top view (b) bottom view [231].

transceiver module at 28 GHz whose 64 dual-polarized antenna elements are integrated together with four transceiver RFICs into a multilayer BGA-based package [113]. The SiGe BiCMOS chipsets include 16 TRX channels per polarization enabling the synthesis of concurrent independent beams in two polarizations either in TX or RX mode. Since the up- and down-conversion stages for the LO and RF signals are monolithically integrated into the RFIC, the AiP provides a 3-GHz IF interface at baseband and an LO interface at around 5 GHz which avoids lossy and complex routing of mm-wave signals between the packages and the PCB. This AiP solution from IBM/Ericsson is capable of beam steering up $\pm 50^\circ$ with a saturated EIRP of 52 dBm. A similar phased array topology for the 5G band at 28 GHz has been presented by Qualcomm [112]. In this implementation, the BGA package is composed of 16 dual-polarized antennas and two transceiver chipsets in a 28-nm bulky CMOS technology. The RFIC uses RF beamforming with RF/IF conversion, whereas the LO signal needs to be injected at 20–23 GHz.

In order to form a 256-element phased array, 16 TRX modules were integrated on a PCB. In a more recent contribution, a dual-polarized and dual-beam phased array transceiver (TRX) working from 28 to 32 GHz has been proposed following an antenna-on-PCB approach as shown in Fig. 30 [231]. Therefore, each SiGe beamformer chip contains four TRX channels per polarization, which are combined into two common RF ports to enable polarization MIMO. As a consequence of that, the 64-element phased array module additionally contains two 1:16 RF distribution networks, similar as proposed in [220]. The authors experimentally verified a EIRP at P_{sat} of 52 dBm per beam and a minimum cross-polarization rejection of 28 dB in a scanning range of $\pm 50^\circ$ in azimuth and $\pm 25^\circ$ in elevation. In [58], the authors present a hybrid beamforming system composed of 16×8 radiating elements and two RF chains. This developed testbed uses a fully-connected hybrid beamforming topology which, in contrast to conventional sub-connected architectures facilitates the use of more sophisticated hybrid beamforming algorithms for higher data throughput. The 128-element phased array as depicted in Fig. 31 operates within a 2 GHz bandwidth

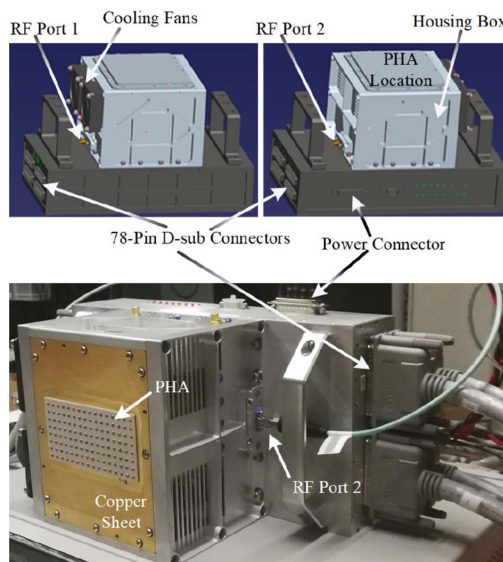


FIGURE 31. Photograph of the hybrid beamforming antenna system at 26 GHz with 16×8 radiating elements [58].

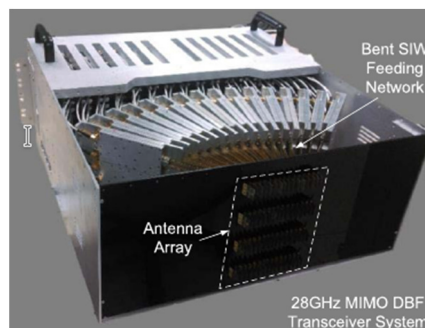


FIGURE 32. Photograph of the 64-channel DBF-based massive MIMO transceiver system at 28 GHz [54].

centered at 26 GHz and provides a flexible control of the two concurrent beams in a scanning range of $\pm 60^\circ$. The electronically steerable antenna system allows to adjust the EIRP between 10 dBm and 60 dBm and thus can it be used either for short- or long-range communication scenarios.

An example of a fully digital beamforming system for 5G massive MIMO applications at 28 GHz has been published in [54]. The planar antenna array makes use of brick architecture and is populated with 16×4 elements in along the horizontal and vertical direction, respectively. To meet a half-wavelength element spacing in the horizontal plane, a fan-shaped arrangement of the transceiver boards is applied (see Fig. 32). In essence, the analog front-end is based on a common-leg architectures as usually found in mm-wave 5G systems relying on time division duplexing, but with the additional of up- and down-conversion stages.

Overall, the DBF-based transceiver array provides an instantaneous signal bandwidth of 500 MHz for all 64 RF chains. In a multiple-user MIMO scenario, the presented system achieves a maximum data throughput of 50.73 Gb/s in

downlink using 20 independent data streams to eight user terminals. In recent years, the deployment of the frequency spectrum around 39 GHz has also gathered increasing momentum. For example, Wang et al. [67] demonstrated a 64-element phased array transceiver system at 39 GHz. In this work, each PCB module comprises of 4×4 single linearly polarized patch antennas which are connected to four quad-channel transceiver RFICs on the backside of the board by means of vertical RF transitions. Apart from that, no further routing of mm-wave signals is necessary because the RFICs internally translate the IF/LO signals at 3.9 GHz to RF domain at 39 GHz, and vice versa. It is interestingly to note that the CMOS-based RFIC includes additionally a built-in calibration circuit block.

The proposed calibration scheme can alleviate phase and amplitude impairments across the TRX elements aiming to ease the deployment of larger phased array transceiver system in base stations. Another tile-based phased array transceiver operating in the band 37–42 GHz was presented in [50]. The module with 64 radiating elements has also been realized using a low-cost PCB technology, whereas the sixteen 4-channel transmit/receive beamformer chips on the bottom side of the PCB are fabricated in SiGe technology. Thus, as expected, the presented RF beamformer IC in this work shows a better performance as the suggested CMOS solution in [67], but at the expense of a higher price tag. Furthermore, the 64 radiating elements are designed as stacked patch antennas for an enhanced operating bandwidth and scanning range. The phased array scans to $\pm 60^\circ$ and $\pm 50^\circ$ in the E- and H-plane, respectively, with a high cross-polarization purity greater than 30 dB, due to the applied feed rotation at 2×2 subarray level.

In addition, a maximum over-the-air data rate of 30 Gb/s with a 64-QAM modulation scheme has been demonstrated. In many ways, a completely different transceiver architecture for the 5G n260 band is shown Fig. 33 [55]. While in most of the current TDD architectures for 5G applications the TX and RX functionalities are usually integrated into a single antenna array, the contribution in [55] proposes the development of separate TX and RX front-ends. This offers the design freedom for asymmetric up- and downlink base station configurations having different requirements on both communication directions in many practical scenarios. Notably, massive MU-MIMO systems for 5G/6G may substantially benefit from this flexibility of having unequal numbers of RF chains for TX and RX, respectively, which potentially result in lower hardware complexity, implementation costs, and power consumption as their symmetrical counterparts [235]. Since this concept does not employ hardware switches in the RF chains, TDD is going to be realized in a shared baseband sub-system. The transmit as well as the receive array are populated with 64 radiating elements using a brick architecture. The uplink and downlink signals are digitally processed in the baseband at element-level forming a fully digital beamforming communication radio across the operating frequency range from 37 GHz to 42.2 GHz with an instantaneous bandwidth of 400 MHz.

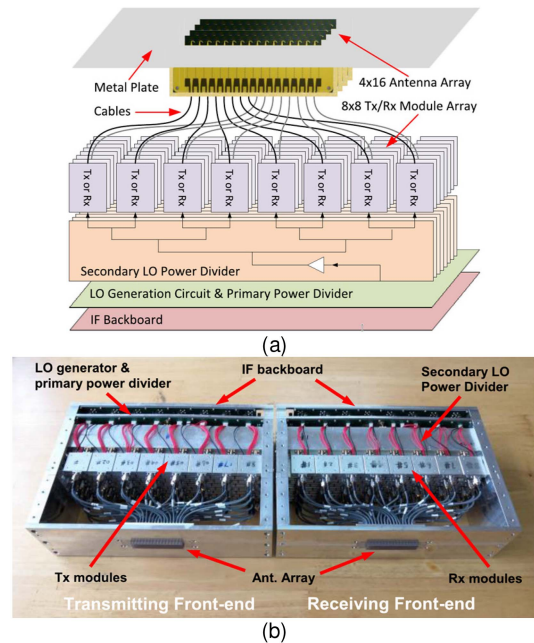


FIGURE 33. Full-Digital beamforming arrays for 5G massive MIMO from 37–42.5 GHz (a) architecture and photograph of the transmitter and receiver front-end [55].

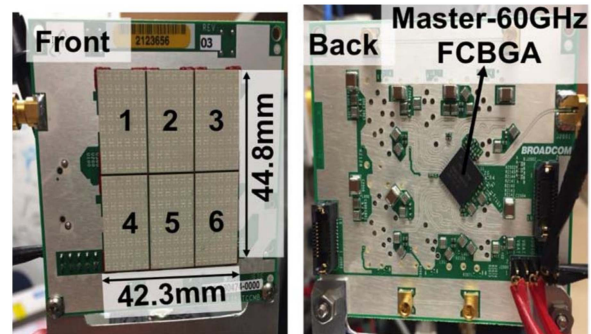


FIGURE 34. 144-channel phased array transceiver composed of 6 packaged tile modules for the 60-GHz band [122].

3) TERRESTRIAL COMMUNICATION FROM V- TO W-BAND

The abundant available spectral resources in the unlicensed 60-GHz bands and in the E-band are particularly suitable for broadband transmission links. In a complementary fashion, the V-band is mainly deployed for small cell backhauling due to the local maximum of the atmospheric absorption around 61 GHz, while long-range backhaul solutions are operating in the E-band. Owing to the promising market potential, numerous developments on electronically steerable antenna systems from both academia and industry have recently been reported. Fig. 34 shows 60-GHz phased-array transceiver from Broadcom for backhaul applications [122]. It consists of 6 tiled LTCC modules with 48 antenna elements each (cf. Fig. 8(d)). Since only a limited scanning capability in the elevation plane is required, a pair of radiating elements are connected to a single RF chain. Two 12-channel transceiver chipsets using analog beamforming drive the upper and lower part of

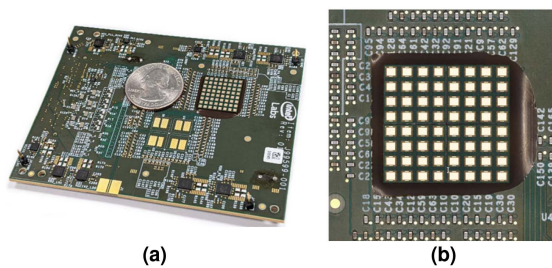


FIGURE 35. Photograph of a E-band phased array transceiver composed of four 8×8 modules (a) motherboards (b) mm-wave antenna array [104].

the array module. They are mounted on the backside of the LTCC module, from where each of the 24 mm-wave I/Os are routed through the WLCS package and the multilayer module to the antenna's power divider/combiner. The phased array transceiver equipped with 288 patch antennas could achieve a maximum EIRP of 51 dBm at boresight and scanning range of $\pm 60^\circ/\pm 10^\circ$ in azimuth/elevation across a wide bandwidth from 57 GHz to 66 GHz.

An alternative design approach for a wideband phased array transceiver module operating in the V-band was pursued by Rupakula et al. [236]. In their contribution, they focus on a low-cost phased array implementation with 128 stacked patch antennas built on a multilayer PCB. Similarly to the solution proposed by Broadcom [122], the planar array is subdivided into rectangular unit cells with a size of $0.5\lambda_0$ and $0.7\lambda_0$ at 60 GHz in the horizontal and vertical plane, respectively. This corresponds to an application-specific scanning range of $\pm 50^\circ$ in azimuth and $\pm 15^\circ$ in elevation. In order to avoid high insertion losses within the on-chip distribution network, a 2×2 SiGe beamformer RFIC was chosen in favor of a high channel-count RFIC. The experimental results of the phased array demonstrator show a flat EIRP of 45 dBm across a RF bandwidth of 9 GHz (54–63 GHz).

Furthermore, a 30-Gbps communication link has been established in the transmit mode using 64-QAM across the full instantaneous bandwidth of 5 GHz. In [104], an electronically steerable transceiver array at E-band was reported more recently by Intel. Fig. 35 illustrates the mainboard on which four packaged phased array modules have been assembled using a $150\text{-}\mu\text{m}$ BGA technology. The unit module is based on an organic prepreg substrate technology which allowed for sophisticated AiP solutions. Each module contains 16 stacked patch antennas fed by four direct-conversion transceiver chips in Intel's 22-nm FinFET process. The packaging and assembly concepts ensure a strictly vertical signal routing and heat removal, in order to create a truly scalable phased array architecture for transmit and receive with excellent scan performance. The 64-element phased array transceiver demonstrates efficient beam steering down to 60° in elevation with less than 5 dB scan loss.

Another organic-based phased-array antenna package with a 100% aperture fill factor but at W-band was pioneered in 2018 by IBM [237]. The package accommodates 64

dual-polarized antenna and a single large SiGe die ($13.5 \text{ mm} \times 11.3 \text{ mm}$) with 4 discrete RFICs for either transmit or receive. In this way, the assembly process for the flip-chip simplifies to just one reflow and underfill step which improves the overall yield of the module package when compared to the integration of four individual flip-chip dies. In order to account for the high-integration density at W-band, a different phased array solution has been proposed by Nokia Bell Labs based on separate TX and RX elements which, however, are interleaved at tile-level to create a full 5G transceiver system [115]. Therefore, two variants of the transceiver RFIC were implemented with 16TX/8RX and 8TX/16RX channels, respectively. By integrating the antennas, the distribution network, and the appropriate RFIC into a BGA-based multilayer tile, a scalable architecture for asymmetrical bidirectional communication scenarios is presented whose intra-tile and inter-tile element spacings are equal. The complete phased array transceiver system consists of 384 elements (256TX/128RX) distributed into sixteen tiles. When all 256 TX were active simultaneously, a maximum saturated EIRP of 60 dBm at 90.7 GHz has been reported. Since the radiating elements are spaced by $0.63\lambda_0$, the TX array has an unambiguous scanning range of $\pm 30^\circ$ in the E- and H-plane.

4) COMPARISON

As thoroughly discussed in the preceding paragraphs, extensive research on direct radiating arrays has been undertaken in the recent years using a large variety of different technologies and system architectures. Table 3 provides a comparison of recently published antenna module and systems for terrestrial and non-terrestrial communication networks. Owing to the large spectral separation of the TX and RX SatCom bands, separate phased array antennas for both communication directions are typically used. In contrast to these FDD systems, terrestrial and aerial communication systems operate in TDD and thus often take a shared aperture approach. Furthermore, SatCom antenna systems exhibit a higher element count and radiation performance reflecting these long-distance communication links, while their antenna counterparts for terrestrial and aerial communication have correspondingly smaller numbers. Another key distinction can be found in the wide range of different beamformer types deployed in terrestrial/aerial systems, whereas SatCom antenna terminals almost exclusively rely on RF beamformers to meet large instantaneous bandwidths. In addition, it can also be observed that direct radiating arrays for SatCom applications provide polarization agility, but implementations for terrestrial communication networks often support the generation of higher beam counts depending on their intended purpose.

B. RECONFIGURABLE QUASI-OPTICAL ANTENNAS

Antenna array architectures based on a space-fed arrangement represents another attractive technique to perform beam steering. Derived from their optical counterparts, these quasi-optical antennas are typically composed of a reflector- or

TABLE 3. Comparison of Reported Direct Radiating Arrays for Communication Applications From Ku- to E-Band

Ref.	Antenna Type	No. of Elements	Comm. direction	Beam-former	Bandwidth (GHz)	Polarization	Scan range (E-/H-plane)	Scan loss (dB)	Max. EIRP @P _{1dB} (dBW)	Max. G/T (dB/K)	No. of beams
[94]	Stacked Patch	4×4 8×8	TX RX	RF	27.5-28.35 12.0-14.5	Dual-circular	60°/60°	≈ 5	-	-	1
[64]	Stacked Patch	16×16	RX	RF	10.6-12.5	Dual	70°/70°	≈ 5.1	-	5.4	1
[52]	Patch	32×32	RX	RF	10.7-12.7	Dual-linear	70°/70°	≈ 5.6	-	10.5	2
[224]	Patch	16×16 16×16	TX RX	RF	17.7-20.2 27.5-31.0	Dual-circular	70°/70°	≈ 4	34.5	-1	1
[63]	Stacked Patch	32×32	TX	RF	29.5-30.0	Dual-circular	60°/60°	≈ 4.5	44	-	1
[225]	Stacked Patch	32×32	TX	RF	27.0-31.0	Dual-linear	70°/70°	≈ 3.3	49.5	-	1
[227]	Stacked Patch	32×32	RX	RF	17.7-20.2	Dual-linear	70°/70°	≈ 3.3	-	8.1	1
[228]	Open ended SIW	16×16	Tx Rx	RF	24.24-27.5	Dual-linear	60°/60°	≈ 4	30 ^s	-	1
[229]	Stacked Patch	16×16	TX RX	RF	17.5-20.0	Dual-circular	65°/65°	-	-	-	1
[236]	Stacked Patch	8×8 16×16	TX RX	RF	54.0-63.0	Linear	50°/15°	≈ 2.5	15	-	1
[238]	Patch	4×8	TX RX	RF	28.5-30.5	Linear	25°/50°	≈ 5	15	-	1
[68]	Dipole	8×1	TX RX	IF	26.5-29.5	Linear	50°/50°	≈ 5	24.8	-	1
[231]	Stacked Patch	8×8	TX RX	RF	28.0-32.0	Dual-linear	50°/25°	≈ 3	22	-	2
[54]	Yagi Uda	16×4	TX RX	Digital	26.5-29.5	Linear	67°/28°	≈ 3	28	-	20
[234]	Tapered Slot	15×1	TX	Digital	23.5-26.5	Linear	45°/45°	≈ 4	-	-	14
[58]	Patch	16×8	TX	Hybrid	25.0-27.0	Linear	60°/60°	≈ 3	30	-	2
[50]	Patch	8×8	TX RX	RF	37.0-42.0	Linear	60°/50°	≈ 4	21	-	1
[55]	Yagi Uda	16x4	TX RX	Digital	37.0-42.0	Linear	30°/65°	≈ 3	17	-	64
[113]	Stacked Patch	8×8	TX RX	IF	29.0-32.0	Dual-linear	50°/50°	≈ 6	34	-	1

Application:	Satcom	Aerial	Terrestrial
---------------------	--------	--------	-------------

lens-based aperture which is illuminated by a primary feed (e.g., horn antenna) in the transmit case, and vice versa for the receive case. Hence, these antenna designs act either as a spatial power splitter or combiner.

In comparison to direct radiating arrays, they feature of a much lower hardware footprint as these high-gain antennas are typically created by using a few active transmit/receive elements in conjunction with a large (reconfigurable) reflector or lens [39], [40], [41], [239]. This leads to dramatically lower implementation costs for large-scaled phased array systems. Furthermore, in particular at higher frequencies, quasi-optical antenna topologies play out their strengths of having a low integration density and no printed RF distribution network.

Note that the latter aspect becomes increasingly pivotal for larger antenna designs as the use of transmission line feeding networks results in increasingly high losses at mm-wave frequencies, which typically diminishes the efficiency of large phased array antennas with hundreds of elements down to less than 40%. Even though the reduced efficiency

can be compensated by additional amplifier stages, this will in turn serve to exacerbate the integration complexity and thermal management of such antenna systems. Reconfigurable quasi-optical antenna systems come in a variety of different forms. However, through the thinning of transceivers, quasi-optical antenna systems must make sacrifices in the radiation characteristics which are commonly very application-specific.

In general terms, it can be stated that quasi-optical antenna systems are particular suitable for point-to-point or point-to-multipoint communication scenarios with high spatial decorrelation regardless of whether ABF or subarray HBF is used. However, due to their simplified architecture, in particular in the analog beamformer part, they are very inappropriate for the implementation of fully-connected HBF topologies. The true virtue of fully-connected HBFs become really apparent in (terrestrial) MU-MIMO applications with large instantaneous bandwidth for which direct radiating array architectures are certainly the better choice to realize all inter-channel connections.

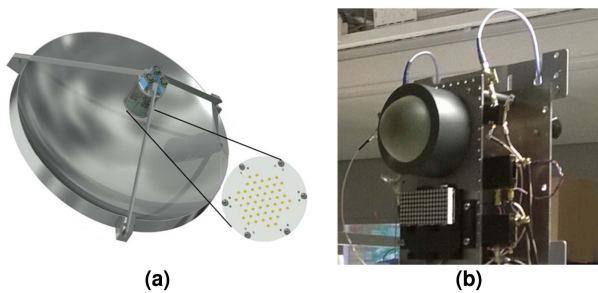


FIGURE 36. Array fed (a) reflector antenna for Ka-band SatCom [240] (b) lens antenna for 5G backhauling [11].

1) ARRAY FED REFLECTOR AND LENS ANTENNAS

An electronically steerable reflector antenna for SatCom at Ka-band was reported in [240]. The quasi-optical configuration is composed of a concave main reflector and a focal plane transmit array as shown in Fig. 36(a). This approach combines the advantages of reflector antennas such as high-gain and simplicity with adaptive beam steering capabilities of phased array antennas at the expense of a reduced scanning range. In this work, the active phased array antenna at 30 GHz is equipped with 49 radiation elements enabling a reconfigurable illumination of the reflector. In this way, the realized quasi-optical system has demonstrated efficient 2D beam steering within a scanning of $\pm 6^\circ$, which makes it suitable for hybrid electronic/mechanical SatCom terminals. An alternative design of a wide-angle array fed reflector antenna for satellites and ground terminals has also been presented very recently by Lockheed Martin [241]. A reflector design with a hybrid geometry and fed by a linear array that combines electronic steering along a first axis and mechanical steering along a second axis was proposed in [242] for VSAT applications. A similar reflector geometry fed by a stack of linear arrays was described in [243], [244] for onboard applications. This hybrid configuration combining a focused design in one plane and an imaging design in the orthogonal plane simplifies greatly the design of the focal array system and in particular the beamforming stage, significantly reducing the losses at the expense of a constrained reconfigurability. These quasi-optical solutions can be of interest for applications with asymmetric scanning requirements, like in base stations.

Deploying the collimating properties of dielectric lenses, Isotropic Systems has developed an active electronically steerable lens antenna for SatCom at Ku-band [245]. The overall terminal antenna contains a plurality of hexagonally shaped lens sets. Owing to the small spectral separation of the uplink and downlink frequency bands, the imaging characteristics of the lenses are sufficiently stable to create a common transmit/receive aperture. Each lens-based subarray includes multiple dual-polarized patch antennas whose dedicated RF chains are connected to a digital beamformer. Depending on which planar antenna element is activated, quasi-optical beam steering up to $\pm 70^\circ$ can be performed based on the element's phase center offset relative to the one of the subarray lens.

Furthermore, as a matter of principle, multiple beams can be synthesized pointing to different satellites simultaneously by activating multiple transmit/receive elements. In the realm of 5G access and backhaul applications, an alternative design of a 64-element array-fed lens antenna in E-band has been reported by Nokia Bell Labs [11], which is capable of continuous beam-switching in a field of view of about $\pm 4^\circ \times \pm 17^\circ$.

2) REFLECTARRAY AND TRANSMITARRAY ANTENNAS

Another class of spatially fed antennas are represented by reflect- and transmitarray antennas. Unlike array-fed reflector or lens systems, these hybrids between aperture antennas and antenna arrays provide electronic beam steering through the reconfigurability of the reflective or transmissive array structure.

There are various different technologies allowing the electronic control of the unit cell properties for instance by PIN diodes, varactor diodes, microelectromechanical systems (MEMS), liquid crystal (LC) substrates, or integrated circuits [39], [41], [40]. Similar technologies are also envisioned for reconfigurable intelligent surfaces (RIS) in the realm of 5G/6G wireless infrastructures, even though they are intended to operate under considerable different environmental conditions compared to classical reflect-/transmitarray antennas [247], [248], [249], [250], [251], [252].

A dual-frequency reconfigurable reflectarray for Ku-band bidirectional SatCom applications has been presented in [253]. Each of the 1600 elementary cells consists of a rectangular patch whose resonance behavior is tuned by a single PIN diode. Since PIN diodes ideally operate as a voltage-controlled switch, the proposed unit cell provides a 1-bit phase resolution and thus a compromise between the aperture efficiency and the radiation performance must be made. However, the complete reflectarray antenna has, in turn, a low-cost and simple structure, which has been demonstrated in a similar reflectarray configuration also at 60 GHz [254]. RF MEMS switches behave similarly to PIN diodes in the sense that both acts as an electronically controlled single-pole switch. Therefore, reflectarray antennas based on MEMS switches are likewise prone to a higher residual side lobe level [78] due to the unit cells' limited phase resolution [255], [256], albeit with lower insertion losses and higher isolation compared to discrete reflectors/lenses with solid state switches. By contrast, the use of varactor diodes supports a continuous control of the reflectarray elements enabling a precise and agile reconfiguration of the radiation characteristics. Very recently, a varactor-based reflectarray antenna for SatCom at Ka-band has been developed in [246]. The transceiver terminal is intended to operate in dual-circular full-duplex mode. In order to provide concurrent receive and transmit functionalities, the interleaved reflectarray unit cell contains a printed 3-arm cross element for each frequency band whose folded arms are reactively loaded with varactor diodes (see Fig. 37). The analysis of the dual-band reflectarray with 48×48 elements shows promising beam steering capabilities up

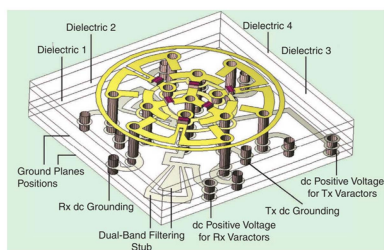


FIGURE 37. Dual-band reconfigurable reflectarray unit cell for Ka-band ground terminal applications [246].

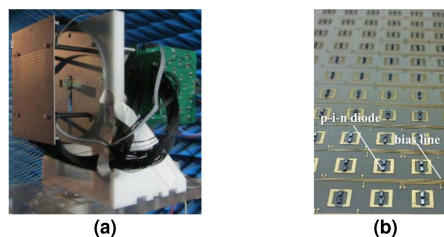


FIGURE 39. Circularly-Polarized Reconfigurable Transmitarray at Ka-Band (a) Fully assembled demonstrator (b) 2×2 submodule [257].

examples a 1-bit reconfigurable transmitarray antenna at Ku-band [260]. In this work, the unit cell features a planar Yagi-Uda and tapered slot antenna as receive and transmit element, respectively. In between, a wideband 180° phase shifter with two PIN diodes has been realized taking advantage of the switching polarity technique. The realized prototype with 16×16 linearly polarized unit cells exhibits a maximum gain of 22.3 dB at 13.6 GHz and covers a 1-dB fractional bandwidth of 14%. Efficient beam steering has been achieved in both the E- and H-planes with a gain degradation of less than 4 dB at 60° off-boresight.

Fig. 39 shows a 400-element circularly-polarized reconfigurable transmitarray in Ka-Band [257]. The proposed multilayer unit cell is composed of two core laminates in which a common ground plane and bias lines have been implemented on the internal metal layers. A derivative of tunable patch antenna element loaded by two PIN-diodes and passive patch antenna element are placed on the bottom layer (receive) and top (transmit) layer, respectively. Furthermore, both patch antennas are galvanically connected by means of a through hole via. Although the 1-bit unit cell operates in linear polarization, the final 20×20 transmitarray antenna supports LHCP/RHCP beam switching by the use of a random sequential rotation technique. The transmitarray prototype obtains a maximum gain of 20.8 dBi at 29 GHz and spans a 3-dB gain bandwidth from 27.4 to 31.7 GHz, while the axial ratio remains below 2 dB. In addition, beam steering capabilities up to $\pm 60^\circ$ were demonstrated. In a different way, an active transmitarray module has been presented in [261] covering both SatCom bands at 30 GHz for uplink and 20 GHz for downlink. In this study, the receive elements are nested into the irregular lattice of the transmitarray to create a shared aperture. Due to the aperiodic array lattices, a significant decrease of the grating lobe levels was achieved. The antenna elements are connected within the submodule to a multi-channel SiGe transceiver RFIC [262] allowing a 16-bit amplitude and phase control.

C. HOLOGRAPHIC ANTENNAS

Despite the many advantages of quasi-optical antennas for electronic beam steering, these topologies essentially require a non-planar RF distribution network preventing their usage in applications where low-profile antennas are preferred. Apart from direct radiating arrays (cf. Section IV-A), a viable solution to the last-mentioned restriction is also provided by

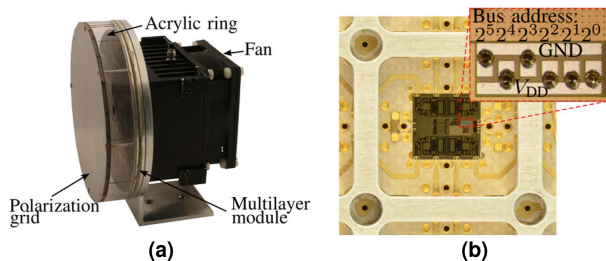


FIGURE 38. Wide-angle scanning folded reflectarray transceiver with 144 dual-polarized elements at 30 GHz (a) Fully assembled demonstrator (b) 2×2 submodule [51], [92].

to 60° and 26° across the RX band (19.3–20.2 GHz) and TX band (29.3–30 GHz), respectively. Furthermore, the sidelobe and cross-polarization levels are sufficiently low because the applied voltage to each varactor diode is controlled by an 8-bit DAC. Quasi-continuous control of the unit cells has also been demonstrated in the mm-wave regime by means of a folded reflectarray antenna based on liquid crystal technology [258]. The antenna demonstrator in E-band has achieved a gain of at least 25.1 dB and a scanning range of $\pm 6^\circ$ from 74 to 78 GHz. Following the same architectural concept of a folded reflectarray antenna, two variants of a 144-element active phased array transceiver at 30 GHz have been reported in [51], [92]. The essential difference between these modules lies in the different chipsets that were deployed. The first variant of the 4-channel mixed-signal transceiver RFIC relies on nMOS SPDT switches to change the communication direction, whereas fully monolithically integrated RF-MEMS components are used in the second version to tackle the lack of low-loss millimeter-wave switches [259]. The module architecture is partitioned into identical 2×2 submodules in which the RFIC is directly connected to four dual-polarized antenna elements through vertical RF transitions (see Fig. 38). As the described system configuration relies on a space-fed arrangement, no lossy RF and LO distribution networks had to be considered further in the multilayer module. In the intended operational band from 29.5 GHz to 31 GHz, both phased array systems have demonstrated excellent scanning performance up to $\pm 60^\circ$ in all azimuth planes.

Besides the aforementioned reflectarray antennas, various electrically reconfigurable transmitarray antennas at micro- and millimeter-wave have been reported. This includes for

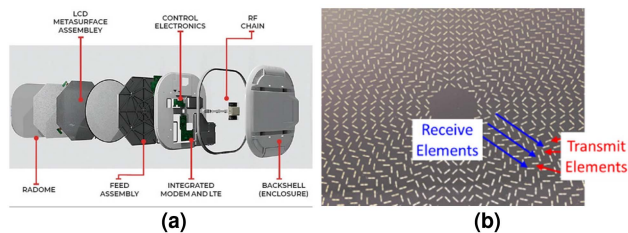


FIGURE 40. LC-based holographic antenna for Ku-band SatCom (a) exploded view of the complete user terminal (b) shared metasurface with interleaved TX and RX elements (Courtesy of Kymeta Corp.).

leaky-wave antennas that are based on the holographic principle [263]. They have recently become subject of considerable attention in academia and industry as the surface impedance-based amplitude and phase synthesis of the aperture field distribution allows a low-complexity and highly flexible beam control [264], [265], [266].

This class of metasurface antennas, as the name already suggests, relies on tailoring the dispersion characteristics of the guided modes in the aperture plane and thus do not require integrated circuits such as amplifiers or phase shifters behind every radiating element. However, in order to dynamically reconfigure holographic antennas, their unit cells must feature some sort of electronic tunability enabling the modulation of the RF signal while propagating along the metasurface. The holographic leaky-wave antenna technology developed by Pivotal Commware [267], for example, comprises of PCB-based antenna array structure whose elements are loaded by varactor diodes. In this way, 2-D holo-graphic beamforming up to $\pm 70^\circ$ in azimuth and $\pm 35^\circ$ in elevation has been achieved for mm-wave 5G network repeater applications at 28 GHz.

Because holographic antennas with their subwavelength-sized unit cells actually exacerbate the requirements on the integration of electronic components, significant efforts have also been devoted to the use of liquid crystals as a tunable dielectric [268], [269], [270]. By leveraging flat panel display manufacturing techniques for high-volume production, Kymeta has recently developed an LC-based holographic antenna for Ku-band SatCom user terminals (see Fig. 40). The radial aperture of the metasurface antenna consists of interleaved TX and RX elements which are specifically distributed to maintain full polarization control, but also to enhance the isolation between both communication directions. Since the radiation properties of each slot are individually tuned by the high-birefringence of the LC material, the holographic antenna can operate within a 75° scan cone across the entire Ku downlink (10.7–12.75 GHz) and uplink (13.75–14.5 GHz) bands, respectively, in full-duplex mode. Furthermore, as a result of this architectural approach, the antenna features a common RF port which in turn interfaces with a single RF chain.

V. SUMMARY

The close-meshed deployment of future heterogeneous communication networks has great potentials to provide

ubiquitous services with high data rates and ultra-low latency. In order to meet these requirements, this new hybrid network is going to be extended in all spatial directions by means of a multi-layer communications architecture consisting of terrestrial (land-/maritime-based), airborne (high altitude platforms, aircraft, drones), and spaceborne (LEO, MEO, GEO satellites) infrastructure platforms.

In the envisioned scenario, micro- and millimeter-wave technologies will play a decisive role in enabling short- and long-distance communication links between the mobile platforms with enhanced capacity and reliability. In light of this, the paper presented an extensive overview of electronically steerable antennas for a plurality of point-to-point/- multipoint communication applications. Various fundamental system architectures were discussed with particular focus on different beamforming techniques as well as array configuration and partitioning aspects.

Subsequently, the current key technologies and components for realizing these reconfigurable antenna systems were reviewed highlighting their pros and cons in terms integration, miniaturization, scalability, and RF performance.

Finally, recent developments of electronically steerable antennas for terrestrial and satellite communications up to 100 GHz were rigorously reported. In order to provide the reader with the latest technical advances in direct radiating arrays, various implementations of array elements as well as active antenna modules and systems were subject of this contribution. Looking forward to the new opportunities and challenges, in particular at mm-wave frequencies, likewise calls for reconfigurable antenna systems with lower hardware footprint and thus lower integration density. To this end, the review of state-of-the-art quasi-optical and holographic antennas concludes this survey.

REFERENCES

- [1] International Telecommunication Union, "IMT vision – Framework and overall objectives of the future development of IMT for 2020 and beyond," Recommendation ITU 2083, Electronic Publication Geneva, Switzerland, 2015. [Online]. Available: <https://www.itu.int/rec/R-REC-M.2083>
- [2] S. Redana et al., "View on 5G architecture, version 4.0," white paper of the 5G-PPP Architecture Working Group, 2021. [Online]. Available: <https://zenodo.org/record/5155657>
- [3] U. Gustavsson et al., "Implementation challenges and opportunities in Beyond-5G and 6G communication," *IEEE J. Microwaves*, vol. 1, no. 1, pp. 86–100, Jan. 2021.
- [4] A. Kapovits, A. Gavras, J. Cosmas, M. Ghorashi, X. Li, and Y. Zhang, "Delivery of 5G services indoors – The wireless wire challenge and solutions," Zenodo, pp. 1–100, 2021. [Online]. Available: <https://zenodo.org/record/4280750>
- [5] A. Ghosh et al., "Millimeter-wave enhanced local area systems: A high-data-rate approach for future wireless networks," *IEEE J. Sel. Areas Commun.*, vol. 32, no. 6, pp. 1152–1163, Jun. 2014.
- [6] A. O. Watanabe et al., "Glass-based IC-embedded antenna-integrated packages for 28-GHz high-speed data communications," in *Proc. IEEE 70th Electron. Compon. Technol. Conf.*, 2020, pp. 89–94.
- [7] K. Kibaroglu, M. Sayginer, and G. M. Rebeiz, "A low-cost scalable 32-element 28-GHz phased array transceiver for 5G communication links based on a 2×2 beamformer flip-chip unit cell," *IEEE J. Solid-State Circuits*, vol. 53, no. 5, pp. 1260–1274, May 2018.

- [8] G. Amendola et al., "Compact E-band I/Q receiver in sige BiCMOS for 5G backhauling applications," *IEEE Trans. Circuits Syst. II, Exp. Briefs*, vol. 68, no. 9, pp. 3098–3102, Sep. 2021.
- [9] S. R. Zahran, L. Boccia, G. Amendola, S. Moscato, M. Oldoni, and D. Tresoldi, "An 8×8 cavity backed waveguide antenna array for D-band backhauling communications," in *Proc. Eur. Conf. Antennas Propag.*, 2020, pp. 1–5.
- [10] M. G. L. Frecassetti et al., "D-band radio solutions for beyond 5G reconfigurable meshed cellular networks," in *Proc. Int. Symp. Wireless Commun. Syst.*, 2019, pp. 427–431.
- [11] J. Ala-Laurinaho et al., "2-D beam-steerable integrated lens antenna system for 5G E-band access and backhaul," *IEEE Trans. Microw. Theory Techn.*, vol. 64, no. 7, pp. 2244–2255, Jul. 2016.
- [12] C. Waldschmidt, J. Hasch, and W. Menzel, "Automotive radar—From first efforts to future systems," *IEEE J. Microwaves*, vol. 1, no. 1, pp. 135–148, Jan. 2021.
- [13] A. Tassi, M. Egan, R. J. Piechocki, and A. Nix, "Modeling and design of millimeter-wave networks for highway vehicular communication," *IEEE Trans. Veh. Technol.*, vol. 66, no. 12, pp. 10676–10691, Dec. 2017.
- [14] F. Jameel, S. Wyne, S. J. Nawaz, and Z. Chang, "Propagation channels for mmWave vehicular communications: State-of-the-art and future research directions," *IEEE Wireless Commun.*, vol. 26, no. 1, pp. 144–150, Feb. 2019.
- [15] L. Yan et al., "Machine learning-based handovers for sub-6 GHz and mmWave integrated vehicular networks," *IEEE Trans. Wireless Commun.*, vol. 18, no. 10, pp. 4873–4885, Oct. 2019.
- [16] L. Giroto de Oliveira, B. Nuss, M. B. Alabd, A. Diewald, M. Pauli, and T. Zwick, "Joint radar-communication systems: Modulation schemes and system design," *IEEE Trans. Microw. Theory Techn.*, vol. 70, no. 3, pp. 1521–1551, Mar. 2022.
- [17] Y. Su, Y. Liu, Y. Zhou, J. Yuan, H. Cao, and J. Shi, "Broadband LEO satellite communications: Architectures and key technologies," *IEEE Wireless Commun.*, vol. 26, no. 2, pp. 55–61, Apr. 2019.
- [18] X. Lin, S. Rommer, S. Euler, E. A. Yavuz, and R. S. Karlsson, "5G from space: An overview of 3GPP non-terrestrial networks," *IEEE Commun. Standards Mag.*, vol. 5, no. 4, pp. 147–153, Dec. 2021.
- [19] T. Duan and V. Dinavahi, "Starlink space network-enhanced cyber-physical power system," *IEEE Trans. Smart Grid*, vol. 12, no. 4, pp. 3673–3675, Jul. 2021.
- [20] TeleSat, "Telesat lightspeed-TM," 2022. [Online]. Available: www.telesat.com/leo-satellites/
- [21] O. Kodheli et al., "Satellite communications in the new space era: A survey and future challenges," *IEEE Commun. Surveys Tuts.*, vol. 23, no. 1, pp. 70–109, Jan.–Mar. 2021.
- [22] S. Liu et al., "LEO satellite constellations for 5G and beyond: How will they reshape vertical domains?," *IEEE Commun. Mag.*, vol. 59, no. 7, pp. 30–36, Jul. 2021.
- [23] Juniper, "IoT—The internet of transformation 2020," 2020. [Online]. Available: <https://www.juniperresearch.com/whitepapers/iot-the-internet-of-transformation-2020>
- [24] M. Centenaro, C. E. Costa, F. Granelli, C. Sacchi, and L. Vangelista, "A survey on technologies, standards and open challenges in satellite IoT," *IEEE Commun. Surveys Tuts.*, vol. 23, no. 3, pp. 1693–1720, Jul.–Sep. 2021.
- [25] X. Cao, P. Yang, M. Alzenad, X. Xi, D. Wu, and H. Yanikomeroglu, "Airborne communication networks: A survey," *IEEE J. Sel. Areas Commun.*, vol. 36, no. 9, pp. 1907–1926, Sep. 2018.
- [26] G. K. Kurt et al., "A vision and framework for the high altitude platform station (HAPS) networks of the future," *IEEE Commun. Surveys Tuts.*, vol. 23, no. 2, pp. 729–779, Apr.–Jun. 2021.
- [27] G. K. Kurt et al., "A vision and framework for the high altitude platform station (HAPS) networks of the future," *IEEE Commun. Surveys Tuts.*, vol. 23, no. 2, pp. 729–779, Apr.–Jun. 2021.
- [28] A. Farajzadeh, M. G. Khoshkholgh, H. Yanikomeroglu, and O. Ercetin, "Self-evolving integrated vertical heterogeneous networks," *arXiv*. 2021. [Online]. Available: <http://arxiv.org/abs/2106.13950>
- [29] M. Geen, "E-band mmWave technology for HAPS and LEO satellite systems," *Microw. J.*, vol. 64, no. 2, pp. 22–52, Feb. 2021.
- [30] H. J. Liebe, P. W. Rosenkranz, and G. A. Hufford, "Atmospheric 60-GHz oxygen spectrum: New laboratory measurements and line parameters," *J. Quantitative Spectrosc. Radiative Transfer*, vol. 48, pp. 629–643, Nov. 1992.
- [31] ITU P.676-12 - Attenuation by atmospheric gases and related effects, 2022. [Online]. Available: <https://www.itu.int/rec/R-REC-P.676>
- [32] M. Mozaffari, W. Saad, M. Bennis, Y.-H. Nam, and M. Debbah, "A tutorial on UAVs for wireless networks: Applications, challenges, and open problems," *IEEE Commun. Surveys Tuts.*, vol. 21, no. 3, pp. 2334–2360, Jul.–Sep. 2019.
- [33] F. Rinaldi et al., "Non-terrestrial networks in 5G & beyond: A survey," *IEEE Access*, vol. 8, pp. 165178–165200, 2020.
- [34] J. R. Bhat and S. A. Alqahtani, "6G ecosystem: Current status and future perspective," *IEEE Access*, vol. 9, pp. 43134–43167, 2021.
- [35] M. Giordani and M. Zorzi, "Non-terrestrial networks in the 6G era: Challenges and opportunities," *IEEE Netw.*, vol. 35, no. 2, pp. 244–251, Mar./Apr. 2021.
- [36] J. S. Herd and M. D. Conway, "The evolution to modern phased array architectures," *Proc. IEEE*, vol. 104, pp. 519–529, Mar. 2016.
- [37] C. Fulton, M. Yearly, D. Thompson, J. Lake, and A. Mitchell, "Digital phased arrays: Challenges and opportunities," *Proc. IEEE*, vol. 104, no. 3, pp. 487–503, Mar. 2016.
- [38] R. Rotman, M. Tur, and L. Yaron, "True time delay in phased arrays," *Proc. IEEE*, vol. 104, no. 3, pp. 504–518, Mar. 2016.
- [39] S. V. Hum and J. Perruisseau-Carrier, "Reconfigurable reflectarrays and array lenses for dynamic antenna beam control: A review," *IEEE Trans. Antennas Propag.*, vol. 62, no. 1, pp. 183–198, Jan. 2014.
- [40] P. Nayeri, F. Yang, and A. Z. Elsherbeni, "Beam-scanning reflectarray antennas: A technical overview and state of the art," *IEEE Antennas Propag. Mag.*, vol. 57, no. 4, pp. 32–47, Aug. 2015.
- [41] J. R. Reis, M. Vala, and R. F. S. Caldeirinha, "Review paper on transmitarray antennas," *IEEE Access*, vol. 7, pp. 94171–94188, 2019.
- [42] Y. J. Guo, M. Ansari, R. W. Ziolkowski, and N. J. G. Fonseca, "Quasi-optical multi-beam antenna technologies for B5G and 6G mmWave and THz networks: A review," *IEEE Open J. Antennas Propag.*, vol. 2, pp. 807–830, 2021.
- [43] Y. Zhang and J. Mao, "An overview of the development of antenna-in-package technology for highly integrated wireless devices," *Proc. IEEE*, vol. 107, no. 11, pp. 2265–2280, Nov. 2019.
- [44] B. Sadhu, X. Gu, and A. Valdes-Garcia, "The more (antennas), the merrier: A survey of silicon-based mm-Wave phased arrays using Multi-IC scaling," *IEEE Microw. Mag.*, vol. 20, no. 12, pp. 32–50, Dec. 2019.
- [45] A. O. Watanabe, M. Ali, S. Y. B. Sayeed, R. R. Tummala, and M. R. Pulugurtha, "A review of 5G front-end systems package integration," *IEEE Trans. Compon. Packag. Manuf. Technol.*, vol. 11, no. 1, pp. 118–133, Jan. 2021.
- [46] X. Gu et al., "Antenna-in-package integration for a wideband scalable 5G millimeter-wave phased-array module," *IEEE Microw. Wireless Compon. Lett.*, vol. 31, no. 6, pp. 682–684, Jun. 2021.
- [47] D. Zhao et al., "Millimeter-wave integrated phased arrays," *IEEE Trans. Circuits Syst. I, Reg. Papers*, vol. 68, no. 10, pp. 3977–3990, Oct. 2021.
- [48] D. Kissingner, G. Kahmen, and R. Weigel, "Millimeter-wave and terahertz transceivers in SiGe BiCMOS technologies," *IEEE Trans. Microw. Theory Techn.*, vol. 69, no. 10, pp. 1557–9670, 2021.
- [49] B. Yang, Z. Yu, R. Zhang, J. Zhou, and W. Hong, "Local oscillator phase shifting and harmonic mixing-based high-precision phased array for 5G millimeter-wave communications," *IEEE Trans. Microw. Theory Techn.*, vol. 67, no. 7, pp. 3162–3173, Jul. 2019.
- [50] Y. Yin et al., "A 37–42-GHz 8×8 phased-array with 48–51-dBm EIRP, 64-QAM 30-Gb/s data rates, and EVM analysis versus channel RMS errors," *IEEE Trans. Microw. Theory Techn.*, vol. 68, no. 11, pp. 4753–4764, Nov. 2020.
- [51] T. Chaloun et al., "Wide-angle scanning active transmit/receive reflectarray," *IET Microw. Antennas Propag.*, vol. 8, pp. 811–818, 2014.
- [52] G. Gültepe, T. Kanar, S. Zehir, and G. M. Rebeiz, "A 1024-element Ku-band SATCOM dual-polarized receiver with $gt;10$ -dB/K G/T and embedded transmit rejection filter," *IEEE Trans. Microw. Theory Techn.*, vol. 69, no. 7, pp. 3484–3495, Jul. 2021.
- [53] M. Sayginer and G. M. Rebeiz, "An eight-element 2–16-GHz programmable phased array receiver with one, two, or four simultaneous beams in SiGe BiCMOS," *IEEE Trans. Microw. Theory Techn.*, vol. 64, no. 12, pp. 4585–4597, Dec. 2016.
- [54] B. Yang, Z. Yu, J. Lan, R. Zhang, J. Zhou, and W. Hong, "Digital beamforming-based massive MIMO transceiver for 5G millimeter-wave communications," *IEEE Trans. Microw. Theory Techn.*, vol. 66, no. 7, pp. 3403–3418, Jul. 2018.
- [55] L. Kuai et al., "A N260 band 64 channel millimeter wave full-digital multi-beam array for 5G massive MIMO applications," *IEEE Access*, vol. 8, pp. 47640–47653, 2020.

- [56] A. Stark et al., "SANTANA: Advanced electronically steerable antennas at Ka-band," in *Proc. Eur. Conf. Antennas Propag.*, 2009, pp. 1557–9670.
- [57] B. Rohrdantz, K. Kuhlmann, A. Stark, A. Geise, and A. F. Jacob, "Digital beamforming antenna array with polarisation multiplexing for mobile high-speed satellite terminals at Ka-band," *J. Eng.*, vol. 2016, pp. 180–188, 2016.
- [58] S. Payami et al., "Developing the first mmwave fully-connected hybrid beamformer with a large antenna array," *IEEE Access*, vol. 8, pp. 141282–141291, 2020.
- [59] R. Zhang, J. Zhou, J. Lan, B. Yang, and Z. Yu, "A high-precision hybrid analog and digital beamforming transceiver system for 5G millimeter-wave communication," *IEEE Access*, vol. 7, pp. 83012–83023, 2019.
- [60] C.-Y. Chu et al., "A Ka-band scalable hybrid phased array based on four-element ICs," *IEEE Trans. Microw. Theory Techn.*, vol. 68, no. 1, pp. 288–300, Jan. 2020.
- [61] S. Mondal, L. R. Carley, and J. Paramesh, "4.4 A 28/37GHz scalable, reconfigurable multi-layer hybrid/digital MIMO transceiver for TDD/FDD and full-duplex communication," in *Proc. IEEE Int. Solid-State Circuits Conf.*, 2020, pp. 82–84.
- [62] C.-Y. Kim, D.-W. Kang, and G. M. Rebeiz, "A 44–46-GHz 16-element SiGe BiCMOS high-linearity transmit/receive phased array," *IEEE Trans. Microw. Theory Techn.*, vol. 60, no. 3, pp. 730–742, Mar. 2012.
- [63] X. Luo et al., "A scalable Ka-band 1024-element transmit dual-circularly-polarized planar phased array for SATCOM application," *IEEE Access*, vol. 8, pp. 156084–156095, 2020.
- [64] A. H. Aljuhani, T. Kanar, S. Zahir, and G. M. Rebeiz, "A 256-element Ku-band polarization agile SATCOM receive phased array with wide-angle scanning and high polarization purity," *IEEE Trans. Microw. Theory Techn.*, vol. 69, no. 5, pp. 2609–2628, May 2021.
- [65] C.-N. Chen et al., "38-GHz phased array transmitter and receiver based on scalable phased array modules with endfire antenna arrays for 5G MMW data links," *IEEE Trans. Microw. Theory Techn.*, vol. 69, no. 1, pp. 980–999, Jan. 2021.
- [66] Y. Yin, B. Ustundag, K. Kibaroglu, M. Sayginer, and G. M. Rebeiz, "Wideband 23.5–29.5-GHz phased arrays for multistandard 5G applications and carrier aggregation," *IEEE Trans. Microw. Theory Techn.*, vol. 69, no. 1, pp. 235–247, Jan. 2021.
- [67] Y. Wang et al., "A 39-GHz 64-element phased-array transceiver with built-in phase and amplitude calibrations for large-array 5G NR in 65-nm CMOS," *IEEE J. Solid-State Circuits*, vol. 55, no. 5, pp. 1249–1269, May 2020.
- [68] J. Pang et al., "A 28-GHz CMOS phased-array transceiver based on LO phase-shifting architecture with gain invariant phase tuning for 5G new radio," *IEEE J. Solid-State Circuits*, vol. 54, no. 5, pp. 1228–1242, May 2019.
- [69] S.-S. Jeon, Y. Wang, Y. Qian, and T. Itoh, "A novel smart antenna system implementation for broad-band wireless communications," *IEEE Trans. Antennas Propag.*, vol. 50, no. 5, pp. 600–606, May 2002.
- [70] N. Naskas et al., "Ka-band integrated transmitter for SATCOM," in *Proc. IEEE Int. Conf. Electron. Circuits Syst.*, 2020, pp. 1–4.
- [71] G. Mangraviti et al., "A 4-antenna-path beamforming transceiver for 60GHz multi-Gb/s communication in 28nm CMOS," in *Proc. IEEE Int. Solid-State Circuits Conf.*, 2016, pp. 246–247.
- [72] S. Pellerano et al., "A scalable 71-to-76 GHz 64-element phased-array transceiver module with 2 × 2 direct-conversion IC in 22 nm FinFET CMOS technology," in *Proc. IEEE Int. Solid-State Circuits Conf.*, 2019, pp. 174–176.
- [73] E. Naviasky, L. Iotti, G. LaCaille, B. Nikolić, E. Alon, and A. M. Niknejad, "A 71-to-86-GHz 16-element by 16-beam multi-user beamforming integrated receiver sub-array for massive MIMO," *IEEE J. Solid-State Circuits*, vol. 56, no. 12, pp. 3811–3826, Dec. 2021.
- [74] R. Garg et al., "A 28 GHz 4-element MIMO beam-space array in 65nm CMOS with simultaneous spatial filtering and single-wire frequency-domain multiplexing," in *Proc. IEEE Int. Solid-State Circuits Conf.*, 2020, pp. 80–82.
- [75] A. S. Y. Poon and M. Taghivand, "Supporting and enabling circuits for antenna arrays in wireless communications," *Proc. IEEE*, vol. 100, no. 7, pp. 2207–2218, Jul. 2012.
- [76] M. Johnson et al., "Code-domain multiplexing for shared IF/LO interfaces in millimeter-wave MIMO arrays," *IEEE J. Solid-State Circuits*, vol. 55, pp. 1270–1281, May 2020.
- [77] D. R. Martinez, R. A. Bond, and M. M. Vai, *High Performance Embedded Computing Handbook: A Systems Perspective*. Boca Raton, FL, USA: CRC, 2018.
- [78] R. J. Mailloux, *Phased Array Antenna Handbook*. Norwood, MA, USA: Artech House, 2005.
- [79] J. Zhang, X. Yu, and K. B. Letaief, "Hybrid beamforming for 5G and beyond millimeter-wave systems: A holistic view," *IEEE Open J. Commun. Soc.*, vol. 1, pp. 77–91, 2020.
- [80] K. B. Letaief, W. Chen, Y. Shi, J. Zhang, and Y.-J. A. Zhang, "The roadmap to 6G: AI empowered wireless networks," *IEEE Commun. Mag.*, vol. 57, no. 8, pp. 84–90, Aug. 2019.
- [81] I. Ahmed et al., "A survey on hybrid beamforming techniques in 5G: Architecture and system model perspectives," *IEEE Commun. Surveys Tuts.*, vol. 20, no. 4, pp. 3060–3097, Oct.–Dec. 2018.
- [82] L. Liang, W. Xu, and X. Dong, "Low-complexity hybrid precoding in massive multiuser MIMO systems," *IEEE Wireless Commun. Lett.*, vol. 3, no. 12, pp. 653–656, Dec. 2014.
- [83] J. A. Kinzel, B. J. Edward, and D. E. Rees, "V-band, space-based phased arrays," *Microw. J.*, vol. 30, pp. 89–102, Jan. 1987.
- [84] R. J. Mailloux, "Antenna array architecture," *Proc. IEEE*, vol. 80, pp. 163–172, Jan. 1992.
- [85] P. Uhlig, A. Friedrich, U. Lewark, and O. Litschke, "Brick or tile? Evaluation of integration concepts for microwave phased array antennas," in *Proc. IEEE 8th Electron. System-Integration Technol. Conf.*, 2020, pp. 80–82.
- [86] R. J. Bolt et al., "Characterization of a dual-polarized connected-dipole array for Ku-band mobile terminals," *IEEE Trans. Antennas Propag.*, vol. 64, no. 2, pp. 591–598, Feb. 2016.
- [87] H. Schumacher, M. Kaynak, V. Valenta, and B. Tillack, "Smarter ICs," *IEEE Microw. Mag.*, vol. 13, no. 11, pp. 33–40, Nov. 2012.
- [88] International Telecommunication Union, "Maximum permissible levels of off-axis E.I.R.P. density from earth stations in geostationary-satellite orbit networks operating in the fixed-satellite service transmitting in the 6 GHz, 13 GHz, 14 GHz and 30 GHz frequency bands," 2006. [Online]. Available: <https://www.itu.int/rec/R-REC-S.524/>
- [89] D. Ha et al., "Large scale array antenna packaging for 5G mmwave base station," in *Proc. 50th Eur. Microw. Conf.*, 2021, pp. 45–48.
- [90] K. Kuang, F. Kim, and S. S. Cahill, *RF and Microwave Microelectronics Packaging*, K. Kuang, F. Kim, and S. S. Cahill, Eds., Berlin, Germany: Springer, 2009.
- [91] S. Holzwarth et al., "Active antenna arrays at Ka-band: Status and outlook of the SANTANA project," in *Proc. 4th Eur. Conf. Antennas Propag.*, 2010, pp. 1–5.
- [92] T. Chaloun, F. Tabarani, S. T. Wipf, M. Kaynak, H. Schumacher, and W. Menzel, "A modular phased array transceiver with RF-MEMS SPDT switches in a 0.25 μm SiGe BiCMOS technology," in *Proc. 12th Eur. Conf. Antennas Propag.*, 2018, pp. 1–5.
- [93] K. K. W. Low, A. Nafe, S. Zahir, T. Kanar, and G. M. Rebeiz, "A scalable circularly-polarized 256-element Ka-band phased-array SATCOM transmitter with ±60° beam scanning and 34.5 dBW EIRP," in *Proc. IEEE MTT-S Int. Microw. Symp.*, 2019, pp. 1064–1067.
- [94] J.-C. S. Chieh et al., "Development of flat panel active phased array antennas using 5G silicon RFICs at Ku- and Ka-bands," *IEEE Access*, vol. 8, pp. 192669–192681, 2020.
- [95] M. Sebastian and H. Jantunen, "Low loss dielectric materials for LTCC applications: A review," *Int. Mater. Rev.*, vol. 53, pp. 57–90, Mar. 2008.
- [96] F. Bechtold, "A comprehensive overview on today's ceramic substrate technologies," in *Proc. Eur. Microelectron. Packag. Conf.*, 2009, pp. 1–12.
- [97] I. Wolff, C. Günner, J. Kassner, R. Kulke, and P. Uhlig, "New heights for satellites: LTCC multilayer technology for future satellites," *IEEE Microw. Mag.*, vol. 19, no. 1, pp. 36–47, Jan. 2018.
- [98] G. M. Rebeiz and K.-J. Koh, "Silicon RFICs for phased arrays," *IEEE Microw. Mag.*, vol. 10, pp. 96–103, May 2009.
- [99] K. Yamamoto et al., "Low loss BT resin for substrates in 5G communication module," in *Proc. IEEE 70th Electron. Compon. Technol. Conf.*, 2020, pp. 1795–1800.
- [100] J. H. Lau, "Recent advances and trends in advanced packaging," *IEEE Trans. Compon. Packag. Manuf. Technol.*, vol. 12, no. 2, pp. 228–252, Feb. 2022.
- [101] A. A. Nawaz, W. T. Khan, and A. C. Ulusoy, "Organically packaged components and modules: Recent advancements for microwave and mm-wave applications," *IEEE Microw. Mag.*, vol. 20, no. 11, pp. 49–72, Nov. 2019.

- [102] T. Zwick, F. Boes, B. Göttel, A. Bhutani, and M. Pauli, "Pea-sized mmW transceivers: QFN-based packaging concepts for millimeter-wave transceivers," *IEEE Microw. Mag.*, vol. 18, no. 9, pp. 79–89, Sep. 2017.
- [103] M. Ali et al., "Package-integrated, wideband power dividing networks and antenna arrays for 28-GHz 5G new radio bands," *IEEE Trans. Compon., Packag. Manuf. Technol.*, vol. 10, no. 9, pp. 1515–1523, Sep. 2020.
- [104] W. J. Lambert et al., "Scalable multichip packaging with integrated antenna array for a 73-GHz transceiver IC," *IEEE Trans. Microw. Theory Techn.*, vol. 69, no. 1, pp. 387–398, Jan. 2021.
- [105] D. G. Kam, D. Liu, A. Natarajan, S. Reynolds, H.-C. Chen, and B. A. Floyd, "LTCC packages with embedded phased-array antennas for 60 GHz communications," *IEEE Microw. Wireless Compon. Lett.*, vol. 21, no. 3, pp. 142–144, Mar. 2011.
- [106] G. M. Rebeiz et al., "Wafer-scale millimeter-wave phased-array RFICs," in *Proc. IEEE Compound Semicond. Integr. Circuit Symp.*, 2014, pp. 1–4.
- [107] S. Zahir, O. D. Gurbuz, A. Kar-Roy, S. Raman, and G. M. Rebeiz, "60-GHz 64- and 256-elements wafer-scale phased-array transmitters using full-reticle and subreticle stitching techniques," *IEEE Trans. Microw. Theory Techn.*, vol. 64, no. 12, pp. 4701–4719, Dec. 2016.
- [108] M. Geiger, P. Grüner, M. Fischer, A. Dürr, T. Chaloun, and C. Waldschmidt, "A multimodal dielectric waveguide-based monopulse radar at 160 GHz," *IEEE Trans. Microw. Theory Techn.*, vol. 68, no. 11, pp. 4825–4834, Nov. 2020.
- [109] T. Galler et al., "Glass package for radar MMICs above 150 GHz," *IEEE J. Microwaves*, vol. 2, no. 1, pp. 97–107, Jan. 2022.
- [110] D. Liu, X. Gu, C. W. Baks, and A. Valdes-Garcia, "Antenna-in-package design considerations for Ka-band 5G communication applications," *IEEE Trans. Antennas Propag.*, vol. 65, no. 12, pp. 6372–6379, Dec. 2017.
- [111] H.-T. Kim et al., "A 28GHz CMOS direct conversion transceiver with packaged antenna arrays for 5G cellular system," in *Proc. IEEE Radio Freq. Integr. Circuits Symp.*, 2017, pp. 69–72.
- [112] J. D. Dunworth et al., "A 28GHz bulk-CMOS dual-polarization phased-array transceiver with 24 channels for 5G user and basestation equipment," in *Proc. IEEE Int. Solid-State Circuits Conf.*, 2018, pp. 69–72.
- [113] X. Gu et al., "Development, implementation, and characterization of a 64-Element dual-polarized phased-array antenna module for 28-GHz high-speed data communications," *IEEE Trans. Microw. Theory Techn.*, vol. 67, no. 7, pp. 2975–2984, Jul. 2019.
- [114] A. L. Amadjikpe, D. Choudhury, C. E. Patterson, B. Lacroix, G. E. Ponchak, and J. Papapolymerou, "Integrated 60-GHz antenna on multilayer organic package with broadside and end-fire radiation," *IEEE Trans. Microw. Theory Techn.*, vol. 61, no. 1, pp. 303–315, Jan. 2013.
- [115] S. Shahramian, M. J. Holyoak, A. Singh, and Y. Baeyens, "A fully integrated 384-element, 16-tile, W-band phased array with self-alignment and self-test," *IEEE J. Solid-State Circuits*, vol. 54, no. 9, pp. 2419–2434, Sep. 2019.
- [116] B. Sadhu et al., "A 250-mW 60-GHz CMOS transceiver SoC integrated with a four-element AiP providing broad angular link coverage," *IEEE J. Solid-State Circuits*, vol. 55, no. 6, pp. 1516–1529, Jun. 2020.
- [117] T. Kamgaing, A. A. Elsherbini, S. N. Oster, and E. Cohen, "Low-profile fully integrated 60 GHz 18 element phased array on multilayer liquid crystal polymer flip chip package," in *Proc. IEEE 65th Electron. Technol. Conf.*, 2015, pp. 994–998.
- [118] D. G. Kam, D. Liu, A. Natarajan, S. K. Reynolds, and B. A. Floyd, "Organic packages with embedded phased-array antennas for 60-GHz wireless chipsets," *IEEE Trans. Compon. Packag. Manuf. Technol.*, vol. 1, no. 11, pp. 1806–1814, Nov. 2011.
- [119] A. Natarajan, A. Valdes-Garcia, B. Sadhu, S. K. Reynolds, and B. D. Parker, "W-band dual-polarization phased-array transceiver front-end in SiGe BiCMOS," *IEEE Trans. Microw. Theory Techn.*, vol. 63, no. 6, pp. 1989–2002, Jun. 2015.
- [120] D. Thompson, O. Tantot, H. Jallageas, G. E. Ponchak, M. M. Tentzeris, and J. Papapolymerou, "Characterization of liquid crystal polymer (LCP) material and transmission lines on LCP substrates from 30 to 110 GHz," *IEEE Trans. Microw. Theory Techn.*, vol. 52, no. 4, pp. 1343–1352, Apr. 2004.
- [121] E. Cohen, M. Ruberto, M. Cohen, O. Degani, S. Ravid, and D. Ritter, "A CMOS bidirectional 32-element phased-array transceiver at 60 GHz with LTCC antenna," *IEEE Trans. Microw. Theory Techn.*, vol. 61, no. 3, pp. 1359–1375, Mar. 2013.
- [122] T. Sowlati et al., "A 60-GHz 144-element phased-array transceiver for backhaul application," *IEEE J. Solid-State Circuits*, vol. 53, no. 12, pp. 3640–3659, Dec. 2018.
- [123] A. Natarajan et al., "A fully-integrated 16-element phased-array receiver in SiGe BiCMOS for 60-GHz communications," *IEEE J. Solid-State Circuits*, vol. 46, no. 5, pp. 1059–1075, May 2011.
- [124] A. Rashidian, S. Jafarlou, A. Tomkins, K. Law, M. Tazlauanu, and K. Hayashi, "Compact 60 GHz phased-array antennas with enhanced radiation properties in flip-chip BGA packages," *IEEE Trans. Antennas Propag.*, vol. 67, no. 3, pp. 1605–1619, Mar. 2019.
- [125] J. Hacker et al., "A 16-element transmit/receive Q-band electronically steerable subarray tile," in *IEEE/MTT-S Int. Microw. Symp. Dig.*, 2012, pp. 1–3.
- [126] A. O. Watanabe et al., "Ultrathin antenna-integrated glass-based millimeter-wave package with through-glass vias," *IEEE Trans. Microw. Theory Techn.*, vol. 68, no. 12, pp. 5082–5092, Dec. 2020.
- [127] T. Galler, T. Frey, C. Waldschmidt, and T. Chaloun, "High-gain millimeter-wave holographic antenna in package using glass technology," *IEEE Antennas Wireless Propag. Lett.*, vol. 19, no. 20, pp. 2067–2071, Dec. 2020.
- [128] K. Wu, M. Bozzi, and N. J. G. Fonseca, "Substrate integrated transmission lines: Review and applications," *IEEE J. Microwaves*, vol. 1, no. 1, pp. 345–363, Jan. 2021.
- [129] E. R. Pillai, "Coax via-A technique to reduce crosstalk and enhance impedance match at vias in high-frequency multilayer packages verified by FDTD and MoM modeling," *IEEE Trans. Microw. Theory Techn.*, vol. 45, no. 10, pp. 1981–1985, Oct. 1997.
- [130] A. Stark and A. F. Jacob, "A broadband vertical transition for millimeter-wave applications," in *Proc. 38th Eur. Microw. Conf.*, 2008, pp. 476–479.
- [131] E. Meniconi, V. Ziegler, R. Sorrentino, and T. Chaloun, "3D integration technologies for a planar dual band active array in Ka-band," in *Proc. Eur. Microw. Conf.*, 2013, pp. 215–218.
- [132] L. Zhu and K. Wu, "Ultrabroad-band vertical transition for multilayer integrated circuits," *IEEE Microw. Guided Wave Lett.*, vol. 9, no. 11, pp. 453–455, Mar. 1999.
- [133] X. Huang and K.-L. Wu, "A broadband and vialess vertical microstrip-to-microstrip transition," *IEEE Trans. Microw. Theory Techn.*, vol. 60, no. 4, pp. 938–944, Apr. 2012.
- [134] W. Heinrich et al., "Connecting chips with more than 100 GHz bandwidth," *IEEE J. Microwaves*, vol. 1, no. 1, pp. 364–373, Jan. 2021.
- [135] S. Beer et al., "An integrated 122-GHz antenna array with wire bond compensation for SMT radar sensors," *IEEE Trans. Antennas Propag.*, vol. 61, no. 12, pp. 5976–5983, Dec. 2013.
- [136] V. Valenta, H. Schumacher, T. Spreng, V. Ziegler, D. Dancila, and A. Rydberg, "Experimental evaluation of differential chip-to-antenna bondwire interconnects above 110 GHz," in *Proc. Eur. Microw. Conf.*, 2014, pp. 1008–1011.
- [137] J. C. Maxwell, "Solutions of problems," *Cambridge Dublin Math. J.*, vol. 9, pp. 9–11, 1854.
- [138] R. K. Luneburg, *Mathematical Theory of Optics*. Providence, RI, USA: Brown Univ., 1944, pp. 189–213.
- [139] M. Šarbot and T. Tyc, "Spherical media and geodesic lenses in geometrical optics," *J. Opt.*, vol. 14, 2012, Art. no. 075705.
- [140] N. J. G. Fonseca, T. Tyc, and O. Quevedo-Teruel, "A solution to the complement of the generalized Luneburg lens problem," *Commun. Phys.*, vol. 4, 2021, Art. no. 270.
- [141] W. Rotman, "Wide-angle scanning with microwave double-layer pill-boxes," *IRE Trans. Antennas Propag.*, vol. 6, pp. 96–105, 1958.
- [142] R. F. Rinehart, "A solution of the problem of rapid scanning for radar antennae," *J. Appl. Phys.*, vol. 19, pp. 860–862, 1948.
- [143] T. Djerafi, N. J. G. Fonseca, and K. Wu, "Design and implementation of a planar 4x4 Butler matrix in SIW technology for wide band high power applications," *Prog. Electromagnetics Res. B*, vol. 35, pp. 29–51, 2011.
- [144] T. Djerafi, N. J. G. Fonseca, and K. Wu, "Planar Ku -band 4 × 4 Nolen matrix in SIW technology," *IEEE Trans. Microw. Theory Techn.*, vol. 58, no. 2, pp. 259–266, Feb. 2010.
- [145] H. E. A. Laue and W. P. du Plessis, "A checkered network for implementing arbitrary overlapped feed networks," *IEEE Trans. Microw. Theory Techn.*, vol. 67, no. 11, pp. 4632–4640, Nov. 2019.

- [146] N. J. G. Fonseca, "Design and implementation of a closed cylindrical BFN-fed circular array antenna for multiple-beam coverage in azimuth," *IEEE Trans. Antennas Propag.*, vol. 60, no. 2, pp. 863–869, Feb. 2012.
- [147] N. J. G. Fonseca, A. Ali, and H. Aubert, "Cancellation of beam squint with frequency in serial beamforming network-fed linear array antennas," *IEEE Antennas Propag. Mag.*, vol. 54, no. 1, pp. 32–39, Jan. 2012.
- [148] J. Blass, "Multidirectional antenna - A new approach to stacked beams," in *Proc. 1958 IRE Int. Conv. Rec.*, 1960, pp. 48–50.
- [149] J. Butler, "Beam-forming matrix simplifies design of electronically scanned antennas," *Electron. Des.*, vol. 9, pp. 170–173, 1961.
- [150] Y. Aslan, A. Roederer, N. J. G. Fonseca, P. Angeletti, and A. Yarovoy, "Orthogonal versus zero-forced beamforming in multibeam antenna systems: Review and challenges for future wireless networks," *IEEE J. Microwaves*, vol. 1, no. 4, pp. 879–901, Oct. 2021.
- [151] J. P. Shelton, "Fast Fourier transforms and Butler matrices," *Proc. IEEE*, vol. 56, no. 3, pp. 350–350, Mar. 1968.
- [152] J. Nolen, "Synthesis of multiple beam networks for arbitrary illuminations," Ph.D. dissertation, Radio Div., Bendix Corp., Baltimore, MD, USA, 1965.
- [153] J. Hirokawa and N. J. G. Fonseca, "Generalized one-dimensional parallel switching matrices with an arbitrary number of beams," *IEEE J. Microwaves*, vol. 1, no. 4, pp. 975–988, Oct. 2021.
- [154] H. Gent, "The bootlace aerial," *Roy. Radar Establishment J.*, vol. 40, pp. 47–57, 1957.
- [155] J. Ruze, "Wide-angle metal-plate optics," *Proc. IRE*, vol. 38, no. 1, pp. 53–59, Jan. 1950.
- [156] W. Rotman and R. Turner, "Wide-angle microwave lens for line source applications," *IEEE Trans. Antennas Propag.*, vol. 11, no. 6, pp. 623–632, Nov. 1963.
- [157] D. Berry, R. Malech, and W. Kennedy, "The reflectarray antenna," *IEEE Trans. Antennas Propag.*, vol. 11, no. 6, pp. 645–651, Nov. 1963.
- [158] D. McGrath, "Planar three-dimensional constrained lenses," *IEEE Trans. Antennas Propag.*, vol. 34, no. 1, pp. 46–50, Jan. 1986.
- [159] Y. J. Guo, M. Ansari, and N. J. G. Fonseca, "Circuit type multiple beamforming networks for antenna arrays in 5G and 6G terrestrial and non-terrestrial networks," *IEEE J. Microwaves*, vol. 1, no. 3, pp. 704–722, Jul. 2021.
- [160] Y. J. Cheng, W. Hong, and K. Wu, "Millimeter-wave substrate integrated waveguide multibeam antenna based on the parabolic reflector principle," *IEEE Trans. Antennas Propag.*, vol. 56, no. 9, pp. 3055–3058, Sep. 2008.
- [161] N. J. G. Fonseca, "The water drop lens: Revisiting the past to shape the future," *Rev. Electromagn.*, vol. 1, pp. 1–4, 2022.
- [162] Y. J. Cheng et al., "Substrate integrated waveguide (SIW) Rotman lens and its Ka-band multibeam array antenna applications," *IEEE Trans. Antennas Propag.*, vol. 56, no. 8, pp. 2504–2513, Aug. 2008.
- [163] S. A. Matos et al., "High gain dual-band beam-steering transmit array for satcom terminals at Ka-band," *IEEE Trans. Antennas Propag.*, vol. 65, no. 7, pp. 3528–3539, Jul. 2017.
- [164] K.-J. Koh and G. M. Rebeiz, "An X- and Ku-band 8-element phased-array receiver in 0.18- μm SiGe BiCMOS technology," *IEEE J. Solid-State Circuits*, vol. 43, no. 6, pp. 1360–1371, Jun. 2008.
- [165] F. Tabarani, T. Chaloun, T. Purtova, M. Kaynak, and H. Schumacher, "0.25 μm BiCMOS system-on-chip with four transceivers for Ka-band active reflectarrays," in *Proc. SBMO/IEEE MTT-S Int. Microw. Optoelectron. Conf.*, 2015, pp. 2325–2339.
- [166] A. C.-W. Wong et al., "A 4Rx, 4Tx Ka-band transceiver in 40nm bulk CMOS technology for satellite terminal applications," in *Proc. IEEE Radio Freq. Integr. Circuits Symp.*, 2021, pp. 211–214.
- [167] B. Sadhu et al., "A 28-GHz 32-element TRX phased-array IC with concurrent dual-polarized operation and orthogonal phase and gain control for 5G communications," *IEEE J. Solid-State Circuits*, vol. 52, no. 12, pp. 3373–3391, Dec. 2017.
- [168] S. Mondal, R. Singh, A. I. Hussein, and J. Paramesh, "A 25–30 GHz fully-connected hybrid beamforming receiver for MIMO communication," *IEEE J. Solid-State Circuits*, vol. 53, no. 5, pp. 1275–1287, May 2018.
- [169] P. Saha, "A quantitative analysis of the power advantage of hybrid beamforming for multibeam phased array receivers," *Microw. J.*, 2021.
- [170] D. Sikri and R. M. Jayasuriya, "Multi-Beam phased array with full digital beamforming for SATCOM and 5G," *Microw. J.*, vol. 62, pp. 64–79, 2019.
- [171] SatixFy, "Beat- Ku band RFIC," Jan. 20, 2022. [Online]. Available: <https://www.satixfy.com/beat/>
- [172] Analog Devices, "ADAR3000 - 17 GHz to 22 GHz, 4-beam and 4-element, Ka-band beamformer," 2022. [Online]. Available: <https://www.analog.com/en/products/adar3000.html>
- [173] V. Joroughi, M. Á. Vázquez, A. I. Pérez-Neira, and B. Devillers, "Onboard beam generation for multibeam satellite systems," *IEEE Trans. Wireless Commun.*, vol. 16, no. 6, pp. 3714–3726, Jun. 2017.
- [174] D. Peng, A. Bandi, Y. Li, S. Chatzinotas, and B. Ottersten, "Hybrid beamforming, user scheduling, and resource allocation for integrated terrestrial-satellite communication," *IEEE Trans. Intell. Veh.*, vol. 70, no. 9, pp. 8868–8882, Sep. 2021.
- [175] A. I. Perez-Neira, M. A. Vazquez, M. R. B. Shankar, S. Maleki, and S. Chatzinotas, "Signal processing for high-throughput satellites: Challenges in new interference-limited scenarios," *IEEE Signal Inf. Process. Mag.*, vol. 36, no. 4, pp. 112–131, Jul. 2019.
- [176] Sivers Semiconductors AB, "TRXBF01 - WiGig/802.11ad beamforming transceiver RFIC from 57 to 71 GHz." [Online]. Available: https://www.sivers-semiconductors.com/wp-content/uploads/2022/01/Product-Brief_TRXBF01_220111-1.pdf
- [177] Sivers Semiconductors AB, "TRX BF/02 - 16+16 channel beamforming IC from 24 to 29.5 GHz for 5G applications." [Online]. Available: <https://www.sivers-semiconductors.com/sivers-wireless/rfics-and-bfics-for-licensed-and-unlicensed-5g/>
- [178] A. Chakrabarti, C. Thakkar, S. Yamada, D. Choudhury, J. Jaussi, and B. Casper, "4.5 A 64 Gb/s 1.4pJ/b/element 60 GHz 2×2 -element phased-array receiver with 8b/symbol polarization MIMO and spatial interference tolerance," in *Proc. IEEE Int. Solid-State Circuits Conf.*, 2020, pp. 84–86.
- [179] SatixFy, "PRIME- Digital beam former ASIC," Jan. 20, 2022. [Online]. Available: <https://www.satixfy.com/prime/>
- [180] Teledyne e2V, "EV12DD700 - Dual channel Ka-band capable 12 GSps DAC," 2022. [Online]. Available: <https://semiconductors.teledyneimaging.com/en/products/digital-to-analog-converters/ev12dd700/>
- [181] E. A. Alwan, S. B. Venkatakrishnan, A. A. Akhiyat, W. Khalil, and J. L. Volakis, "Code optimization for a code-modulated RF front end," *IEEE Access*, vol. 3, pp. 260–273, 2015.
- [182] P. M. Asbeck, N. Rostomyan, M. Özen, B. Rabet, and J. A. Jayamon, "Power amplifiers for mm-wave 5G applications: Technology comparisons and CMOS-SOI demonstration circuits," *IEEE Trans. Microw. Theory Techn.*, vol. 67, no. 7, pp. 3099–3109, Jul. 2019.
- [183] Z. Chbili and A. Kerber, "Self-heating impact on TDD in bulk FinFET devices: Uniform vs non-uniform stress," in *Proc. IEEE Int. Integr. Rel. Workshop*, 2016, pp. 45–48.
- [184] C. Zhang, F. Zhang, S. Syed, M. Otto, and A. Bellaouar, "A low noise figure 28GHz LNA in 22nm FDSOI technology," in *Proc. IEEE Radio Freq. Integr. Circuits Symp.*, 2019, pp. 207–210.
- [185] G. H. Knittel, A. Hessel, and A. A. Oliner, "Element pattern nulls in phased arrays and their relation to guided waves," *Proc. IEEE*, vol. 56, pp. 1822–1836, Nov. 1968.
- [186] A. K. Bhattacharyya, *Phased Array Antennas: Floquet Analysis, Synthesis, BFNs and Active Array Systems*. Hoboken, NJ, USA: Wiley, 2006.
- [187] H. Kähkönen, J. Ala-Laurinaho, and V. Viikari, "Surface-mounted Ka-band Vivaldi antenna array," *IEEE Open J. Antennas Propag.*, vol. 2, pp. 126–137, 2021.
- [188] J. A. Kasemodel, C.-C. Chen, and J. L. Volakis, "Wideband planar array with integrated feed and matching network for wide-angle scanning," *IEEE Trans. Antennas Propag.*, vol. 61, pp. 4528–4537, Jun. 2013.
- [189] M. H. Novak, F. A. Miranda, and J. L. Volakis, "Ultra-wideband phased array for millimeter-wave ISM and 5G bands, realized in PCB," *IEEE Trans. Antennas Propag.*, vol. 66, no. 12, pp. 6930–6938, Dec. 2018.
- [190] S. S. Holland, D. H. Schaubert, and M. N. Vouvakis, "A 7–21 GHz dual-polarized planar ultrawideband modular antenna (PUMA) array," *IEEE Trans. Antennas Propag.*, vol. 60, no. 10, pp. 4589–4600, Oct. 2012.
- [191] R. Kindt, R. Mital, and M. Vouvakis, "3:1-bandwidth millimeter-wave PUMA array," in *Proc. IEEE Int. Symp. Antennas Propag.*, 2016, pp. 1867–1868.

- [192] J. T. Logan, R. W. Kindt, M. Y. Lee, and M. N. Vouvakis, "A new class of planar ultrawideband modular antenna arrays with improved bandwidth," *IEEE Trans. Antennas Propag.*, vol. 66, no. 2, pp. 692–701, Feb. 2018.
- [193] S. Hussain, S.-W. Qu, W.-L. Zhou, P. Zhang, and S. Yang, "Design and fabrication of wideband dual-polarized dipole array for 5G wireless systems," *IEEE Access*, vol. 8, pp. 65155–65163, 2020.
- [194] D. Cavallo, W. H. Syed, and A. Neto, "Connected-slot array with artificial dielectrics: A 6 to 15 GHz dual-pol wide-scan prototype," *IEEE Trans. Antennas Propag.*, vol. 66, no. 6, pp. 3201–3206, Jun. 2018.
- [195] B. Yu et al., "A wideband mmwave antenna in fan-out wafer level packaging with tall vertical interconnects for 5G wireless communication," *IEEE Trans. Antennas Propag.*, vol. 69, no. 10, pp. 1867–1868, Oct. 2021.
- [196] Y. Li, C. Wang, and Y. X. Guo, "A Ka-band wideband dual-polarized magneto-electric dipole antenna array on LTCC," *IEEE Trans. Antennas Propag.*, vol. 68, no. 6, pp. 4985–4990, Jun. 2020.
- [197] Y. Li and K.-M. Luk, "60-GHz dual-polarized two-dimensional switch-beam wideband antenna array of aperture-coupled magneto-electric dipoles," *IEEE Trans. Antennas Propag.*, no. 2, vol. 64, pp. 554–563, Feb. 2016.
- [198] Y. Li and K.-M. Luk, "A multibeam end-fire magneto-electric dipole antenna array for millimeter-wave applications," *IEEE Trans. Antennas Propag.*, vol. 64, no. 7, pp. 2894–2904, Jul. 2016.
- [199] T. Chaloun, V. Ziegler, and W. Menzel, "Design of a dual-polarized stacked patch antenna for wide angle scanning reflectarrays," *IEEE Trans. Antennas Propag.*, vol. 64, no. 8, pp. 3380–3390, Aug. 2016.
- [200] H. Liu, A. Qing, T. Chen, Z. Yu, and Z. Zhang, "A switchable 256 elements Ka band circularly polarized phased array using 45 degree linearly polarized element," in *Proc. IEEE Asia-Pacific Microw. Conf.*, 2020, pp. 985–987.
- [201] Swissto12, "Next generation active antennas for satellite communications," Jan. 20, 2022. [Online]. Available: <https://swissto12.com/products/electronically-steered-antenna-arrays/>
- [202] I. Nistal-González et al., "Planar phased array antenna for nomadic satellite communication in Ka-band," in *Proc. 11th Eur. Radar Conf.*, pp. 396–399, 2014.
- [203] F. Bongard, M. Gimersky, S. Doherty, X. Aubry, and M. Krummen, "3D-printed Ka-band waveguide array antenna for mobile SATCOM applications," in *Proc. 11th Eur. Conf. Antennas Propag.*, 2017, pp. 579–583.
- [204] M. Ferrando-Rocher, J. I. Herranz-Herruzo, A. Valero-Nogueira, and B. Bernardo-Clemente, "Dual circularly polarized aperture array antenna in gap waveguide for high-efficiency Ka-band satellite communications," *IEEE Open J. Antennas Propag.*, vol. 1, pp. 283–289, 2020.
- [205] K. Kuhlmann, K. Rezer, and A. F. Jacob, "Far field measurement on Ka-band substrate-integrated waveguide antenna array with polarization multiplexing," in *Proc. IEEE/MTT-S Int. Microw. Symp.*, 2008, pp. 1337–1340.
- [206] K. Kuhlmann, B. Rohrdantz, and A. F. Jacob, "Performance assessment and optimization of an active Ka-band antenna array with polarization multiplexing," in *Proc. Eur. Microw. Conf.*, 2014, pp. 239–242.
- [207] R. Kindt and D. Taylor, "Polarization correction in dual-polarized phased arrays of flared notches," in *Proc. IEEE Int. Symp. Antennas Propag.*, 2011, pp. 1961–1964.
- [208] Hansen, "Linear connected arrays [coupled dipole arrays]," *IEEE Antennas Wireless Propag. Lett.*, vol. 3, pp. 154–156, 2004.
- [209] A. Neto, D. Cavallo, G. Gerini, and G. Toso, "Scanning performances of wideband connected arrays in the presence of a backing reflector," *IEEE Trans. Antennas Propag.*, vol. 57, no. 10, pp. 3092–3102, Oct. 2009.
- [210] J. P. Doane, K. Sertel, and J. L. Volakis, "Matching bandwidth limits for arrays backed by a conducting ground plane," *IEEE Trans. Antennas Propag.*, vol. 61, no. 5, pp. 2511–2518, 2013.
- [211] D. Cavallo et al., "Ku-band dual-polarized array of connected dipoles for satcom terminals: Theory and hardware validation," in *Proc. Eur. Conf. Antennas Propag.*, 2013, pp. 459–460.
- [212] Y. Zhou et al., "Tightly coupled array antennas for ultra-wideband wireless systems," *IEEE Access*, vol. 6, pp. 61851–61866, 2018.
- [213] S. S. Holland and M. N. Vouvakis, "Planar ultrawideband modular antenna array," U.S. Patent Appl. 12/848,301, Jun. 2012.
- [214] A. J. v. Katwijk, A. Neto, G. Toso, and D. Cavallo, "Design of wideband wide-scanning dual-polarized phased array covering simultaneously both the Ku- and the Ka-satcom bands," in *Proc. Eur. Conf. Antennas Propag.*, 2020, pp. 1–3.
- [215] J. Sun, A. Li, and K.-M. Luk, "A high-gain millimeter-wave magneto-electric dipole array with packaged microstrip line feed network," *IEEE Antennas Wireless Propag. Lett.*, vol. 19, no. 10, pp. 1669–1673, Oct. 2020.
- [216] Y. C. Chang, C. C. Hsu, M. I. Magray, H. Y. Chang, and J.-H. Tarnq, "A novel dual-polarized wideband and miniaturized low profile magneto-electric dipole antenna array for mmwave 5G applications," *IEEE Open J. Antennas Propag.*, vol. 2, pp. 326–334, 2021.
- [217] J. Wang et al., "A low-profile vertically polarized magneto-electric monopole antenna with a 60% bandwidth for millimeter-wave applications," *IEEE Trans. Antennas Propag.*, vol. 69, no. 1, pp. 3–13, Jan. 2021.
- [218] T. Lambard, O. Lafond, M. Himdi, H. Jeuland, S. Bolioli, and L. Le Coq, "Design of a Ka-band wide scanning phased array antenna," in *Proc. Eur. Conf. Antennas Propag.*, 2009, pp. 1247–1251.
- [219] Anokiwave, "Ku band intelligent gain block IC," Jan. 20, 2022. [Online]. Available: <https://www.anokiwave.com/products/awmf-0117/index.html>
- [220] G. Gültepe and G. M. Rebeiz, "A 256-element dual-beam dual-polarization Ku-band phased-array with 5 dB/K G/T for simultaneous multi-satellite reception," in *Proc. IEEE MTT-S Int. Microw. Symp.*, 2021, pp. 629–631.
- [221] I. del Portillo, B. G. Cameron, and E. F. Crawley, "A technical comparison of three low earth orbit satellite constellation systems to provide global broadband," *Acta Astronautica*, vol. 159, pp. 123–135, Jun. 2019.
- [222] N. Pachler, I. del Portillo, E. F. Crawley, and B. G. Cameron, "An updated comparison of four low earth orbit satellite constellation systems to provide global broadband," in *Proc. IEEE Int. Conf. Comm. Workshops*, 2021, pp. 1–7.
- [223] B. Canpolat, D. Sikri, and C. Altan, "Electronically steered multi-beam antenna array performance and beam tracking in mobility," in *Proc. Ka Broadband Commun. Conf.*, 2019, pp. 1–20.
- [224] W. M. Abdel-Wahab et al., "A modular architecture for wide scan angle phased array antenna for K/Ka mobile SATCOM," in *Proc. IEEE/MTT-S Int. Microw. Symp.*, 2019, pp. 1076–1079.
- [225] K. K. W. Low, S. Zahir, T. Kanar, and G. M. Rebeiz, "A 27-31-GHz 1024-element Ka-band SATCOM phased-array transmitter with 49.5-dBW peak EIRP, 1-dB AR, and $\pm 70^\circ$ beam scanning," *IEEE Trans. Microw. Theory Techn.*, vol. 70, no. 3, pp. 1757–1768, Mar. 2022.
- [226] Renesas, "F6522 - 8-Channel Transmit Active Beamforming IC for Ka-Band SATCOM." [Online]. Available: <https://www.renesas.com/us/en/products/rf-products/phased-array-beamformers/f6522-8-channel-transmit-active-beamforming-ic-ka-band-satcom>
- [227] K. K. W. Low, T. Kanar, S. Zahir, and G. M. Rebeiz, "A 17.7-20.2-GHz 1024-element K-band SATCOM phased-array receiver with 8.1-dB/K G/T, $\pm 70^\circ$ beam scanning, and high transmit isolation," *IEEE Trans. Microw. Theory Techn.*, vol. 70, no. 3, pp. 1769–1778, Mar. 2022.
- [228] M. Stoneback and K. Madsen, "A planar all-silicon 256-element Ka-band phased array for high-altitude platforms (HAPs) application," in *Proc. IEEE/MTT-S Int. Microw. Symp.*, 2018, pp. 783–786.
- [229] W. Theunissen, V. Jain, and G. Menon, "Development of a receive phased array antenna for high altitude platform stations using integrated beamformer modules," in *Proc. IEEE/MTT-S Int. Microw. Symp.*, 2018, pp. 779–782.
- [230] J. Dunworth et al., "28GHz phased array transceiver in 28nm bulk CMOS for 5G prototype user equipment and base stations," in *Proc. IEEE/MTT-S Int. Microw. Symp.*, 2018, pp. 783–786.
- [231] A. Nafe, M. Sayginer, K. Kibaroglu, and G. M. Rebeiz, "2 × 64-element dual-polarized dual-beam single-aperture 28-GHz phased array with 2 × 30 Gb/s links for 5G polarization MIMO," *IEEE Trans. Microw. Theory Techn.*, vol. 68, no. 9, pp. 3872–3884, Sep. 2020.
- [232] Y. Hu and W. Hong, "A novel hybrid analog-digital multibeam antenna array for massive MIMO applications," in *Proc. IEEE Asia-Pacific Conf. Antennas Propag.*, 2018, pp. 42–45.
- [233] C. Yu et al., "Full-angle digital predistortion of 5G millimeter-wave massive MIMO transmitters," *IEEE Trans. Microw. Theory Techn.*, vol. 67, no. 7, pp. 2847–2860, Jul. 2019.
- [234] Y. Yu, W. Hong, Z. H. Jiang, H. Zhang, and C. Guo, "Multibeam generation and measurement of a DDS-based digital beamforming array transmitter at Ka-band," *IEEE Trans. Antennas Propag.*, vol. 67, no. 5, pp. 3030–3039, May 2019.

- [235] W. Hong et al., "The role of millimeter-wave technologies in 5G/6G wireless communications," *IEEE J. Microwaves*, vol. 1, no. 1, pp. 101–122, Jan. 2021.
- [236] B. Rupakula, S. Zihir, and G. M. Rebeiz, "Low complexity 54–63-GHz transmit/receive 64- and 128-element 2-D-scanning phased-arrays on multilayer organic substrates with 64-QAM 30-Gbps data rates," *IEEE Trans. Microw. Theory Techn.*, vol. 67, no. 12, pp. 5268–5281, Dec. 2019.
- [237] X. Gu, D. Liu, C. Baks, J.-O. Plouchart, W. Lee, and A. Valdes-Garcia, "An enhanced 64-element dual-polarization antenna array package for W-band communication and imaging applications," in *Proc. IEEE Electron. Compon. Technol. Conf.*, 2018, pp. 197–201.
- [238] K. Kibaroglu, M. Sayginer, T. Phelps, and G. M. Rebeiz, "A 64-element 28-GHz phased-array transceiver with 52-dBm EIRP and 8–12-Gb/s 5G link at 300 meters without any calibration," *IEEE Trans. Microw. Theory Techn.*, vol. 66, no. 12, pp. 5796–5811, Dec. 2018.
- [239] J. Huang and J. A. Encinar, *Reflectarray Antennas*, Hoboken, NJ, USA: Wiley, 2007.
- [240] B. Rohrdantz, T. Jaschke, T. Reuschel, S. Radziejewski, A. Sieganschin, and A. F. Jacob, "An electronically steerable reflector antenna using a planar active array feed at Ka-band," *IEEE Trans. Microw. Theory Techn.*, vol. 65, no. 5, pp. 1650–1661, May 2017.
- [241] L. Martin, "Lockheed martin develops hybrid antenna for 5G, radar and remote sensing applications," 2021. Accessed: Mar. 11, 2022. [Online]. Available: <https://www.microwavejournal.com/articles/36588-lockheed-martin-develops-hybrid-antenna-for-5g-radar-and-remote-sensing-applications>
- [242] Y.-B. Jung, S.-Y. Eom, S.-I. Jeon, A. V. Shishlov, and C.-J. Kim, "Novel hybrid antenna design having a shaped reflector for mobile satellite communication applications," in *Proc. IEEE Antennas Propag. Int. Symp.*, 2010, pp. 1–4.
- [243] N. J. G. Fonseca, E. Girard, and H. Legay, "Doubly curved reflector design for hybrid array fed reflector antennas," *IEEE Trans. Antennas Propag.*, vol. 66, no. 4, pp. 2079–2083, Apr. 2018.
- [244] N. J. G. Fonseca, E. Girard, and H. Legay, "Doubly curved reflector antenna design trade-offs for a hexagonal lattice of beams," in *Proc. Int. Symp. Antennas Propag.*, 2021, pp. 581–582.
- [245] C. P. Scarborough, J. P. Turpin, D. F. Difonzo, and J. Finney, "Lens antenna system," Patent EP3376595A1, 2017.
- [246] J.-M. Baracco, P. Ratajczak, P. Brachat, J.-M. Fargeas, and G. Toso, "Ka-band reconfigurable reflectarrays using varactor technology for space applications: A proposed design," *IEEE Antennas Propag. Mag.*, vol. 64, no. 1, pp. 27–38, Feb. 2022.
- [247] E. Basar, M. Di Renzo, J. De Rosny, M. Debbah, M.-S. Alouini, and R. Zhang, "Wireless communications through reconfigurable intelligent surfaces," *IEEE Access*, vol. 7, pp. 116753–116773, 2019.
- [248] Q. Wu and R. Zhang, "Intelligent reflecting surface enhanced wireless network via joint active and passive beamforming," *IEEE Trans. Wireless Commun.*, vol. 18, no. 11, pp. 5394–5409, Nov. 2019.
- [249] J. A. Hodge, K. V. Mishra, and A. I. Zaghoul, "Intelligent time-varying metasurface transceiver for index modulation in 6G wireless networks," *IEEE Antennas Wireless Propag. Lett.*, vol. 19, no. 11, pp. 1891–1895, Nov. 2020.
- [250] Q. Wu and R. Zhang, "Towards smart and reconfigurable environment: Intelligent reflecting surface aided wireless network," *IEEE Commun. Mag.*, vol. 58, no. 1, pp. 106–112, Jan. 2020.
- [251] A. Araghi et al., "Reconfigurable intelligent surface (RIS) in the sub-6 GHz band: Design, implementation, and real-world demonstration," *IEEE Access*, vol. 10, pp. 2646–2655, 2022.
- [252] Y. Han, X. Li, W. Tang, S. Jin, Q. Cheng, and T. J. Cui, "Dual-polarized RIS-assisted mobile communications," *IEEE Trans. Wireless Commun.*, vol. 21, no. 1, pp. 591–606, Jan. 2022.
- [253] H. Yang et al., "A 1600-element dual-frequency electronically reconfigurable reflectarray at X/Ku-band," *IEEE Trans. Antennas Propag.*, vol. 65, no. 6, pp. 3024–3032, Jun. 2017.
- [254] H. Kamoda, T. Iwasaki, J. Tsumochi, T. Kuki, and O. Hashimoto, "60-GHz electronically reconfigurable large reflectarray using single-bit phase shifters," *IEEE Trans. Antennas Propag.*, vol. 59, no. 7, pp. 2524–2531, Jul. 2011.
- [255] O. Bayraktar, O. A. Civi, and T. Akin, "Beam switching reflectarray monolithically integrated with RF MEMS switches," *IEEE Trans. Antennas Propag.*, vol. 60, no. 2, pp. 854–862, Feb. 2012.
- [256] T. Debogovic and J. Perruisseau-Carrier, "Low loss MEMS-reconfigurable 1-bit reflectarray cell with dual-linear polarization," *IEEE Trans. Antennas Propag.*, vol. 62, no. 10, pp. 5055–5060, Oct. 2014.
- [257] L. D. Palma, A. Clemente, L. Dussopt, R. Sauleau, P. Potier, and P. Pouliguen, "Circularly-polarized reconfigurable transmitarray in Ka-band with beam scanning and polarization switching capabilities," *IEEE Trans. Antennas Propag.*, vol. 65, no. 2, pp. 529–540, Feb. 2017.
- [258] S. Bildik, S. Dieter, C. Fritzsche, W. Menzel, and R. Jakoby, "Reconfigurable folded reflectarray antenna based upon liquid crystal technology," *IEEE Trans. Antennas Propag.*, vol. 63, no. 1, pp. 122–132, Jan. 2015.
- [259] F. Tabarani, T. Chaloun, T. Purtova, M. Kaynak, and H. Schumacher, "0.25 μ m BiCMOS system-on-chip with four transceivers for Ka-band active reflectarrays," in *Proc. SBMO/IEEE MTT-S Int. Microw. Optoelectron. Conf.*, Porto de Galinhas, Pernambuco, Brazil, 2015, pp. 1–5.
- [260] Y. Xiao, F. Yang, S. Xu, M. Li, K. Zhu, and H. Sun, "Design and implementation of a wideband 1-bit transmitarray based on a Yagi-Vivaldi unit cell," *IEEE Trans. Antennas Propag.*, vol. 69, no. 7, pp. 4229–4234, Jul. 2021.
- [261] T. Chaloun, C. Hillebrand, C. Waldschmidt, and W. Menzel, "Active transmitarray submodule for K/Ka band satcom applications," in *Proc. German Microw. Conf.*, 2015, pp. 198–201.
- [262] F. Tabarani, L. Boccia, T. Purtova, A. Shamsafar, H. Schumacher, and G. Amendola, "0.25- μ m BiCMOS system-on-chip for K-/Ka-band satellite communication transmit-receive active phased arrays," *IEEE Trans. Microw. Theory Techn.*, vol. 66, no. 5, pp. 2325–2339, May 2018.
- [263] A. Oliner and A. Hessel, "Guided waves on sinusoidally-modulated reactance surfaces," *IRE Trans. Antennas Propag.*, vol. TAP-7, no. 5, pp. 201–208, Dec. 1959.
- [264] G. Minatti et al., "Modulated metasurface antennas for space: Synthesis, analysis and realizations," *IEEE Trans. Antennas Propag.*, vol. 63, no. 4, pp. 1288–1300, Apr. 2015.
- [265] D. González-Ovejero, G. Minatti, G. Chattopadhyay, and S. Maci, "Multibeam by metasurface antennas," *IEEE Trans. Antennas Propag.*, vol. 65, no. 6, pp. 2923–2930, Jun. 2017.
- [266] T. Frey, M. Döring, C. Waldschmidt, and T. Chaloun, "Towards holographic antenna systems for MIMO radar and communication applications," in *Proc. Eur. Conf. Antennas Propag.*, Madrid, 2022, pp. 1–5.
- [267] P. Commware, "Holographic beam forming technology – Pivotal commware," Accessed: Mar. 22, 2022. [Online]. Available: <https://pivotalcommware.com/technology/>
- [268] A. Bily, J. Dallas, R. J. Hannigan, N. Kundtz, D. R. Nash, and R. A. Stevenson, "Surface scattering antenna improvements," Patent US20140266946A1, 2013.
- [269] R. Stevenson, M. Sazegar, A. Bily, M. Johnson, and N. Kundtz, "Metamaterial surface antenna technology: Commercialization through diffractive metamaterials and liquid crystal display manufacturing," in *Proc. 10th Int. Congr. Adv. Electromagn. Materials Microw. Opt.*, 2016, pp. 349–351.
- [270] S. C. Pavone, E. Martini, F. Caminita, M. Albani, and S. Maci, "Surface wave dispersion for a tunable grounded liquid crystal substrate without and with metasurface on top," *IEEE Trans. Antennas Propag.*, vol. 65, no. 7, pp. 3540–3548, Jul. 2017.



TOBIAS CHALOUN (Member, IEEE) received the Dipl.-Ing. degree and the Dr.-Ing. degree (with hon.) in electrical engineering from the University of Ulm, Ulm, Germany, in 2010 and 2016, respectively. From 2010 to 2016, he was a Research Assistant with the Institute of Microwave Engineering, Ulm University, Germany, where he conducted his doctoral studies in the field of highly integrated antenna systems for communication applications at millimeter wave frequencies. Since January 2017, he has been a Senior Researcher and

Lecturer with the Institute of Microwave Engineering, University of Ulm. His research interest include multilayer antennas and circuits, millimeter-wave packaging and interconnects, phased array antenna systems, and millimeter-wave radar sensors. Dr. Chaloun is a member of the European Microwave Association. He is also a Founding Member of the IEEE MTT-S Technical Committee 29 on Microwave Aerospace Systems. He is currently a reviewer for multiple IEEE journals and conferences. He was the recipient of the Best Paper Award of the German Microwave Conference in 2015. In 2016, he was awarded the Best Paper in *IET Microwaves, Antennas & Propagation*.



LUIGI BOCCIA (Senior Member, IEEE) was born in Lungro, Italy, in 1975. He received a degree in information technology engineering from the University of Calabria, Rende, Italy, in 2000, and the Ph.D. degree in electronics engineering from the University Mediterranea of Reggio Calabria, Reggio Calabria, Italy, in 2003. Since 2021, he has been an Associate Professor of electromagnetics with the University of Calabria. His research interests include antennas for telecommunications, radar and Earth observation applications, mono-

lithically integrated RF circuits for phased array applications, and RF system integration technologies. He was an Associated Editor for the *International Journal of Microwave and Wireless Technologies* (Cambridge University Press) and IEEE MICROWAVE AND WIRELESS COMPONENTS LETTERS. He was also the Co-Editor of the book titled *Space Antenna Handbook* (Wiley, 2012).



EMILIO ARNERI (Member, IEEE) was born in Cosenza, Italy, in 1977. He received the Degree (Hons.) in information technology engineering from the University of Calabria, Rende, Italy, in 2003, and the Ph.D. degree in electronics engineering from the University Mediterranea of Reggio Calabria, Reggio Calabria, Italy, in 2007. He is currently an Assistant Professor with the Department of Informatics, Modeling, Electronics and System Engineering, University of Calabria, where he has participated in several national, European Union,

and ESA projects. He has coauthored more than 80 articles published in international journals and proceedings of international conferences. His research interests include circular polarizers, the development of dual-band antennas and millimeter-wave components, synthetic aperture radar, and beam scanning antennas. Dr. Arneri was selected as a finalist for the Best Paper Award in Antenna Design at the 13th European Conference on Antennas and Propagation (EuCap 2019). He was an Associate Editor for IEEE ANTENNAS AND WIRELESS PROPAGATION LETTERS, an Advisory Editor for the *Wiley Engineering Reports*, and a Guest Editor for *MDPI Sensors* and *MDPI Electronics*. He is the Co-Founder of the academic spinoff Antecnica.



MICHAEL FISCHER (Student Member, IEEE) received the M.Sc. degree in electrical engineering from Ulm University, Ulm, Germany in 2019, where he is currently working toward the Ph.D. degree. In 2019, he joined the Institute of Microwave Engineering, Ulm University, Germany. His research focuses on the development of electronically steerable antenna arrays with a focus on highly integrated and broadband antenna systems for communication applications at millimeter-wave frequencies.



VACLAV VALENTA (Member, IEEE) received the dual Doctoral degree in radio-engineering from ESIEE Paris, France, and the Brno University of Technology, Brno, Czechia. Since 2016, he has been with the European Space Agency, Noordwijk, The Netherlands. With over a decade of experience in RFIC design, he is running internal research and industrial R&D contracts in the area of RF equipment and technology, covering radar, navigation and satcom applications. His research interests include frequency generation and timing, high-power

amplification, and beamforming concepts in active antenna arrays and FMCW radars. He is the ESA Lead Engineer of a radio-scientific instrument LaRa embarked on the ExoMars surface platform Kozachok.



NELSON J. G. FONSECA (Senior Member, IEEE) received the M.Eng. degree in electrical engineering from Ecole Nationale Supérieure d'Electrotechnique, Electronique, Informatique, Hydraulique et Télécommunications (ENSEEIH), Toulouse, France, in 2003, the M.Sc. degree in electrical engineering from the Ecole Polytechnique de Montréal, Montréal, QC, Canada, in 2003, and the Ph.D. degree in electrical engineering from the Institut National Polytechnique de Toulouse, Université de

Toulouse, Toulouse, France, in 2010. He is currently an Antenna Engineer with the Antenna and Sub-Millimetre Waves Section, European Space Agency, Noordwijk, The Netherlands. Since November 2020, he has held an Honorary Appointment as a Professional Fellow with the University of Technology Sydney, Ultimo, Australia. He has authored or coauthored more than 250 papers in peer-reviewed journals and conferences and has more than 50 patents issued or pending. His research interests include multiple beam antennas for space missions, beam-former theory and design, ground terminal antennas and novel manufacturing techniques. Dr. Fonseca is an Associate Editor for *IET Microwave, Antennas and Propagation* and IEEE TRANSACTIONS ON MICROWAVE THEORY AND TECHNIQUES, and a Topic Editor for IEEE JOURNAL OF MICROWAVES. He is also Chair of the newly founded IEEE MTT-S Technical Committee 29 on Microwave Aerospace Systems. Since January 2019, he has been a Board Member of the European School of Antennas and is actively involved as a lecturer and a coordinator in courses related to space and ground antennas. From 2021 to 2023, he is the Elected EurAAP Regional Delegate representing Benelux. He was the recipient of the several prizes and awards, including the Best Young Engineer Paper Award at the 29th ESA Workshop on Antennas in 2007, an ESA Teamwork Excellence Award in 2020, and several ESA Technical Improvement Awards.



CHRISTIAN WALDSCHMIDT (Fellow, IEEE) received the Dipl.-Ing. (M.S.E.E.) and Dr.-Ing. (Ph.D.E.E.) degrees from University Karlsruhe, Karlsruhe, Germany, in 2001 and 2004, respectively. From 2001 to 2004, he was a Research Assistant with the Institut für Höchstfrequenztechnik und Elektronik (IHE), Universität Karlsruhe. Since 2004, he has been with Robert Bosch GmbH, in the business units Corporate Research and Chassis Systems. He was heading different research and development teams in microwave engineering,

RF-sensing, and automotive radar. In 2013, he returned to academia. He was appointed as the Director of the Institute of Microwave Engineering with University Ulm, Ulm, Germany, as a Full Professor. He has authored or coauthored more than 250 scientific publications and more than 20 patents. His research interests include radar and RF-sensing, mm-wave and submillimeter-wave engineering, antennas and antenna arrays, RF, and array signal processing. He is a member of the executive committee board of the German MTT/AP joint chapter and a member of the German Information Technology Society. He was Chair of the IEEE MTT-29 Technical Committee on Microwave Aerospace Systems and Chair of the MTT-27 Technical Committee on Wireless Enabled Automotive and Vehicular Applications. He was the two-time TPC Chair and General Chair of the IEEE MTT International Conference on Microwaves for Intelligent Mobility. Since 2018, he has been an Associate Editor for IEEE MICROWAVE WIRELESS COMPONENTS LETTERS. He is a reviewer for multiple IEEE transactions and many IEEE conferences in the field of microwaves. He was co-recipient of 12 best paper awards.